Finite memory observer design for continuous-time nonlinear systems with discrete-time measurements: application to diagnosis

Tingting Zhang

INSA INSTITUT NATIONAL DES SCIENCES APPLIQUÉES CENTRE VAL DE LOIRE

INSA Centre Val de Loire

ÉCOLE DOCTORALE

MATHÉMATIQUES, INFORMATIQUE, PHYSIQUE THÉORIQUE ET INGÉNIERIE DES SYSTÈMES

Laboratoire PRISME

THÈSE présentée par :

Tingting ZHANG

soutenue le : **14 Janvier 2021**

pour obtenir le grade de : **Docteur de l'INSA Centre Val de Loire**

Discipline / Spécialité : Sciences et Technologies Industrielles / Automatique

---

Finite Memory Observer Design for Continuous-Time Nonlinear Systems with Discrete-Time Measurements: Application to Diagnosis

---

THÈSE dirigée par :	
Frédéric KRATZ	Professeur, INSA Centre Val de Loire, PRISME
Co-encadrant :	
Vincent IDASIAK	Maître de conférences, INSA Centre Val de Loire, PRISME
Yunhui HOU	Maître de conférences, INSA Centre Val de Loire, PRISME
RAPPORTEURS :	
Gabriela Iuliana BARA	Maître de conférences, Université de Strasbourg, ICube
Samira EL YACOUBI	Professeur, Université de Perpignan, IMAGES Espace-Dev

---

JURY :	
Youssoufi TOURE (Président)	Professeur, Université d'Orléans, PRISME
Mustapha OULADSINE	Professeur, Aix-Marseille Université, LIS
Gabriela Iuliana BARA	Maître de conférences, Université de Strasbourg, ICube
Samira EL YACOUBI	Professeur, Université de Perpignan, IMAGES Espace-Dev
Nicolas LANGLOIS	Directeur de la Formation par la Recherche, ESIGELEC
Vincent IDASIAK	Maître de conférences, INSA Centre Val de Loire, PRISME
Frédéric KRATZ	Professeur, INSA Centre Val de Loire, PRISME
Yunhui HOU	Maître de conférences, INSA Centre Val de Loire, PRISME

To my beloved parents

To my dear brother

To my family

Acknowledgements

The work presented in this PhD thesis was supported by the China Scholarship Council (CSC), and has been carried out within Laboratory PRISME (Pluridisciplinaire de Recherche en Ingénierie des Systèmes, Mécanique et Énergétique) at INSA Centre Val de Loire.

There are many people whom I would like to thank for their contributions and support, both directly and indirectly, to this PhD thesis. First and foremost, I wish to thank all my committee members who were more than generous with their expertise and precious time. A special thanks to Mr. Youssoufi TOURE for accepting being the committee chairman in spite of the pandemic. My gratitude extends to Mrs Gabriela Iuliana BARA and Mrs Samira EL YACOUBI for their kind acceptances to review my work. Thanks to Mr. Nicolas LANGLOIS and Mr. Mustapha OULADSINE to be the committee members.

I owe my deepest gratitude to my supervisor Mr. Frédéric KRATZ for his invaluable advice, continuous support, and tremendous patience during my PhD study. His immense knowledge and plentiful experience have encouraged me in all the time of my academic research and daily life in France. I would never forget the trust and motivation he placed in me, especially during those self-doubt moments of mine. Without his guidance and persistent help, this thesis would not have been possible. He is my research mentor and a better advisor for my doctoral study beyond the imagination. Those talks and laughs during coffee breaks with him have also enriched my daily life in France. Apart from my supervisor, I won't forget to express my appreciation to Mr. Vincent IDASIAK and Mrs. Yunhui HOU, for being my co-supervisors and for giving me their full support during the course of this thesis.

Many thanks to my fellow lab mates (both past and present): Rudy, Julien, Bassem, Dian, Lestari, Yanqiao, Ruipeng, Lifei etc. I would always remember those fun time we spent together as well as those discussions that gave me the courage to complete tasks before deadlines. Special thanks also goes to our "Squad Châteauroux" Pascal and David.

I would like to thank Mrs. Laura GUILLET and Mr. Antoine FERREIRA, who always supported me when I was representative of the MIPTIS PhD students. I am also grateful to acknowledge Mr. Driss BOUTAT for providing me an opportunity to apply the position ATER, which is very meaningful for my future career as a lecture and researcher.

My most sincere appreciation must go to my parents and my little brother Chen-guang. They've given me so much support and encouragement to accomplish my personal goals without any obstacle on the way. I consider myself nothing without them. This thesis is also dedicated to the memory of my beloved grandparents.

Bourges, January 2021

Tingting ZHANG

Abstract

Observer-based estimation provides the basis of implementing many important engineering applications over past decades, especially fault diagnosis of different fields. As the real physical systems become more and more complex, the requirements of fault diagnosis are therefore much more important since they are crucial means to maintain the safety and reliability of system. The corresponding growing demand of nonlinear observer design have therefore gained increasing consideration as well.

The aim of this thesis is to design a nonlinear observer as part of a diagnostic tool for continuous-time nonlinear systems with discrete-time measurements. We begin with the study of observability notions concerning the considered nonlinear systems, following by the presents of three typical optimization-based nonlinear observers and observer-based diagnostic methods. Inspired by the existing approaches, a finite memory observer is then designed for a class of nonlinear systems in the presence of both process and measurement noises, where a one-step prediction algorithm incorporated with an iterative-update scheme is performed to solve the integral problem caused by system nonlinearity, and an analysis of the unbiased estimation property has been proved in both deterministic and stochastic case. Residuals are employed to implement fault detection cooperated with the CUSUM algorithm, while a bank of observers are used to realize fault isolation for different sensor and actuator faults of a considered nonlinear robotic systems. In the second part, a nonlinear observer based on augmented model is then designed to simultaneously estimate both system states and unknown inputs. The robustness with respect to the diverse noises is studied, as well as the study of the minimum amplitude of fault for detection purpose. The EWMA algorithm was also introduced and analyzed for its performance in fault diagnosis. Moreover, fault detection and identification of multiple simultaneous sensor and actuator faults are also performed thanks to the actuator fault estimation and compensation by the proposed unknown input observer. In the last part of this thesis, a finite memory observer is then designed for the nonlinear time-varying systems on the basis of the fundamental synthesis and analyses for linear time-varying systems first, where the detailed proofs and illustration are studied as well to show the performance of the proposed observer in time-varying case.

Keywords: Observer design; Nonlinear dynamical systems; Fault diagnosis; Unknown input; Time-varying; Finite memory observer.

Contents

List of figures

List of tables

Acronyms

BLUE Best Linear Unbiased Estimator

CD Continuous-Discrete

CL the Center Line

CRLB Cramér-Rao Lower Bound

CT Continuous Time

CUSUM Cumulative Sum

DT Discrete Time

EKF Extended Kalman Filter

EWMA Exponentially Weighted Moving Average

FDI Fault Detection and Isolation

FMO Finite Memory Observer

KF Kalman Filter

LTI Linear Time-Invariant

LTV Linear Time-Varying

MC Monte Carlo

MHO Moving Horizon Observer

MSF Multiple Simultaneous Faults

SF Single Fault

NLO Nonlinear Observer

NLTV Nonlinear Time-Varying

ODE Ordinary Differential Equation

RE Riccati Equation

RMSE Root Mean Square Error

SD Standard Derivation

LCL the Lower Control Limit

UCL the Upper Control Limit

UI Unknown Input

UIO Unknown Input Observer

Chapter 1

General Introduction

1.1 Context

Most geometric control design methods for nonlinear systems assume that all state variables are available for feedback in real time [Rajamani 2017]. Unfortunately, the entire state is usually too expensive or impossible to measure, and certain form of estimation is necessary. A common way to solve this problem is to set several sensors in the real physical system and design an algorithm, so-called observer, whose role is to perform a reliable estimate of the whole system state through the information provided by the sensors. It is worth to mention that such an algorithm can exist only if the measurements from the sensors contain enough amount of information to uniquely determine the system states, which is what we[1] said "the system is observable". Observer is commonly seen as a "soft sensor".

Meanwhile, it can be noticed that observer-based estimation provides the basis of implementing many important engineering applications over past decades, especially fault diagnosis of different fields. As the real physical systems become more and more complex, more and more system components are involved. The requirements of fault diagnosis are therefore much more important since they are crucial means to maintain system safety and reliability, namely to ensure that the system is well functioning. Under such circumstances, the corresponding growing demand of nonlinear observer design have gained increasing consideration as well. However, unlike linear time-invariant systems, the design of a stable observer for nonlinear systems still suffers from a significant lack of general systematic method despite the existing developed techniques, including Luenberger-like nonlinear observer [Ciccarella et al. 1993, Rajamani 1998], linear matrix inequalities (LMI) [Zemouche and Boutayeb 2013], high-gain observer [Ahrens and Khalil 2009, Sanfelice 2011, Prasov and Khalil 2013].

[1] In this thesis, the word *we* is often used to refer to my colleagues and myself. Sometimes, *we* also indicates that the control and estimation community. The distinction should be clear from the context. However, we encourage the reader not to read too much into my use of the word *we*, it is more a matter of personal preference and style rather than a claim to authority.

1.2 Motivations and Objective

The above context reveals the needs of observer design techniques as well as observer-based fault diagnosis tool for nonlinear dynamical systems. This motivates me to look for some contributions to this subject. Meanwhile, when I started my thesis, some preliminary results about finite memory observer design had already been obtained in the case of time-invariant linear systems, where the nonlinear and time-varying cases remained to be developed. It then brought the beginning of my work in this thesis.

In the literature or textbooks of control theory, the general continuous-time dynamical models for nonlinear systems is under the form

$$\dot{x}(t) = f(x(t), u(u))$$
$$y(t) = h(x(t), u(t))$$

where $x(t)$ is the state, $u(t)$ is the control input and $y(t)$ is the measurement at time instant t. However, it may be worth noting that: *If either the state equation or the output equation has nonlinear terms, then the system is called a nonlinear system.* This means that the measurement equation $h(\cdot)$ of a nonlinear system does not have to be always nonlinear.

As the dynamics of most engineering systems are naturally continuous, e.g., trajectories of vehicles and flow of electric current, it is therefore more convenient and accurate to model the physical processes in continuous time with nonlinear differential equations. However, observations or measurements are usually taken at discrete time instants using digital sensors, which are massively used in today's "digital era". For this reason, the observer designed in this thesis are investigated based on a discrete-time measurement model.

Note that the purpose of the observer design in this work is to support the fault diagnosis for practical systems, the considered nonlinear systems should be as close as possible to the practical one, in which the disturbance and uncertainty is inevitable. The measurement noise, system uncertainties including process noise and modeling uncertainties are therefore taken into consideration in this thesis.

In general, most practical systems can be described by time-invariant model, however, there are some systems that still cannot be modeled by assuming that they are time invariant, such as aircraft [Cook 2013] and the human vocal tract [Strube 1982]. In the meantime, it should be noted that the linearization of a *time-invariant* nonlinear system also (when the nominal solution is not a constant) gives rise to *time-varying* systems, and this is actually one of the chief ways time-varying systems are encountered in system analysis [Kailath 1980]. This is why we also devote part of our efforts to study time-varying systems (linear case and nonlinear case). The overall scheme is shown in Figure 1.1.

Based on the context introduced in section 1.1 and the above presented motivations, our objective in this thesis is to design a nonlinear observer for a class of continuous-time nonlinear systems with discrete-time measurements in the presence of measurement noise and process noise in order to perform fault diagnosis.

1.3 Outline of Manuscript

This manuscript is organized as follows:

Chapter 1 The thesis begins with this chapter by a brief introduction, which presents the context of this work, the problem statements and the organization of the manuscript.

Chapter 2 A review of the relevant definitions and notations of observability is firstly recalled in this chapter. Then there follows three typical optimization-based moving horizon nonlinear observer design techniques. Observer-based fault diagnosis (fault detection and isolation) is performed at the end of this chapter as well.

Chapter 3 This chapter is devoted to develop a continuous-discrete finite memory observer for a class of nonlinear systems under the presence of both process noise and measurement noise. The properties of estimation performance have been theoretically proved and practically validated by simulations. For the diagnosis purpose, the designed nonlinear observer is used to realize fault detection and isolation of different sensor and actuator faults of a nonlinear robotic arm system.

Chapter 4 Based on chapter 3, a nonlinear observer with unknown input is proposed in this chapter by an augmented model. It is then applied to an actuator fault detection and estimation, where the actuator fault is modeled as unknown input. Moreover, multiple simultaneous sensor and actuator faults are successfully detected and isolated thanks to the unknown input estimation.

Chapter 5 A time-varying observer is designed for both linear and nonlinear time-varying systems in this chapter. The detailed illustration and proofs of the proposed observer are firstly provided for linear case, then further extended to nonlinear case.

Chapter 6 Conclusions and perspectives are summarized in this final chapter.

A Note on Symbols: In this thesis, we may sometimes use the same alphabet letter, Greek or Romain symbols representing different variables in different chapters. The specific meaning needs to be inferred from the context.

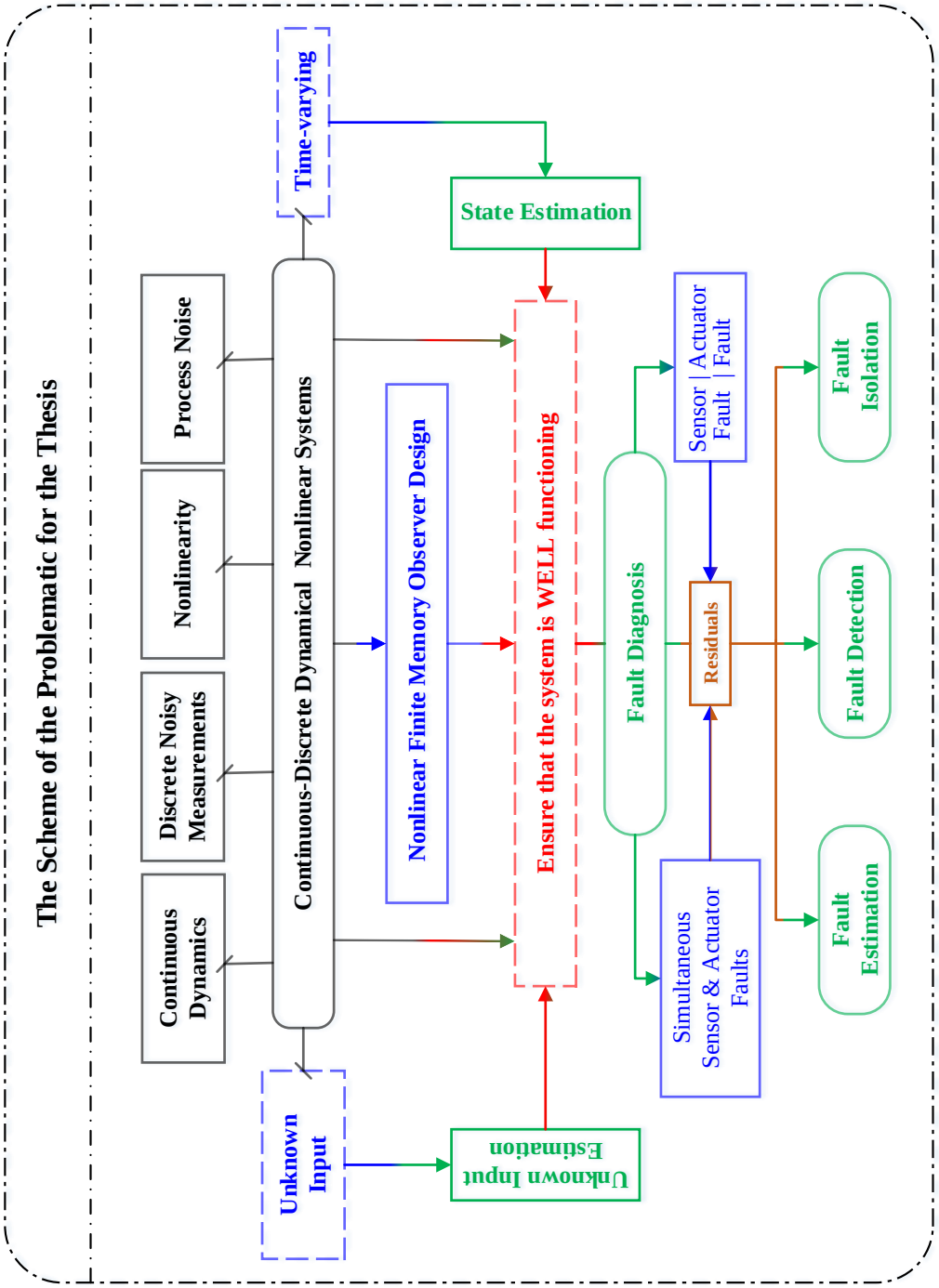

Figure 1.1: The Scheme of the problematic for the thesis

Chapter 2

On Some Nonlinear Observers (NLOs) and Fault Diagnosis

"If I have seen further, it is by standing on the shoulders of Giants."
- Isaac Newton, 1675

Contents of chapter

Résumé en français :

Suite aux motivations et contextes introduits dans le chapitre précédent, nous allons présenter dans ce chapitre quelques observateurs non linéaires et méthodes de diagnostic de défauts basées sur observateurs. Comme nous l'avons mentionné précédemment, la synthèse d'un observateur stable pour les systèmes non linéaires est un défi très important depuis des décennies, et ce défi a été abordé dans la littérature grâce au développement de diverses techniques de synthèse dans le cadre non linéaire. Il convient de noter que notre objectif dans ce chapitre n'est pas de fournir un aperçu exhaustif des observateurs non linéaires, mais plutôt de situer notre contribution et d'introduire une synthèse basée sur l'optimisation, en particulier des techniques à horizon glissant. En plus, quelques méthodes de diagnostic à base d'observateur, des définitions/concepts de base mais importants et des étapes de diagnostic, qui sont nécessaires dans le reste de cette thèse, seront également établis à la fin de ce chapitre.

2.1 Introduction

Based on the motivations and backgrounds introduced in the previous chapter, we are going to review in this chapter some nonlinear observers and observer-based fault diagnostic methods. As we mentioned before, the design of a stable observer for nonlinear systems has been a significant challenge over the past decades, and this challenge has been addressed in the literature through the development of various observer design techniques specific to nonlinear systems. Our intension in this chapter is not to provide an exhaustive overview on nonlinear observer design, but rather to situate our contribution and introduce some optimization-based methods, specifically moving horizon techniques. Moreover, some observer-based diagnostic methods, basic but important definitions/concepts and diagnostic steps, which are needed in the rest of this thesis, will also be established at the end of this chapter.

2.2 Observability of Dynamical Systems

Consider the following general nonlinear system:

$$\begin{aligned} \dot{x}(t) &= f(x,u,t) \\ y(t) &= h(x) \end{aligned} \tag{2.1}$$

with system state noted as $x \triangleq [x_1, \cdots, x_n]^{\mathrm{T}} \in M$, where M is a smooth manifold of $\mathbb{R}^n$; $u \triangleq [u_1, \cdots, u_m]^{\mathrm{T}} \in U \subset \mathbb{R}^m$ represents input while $y \triangleq [y_1, \cdots, y_p]^{\mathrm{T}} \in Y \subset \mathbb{R}^p$ is output. The

two mappings $f \triangleq [f_1, \cdots, f_n]^{\mathrm{T}}$ (with $f : M \times U \to M$) and $h \triangleq [h_1, \cdots, h_p]^{\mathrm{T}}$ (with $h : M \to Y$) are the vectorfields defined on M. Denote $x(t, x_0, u)$ as the state solution of system (2.1) at instant t due to the initial state $x_0 = x(t_0)$ and the input u over $[t_0, t]$, and the corresponding output is denoted as $y(t, x_0, u)$.

2.2.1 Observability problem and definitions

In control theory, *observability* [Canuto et al. 2018] concerns the problem of how to estimate the state vector $x(t)$ from incomplete and possibly inaccurate observations (measurements), collected over a finite time $t_f - t_0 < \infty$. The observations on which to rely are the input and output temporal profiles $u(t)$ and $y(t)$ with $t \in [t_0, t_f]$. The following problem is generally considered:

Observability problem: Given t_0, find a final time $t_f > t_0$, such that x_0 can be uniquely determined from input $u(t)$ and output $y(t)$ with $t \in [t_0, t_f]$.

As stated in Nijmeijer and Schaft [2016] and Hermann and Krener [1977], the observability of systems (2.1) is defined from the *indistinguishability* concept, which is:

Definition 2.1 (Indistinguishable)**.** *For system (2.1), two initial states $x_0^1 \in M$ and $x_0^2 \in M$ are said to be indistinguishable if for any admissible system input $u(t)$ (for all $t > 0$), the corresponding outputs $y(t, x_0^1, u)$ and $y(t, x_0^2, u)$ are equal.*

According to **Definition** 2.1, the observability definition is then given as:

Definition 2.2 (Observable)**.** *For different initial states of system (2.1), if there is no indistinguishable pair $\{x_0^1, x_0^2\}$, then system (2.1) is said to be observable at x_0. Moreover, if the system is observable at every $x \in M$, then we say that system (2.1) is observable.*

Note that the observability defined above is a global concept, which means globally observable. Since our aim afterward is to focus on the rank condition study, the observability in this case will inherently be a local condition for nonlinear systems, which leads to the following definitions :

Definition 2.3 (V-Indistinguishable)**.** *Given two initial states $x_0^1 \in M$ and $x_0^2 \in M$, let V be a subset of M containing x_0^1 as well as x_0^2, we say x_0^1 is V-indistinguishable from x_0^2 if for every admissible input $u(t)$ (all $t > 0$) whose trajectories $x(t, x_0^1, u)$ and $x(t, x_0^2, u)$ both remain in V, the corresponding outputs $y(t, x_0^1, u)$ and $y(t, x_0^2, u)$ are the same.*

Definition 2.4 (Locally Observable)**.** *The system (2.1) is called locally observable at x_0 if there exists a neighborhood W around x_0 such that for every neighborhood $V \subset W$ of x_0, $y(t, x_0^1, u) = y(t, x_0^2, u)$ implies $x_0^1 = x_0^2$. If the system (2.1) is locally observable at each x_0, then we call it locally observable.*

Remark 2.1 (Detectability)**.** *System* (2.1) *is said to be detectable if all the unobservable states are stable.*

Notice that another concept, *stability (stable)*, is mentioned in **Remark** 2.1. It will be analyzed later according to the specific study case, which means it will not be detailed here. Please see Nijmeijer and Schaft [2016], Hermann and Krener [1977], Fossard and Normand-Cyrot [1995] and the references therein for more details if needed. The same strategy was also used for the concept of *controllability (controllable)*, which is a dual concept of observability. Roughly speaking, the concept of controllability denotes the ability to move a system around in its entire configuration space using only certain admissible manipulations. The exact definition may varies slightly within the framework or the type of models applied.

So far, we have presented the general and fundamental concepts of observability. As we known, observability indicates whether or not we can uniquely determine the system state $x(t)$ from the input u and measurements $y = h(x)$, which can be directly measured. As a matter of fact, the derivatives of output $y = h(x)$ also contain the information of system state $x(t)$. This fact leads us to the *Lie derivatives*-based "rank condition" study for observability in next subsection.

2.2.2 Observability rank condition

Considering system (2.1), let us assume that input $u = u_c$ is constant. Firstly we define

Definition 2.5 (Observation Space)**.** *The observation space O for system* (2.1) *is defined as the linear vectorial subspace (over $\mathbb{R}$) of functions on M, including output function $h \in \mathbb{R}^p$, and all its repeated Lie derivatives $\{\mathscr{L}^1_{f_u} h, \mathscr{L}^2_{f_u} h, \cdots, \mathscr{L}^k_{f_u} h\}$ with respect to vectorfields $f_u = f(x,u)$ with $u = u_c$ being fixed.*

According to the definition of Lie derivative, it is easy to see that $h = \mathscr{L}^0_{f_u} h$, then we can write the observation space $O(x,u_c)$ as follows:

$$O(x,u_c) := \begin{pmatrix} \mathscr{L}^0_{f_u} h \\ \mathscr{L}^1_{f_u} h \\ \vdots \\ \mathscr{L}^k_{f_u} h \end{pmatrix} = \begin{pmatrix} y \\ \dot{y} \\ \vdots \\ y^{(k)} \end{pmatrix} \tag{2.2}$$

where $y^{(k)}$ represents the k-th time derivative of y. Note $\mathrm{d}O(x,u_c)|_x$ as the differential space of $O(x,u_c)$ and $\mathrm{d}O(x,u_c)|_{x=x_0}$ as the differential space evaluated at x_0. The observability rank condition is thus denoted as:

Definition 2.6 (Observability Rank Condition)**.** *Suppose $u = u_c$, system (2.1) is said to be locally weakly observable at x_0 if the dimension of $\mathrm{d}O(x_0, u_c)$ equals to n, namely*

$$\dim\{\mathrm{d}O(x,u_c)|_{x=x_0}\} = rank\begin{pmatrix} \mathrm{d}\mathscr{L}^0_{f_u}h \\ \mathrm{d}\mathscr{L}^1_{f_u}h \\ \vdots \\ \mathrm{d}\mathscr{L}^k_{f_u}h \end{pmatrix} = rank\begin{pmatrix} \mathrm{d}y \\ \mathrm{d}\dot{y} \\ \vdots \\ \mathrm{d}y^{(k)} \end{pmatrix} = n \tag{2.3}$$

In addition, the system is said to satisfy the observability rank condition if the above rank condition (2.3) holds for all x_0.

The rank condition states that $\mathrm{d}O(x_0, u_c)$ contains n linearly independent vectors. It may be worth mentioning that $k = n-1$ when the dynamical system is *linear* thanks to Cayley–Hamilton theorem, while there does not exist a fixed value k for *nonlinear* dynamical system in general. In fact, if we try to see the rank condition from the linear algebraic point of view, it is easy to understand that it means the *kernel* of $\mathrm{d}O(x_0, u_c)$ is reduced to the zero subspace. That is why both the output h and its Lie derivatives $\mathscr{L}^i_{f_u}h$ $(i = 1, 2, \cdots, n-1)$ in the direction of f_u will change as the state x change, this is exactly what we called "observable".

Remark 2.2. *The following remarks are worth mentioning concerning the observability rank condition in **Definition** 2.6 :*

1. *It is only a "local" condition for nonlinear systems.*
2. *Unlike the linear case, it is only a necessary but "non" sufficient condition to build an observer for a nonlinear system. It may need to take into account the input properties in some cases.*

Assumption 2.1 (Universal Inputs Assumption)**.** *It can be seen that the control input $u = u_c$, taken as a constant during the entire illustrations above and there is no doubt that input u will affect the observability of nonlinear system (2.1). However, since the nonlinear systems considered in this thesis are assumed in the case where control input u are "universal inputs", the influence of input u on observability will no longer be detailed here. Please refer to Hermann and Krener [1977] for a synthesis of this problem.*

Up to nowadays, there is still no complete theory that allows to design an observer for general observable systems. **Assumption** 2.1 brings us to an interesting class of nonlinear systems, which are observable in the following sens [Hammouri and Farza 2003]:

Definition 2.7 (Uniformly Observable)**.** *If the observability of system (2.1) does NOT depend on the input control $u(t)$, i.e. all the inputs are universal, then system (2.1) is said to be*

uniformly observable. If for any $t > 0$, input u is universal on $[0,t]$, then system (2.1) is uniformly locally observable.

So far, the aforementioned part is the general rank condition of observability for general nonlinear system (2.1). In what follows, we will spend a little bit more space in this section to show the counterpart of observability rank condition in the cases of linear time-invariant (LTI) systems and linear time-varying (LTV) systems, which have been known as two typical linear systems.

Consider the following LTV systems with $x \in \mathbb{R}^n$, $u \in \mathbb{R}^m$ and $y \in \mathbb{R}^p$:

$$\text{LTV systems:} \begin{cases} \dot{x}(t) = A(t)x(t) + B(t)u(t) \\ y(t) = C(t)x(t) \end{cases} \tag{2.4}$$

Definition 2.8 (Observability Gramian)**.** *System (2.4) is said to be observable at time t_0 if and only if there exists a finite $t_f > t_0$ such that $\mathbb{O}_{ob}(t_0,t_f) \in \mathbb{R}^{n\times n}$, defined by*

$$\mathbb{O}_{ob}(t_0,t_f) := \int_{t_0}^{t_f} \Phi^T(\theta,t_0)C^T(\theta)C(\theta)\Phi(\theta,t_0)\,\mathrm{d}\theta \tag{2.5}$$

*is nonsingular. Here, $\Phi(\theta,t_0) \in \mathbb{R}^{n\times n}$ is so-called **state transition matrix** from t_0 to θ with $\theta \in [t_0,t_f]$, which satisfies the following differential equation:*

$$\begin{cases} \dfrac{\mathrm{d}\Phi(\theta,t_0)}{\mathrm{d}\theta} = A(\theta)\Phi(\theta,t_0) \\ \Phi(t_0,t_0) = I_n \qquad I_n \text{ is identity matrix of size } n \end{cases} \tag{2.6}$$

Remark 2.3. *Various methods of calculating state transition matrix $\Phi(\cdot,\cdot)$ can be found in the literatures, see Kailath [1980] and Chen [1999] for example. It may be worth mentioning here the properties of state transition matrix $\Phi(\cdot,\cdot)$, which includes*

- $\Phi^{-1}(t_2,t_1) = \Phi(t_1,t_2)$ *for any* $t_1,t_2 \in [t_0,t_f]$;
- $\Phi(t_1,t_3)\Phi(t_3,t_2) = \Phi(t_1,t_2)$ *for any* $t_1,t_2,t_3 \in [t_0,t_f]$;
- $\Phi(t,t) = I_n$ *holds for all* $t \in [t_0,t_f]$;
- $\Phi(\cdot,\cdot)$ *is never singular.*

For LTV systems (2.4), **Definition** 2.8 tells us that it is impossible to distinguish the initial state x_0^1 from x_0^2 if $x_0^1 - x_0^2$ lies in the kernel of $\mathbb{O}_{ob}(t_0,t_f)$. Also, it is easy to see that the observability gramian matrix $\mathbb{O}_{ob}(t_0,t_f)$ has the following properties:

- $\mathbb{O}_{ob}(t_0,t_f)$ is symmetric;
- For all $t_f > t_0$, $\mathbb{O}_{ob}(t_0,t_f)$ is positive semidefinite;

Suppose the matrices $A(\cdot)$ and $C(\cdot)$ in (2.4) have real-analytic entries, then the observability rank condition in 2.6 is equivalent as follows

Definition 2.9 (Observability Rank Condition for LTV Systems [Sontag 1998])**.** *System* (2.4) *is said to be observable on* $[t_0,t_f]$ *if there exists an arbitrary* $t \in [t_0,t_f]$*, so that*

$$\dim\{\mathrm{d}O\} = rank \begin{pmatrix} \mathbb{C}_0(t) \\ \mathbb{C}_1(t) \\ \vdots \\ \mathbb{C}_k(t) \end{pmatrix} = n \qquad for\ some\ k \tag{2.7}$$

with

$$\begin{cases} \mathbb{C}_0(t) \coloneqq C(0) & i = 0 \\ \mathbb{C}_{i+1}(t) \coloneqq \mathbb{C}_i(t)A(t) + \dfrac{\mathrm{d}}{\mathrm{d}t}\mathbb{C}_i(t) & i \geq 1 \end{cases}$$

Now consider that system (2.4) has the constant parameters A, B and C, namely it becomes the LTI systems

$$\text{LTI systems: } \begin{cases} \dot{x}(t) = Ax(t) + Bu(t) \\ y(t) = Cx(t) \end{cases} \tag{2.8}$$

Based upon the observability rank condition above for LTV systems, the equivalent studies for LTI systems (2.8) are easy to obtain as:

Definition 2.10 (Observability Gramian for LTI)**.** *System* (2.8) *is said to be observable if and only if the following* $n \times n$ *matrix*

$$\mathbb{O}_{ob}(t_0,t) \coloneqq \int_{t_0}^{t} e^{A^T(\theta - t_0)} C^T C e^{A(\theta - t_0)}\, \mathrm{d}\theta \tag{2.9}$$

is nonsingular. It is worth noting that the term $e^{A(\theta - t_0)}$ *in* (2.9) *is the state transition matrix* $\Phi(\theta,t_0)$ *from* t_0 *to* θ *in the case of LTI systems.*

Definition 2.11 (Observability Rank Condition for LTI Systems)**.** *System* (2.8) *is said to be observable if*

$$\dim\{\mathrm{d}O\} = rank \begin{pmatrix} C \\ CA \\ \vdots \\ CA^{n-1} \end{pmatrix} = n \tag{2.10}$$

Note that there is no state x involved in the observability rank condition (2.7) and (2.10) for LTV and LTI systems. It means that unlike the nonlinear case, the observability rank condition for linear system is *global*, which is well-known as the "Kalman rank condition" [Kalman 1963].

2.3 Some Optimization-based Nonlinear Observers

Among all the observer design methods for nonlinear systems, the optimization-based moving horizon technique is the one on which we are going to focus in this section. More specifically, this kind of method turns the state estimation problem into an optimization problem, which generally aims at minimizing the difference between real measurement and the predicted one obtained by using some suitable algorithms on a predetermined moving time horizon. Newton's method and least square method (Levenberg-Marquardt algorithm) are the two main optimization approaches for the NLOs introduced in this section. For the sake of brevity, we have included only some of the many techniques and the references listed in this part are therefore by no means exhaustive.

2.3.1 Moving horizon observers (MHOs)

The name of moving horizon observers (MHOs) was first used by H. Michalska and D. Q. Mayne in the early 1990s [Mayne and Michalska 1992, Michalska and Mayne 1993], which deals with the continuous-time nonlinear systems (2.1) recalled here as:

$$\dot{x}(t) = f(x,u) \tag{2.11a}$$
$$y(t) = h(x) \tag{2.11b}$$

where the uniform observability assumption in **Definition** 2.7 is required and the functions f and h are assumed locally Lipschitz continuous. Then an on-line approximation of a cost function J is defined under the form of Euclidean norm, which described the difference

between the real system output and estimated one over the interval $[t_1, t_2]$ as:

$$J(w;t_1,t_2) \triangleq \int_{t_1}^{t_2} \|h(X(s;w,t_1)) - y(s)\|^2 \, \mathrm{d}s \tag{2.12}$$

here $y(\cdot)$ is the real system output with the true (but unknown) initial condition x_0 at initial time instant t_0. Let $X(\cdot;w,t_1)$ represent the solution of (2.11a) passing through state w at time instant t_1, so it is obvious that $x(t) = X(t,x_0,t_0)$, i.e. $y(\cdot) = h(x(\cdot)) = h(X(\cdot;x_0,t_0))$. The minimization strategy for the cost function (2.12) is well defined using a gradient-based descent approach on the interval $[t-T,t]$ where there always exists a better estimation $w(t)$ for state $x(t)$ of each interval in the case of no measurement noise and no model discrepancy [Michalska and Mayne 1995].

It should be mentioned that the above optimization problem has to be solved at each sampling time instant, this may present some serious drawbacks in the case that one may not be able to control the required time to satisfy a given estimation accuracy. However, this kind of observer design idea establishes a cornerstone for the numerous contributions on continuous-time nonlinear observer synthesis, such as approaches based Newton's method [Moraal and Grizzle 1995, Zimmer 1993a; 1994], which we will get back to detail in next subsection. Moreover, the improved and developed MHOs were studied and revisited by Alamir, which the developed ideas are closely connected to those when the real time implementation of model predictive control is addressed, see Alamir [1999] and Alamir [2007] for more information.

At the end of this part, we would like to share our opinion on the name "moving horizon observer (MHO)": Michalska and Mayne indeed used MHO for their proposed observer, however this name should not be only dedicated to this single method. We believe that all the observers synthesis approaches based on a moving horizon technique can be called MHO. MHO speaks for a class of observers, for instance, finite memory observer is also a kind of MHO, so are the observers introduced in next section.

2.3.2 Nonlinear observers based on Newton's method

Newton's method or in some cases a quasi-Newton method was first introduced for the observer design to discrete-time systems by Grizzle and Moraal in Grizzle and Moraal [1990] and then improved in Moraal [1994] and Moraal and Grizzle [1995]. Meanwhile, Zimmer has also proposed the nonlinear observer design methods for continuous-time systems. In article Zimmer [1993a], the gradient descent method is applied to deal with the problem of minimizing a cost function (a large consumption of computation time). In Zimmer [1993b] and Zimmer [1994], Newton's method is taken to minimize the cost function by using

curvature information (i.e. the second derivative) to take a more direct path than gradient descent. Let's take Newton's method in Zimmer [1994] as an example to explain it in detail.

The considered nonlinear system is described by:

$$\begin{cases} \dot{x} = f(x,u) \\ y = g(x) \end{cases} \tag{2.13}$$

where the vectors x, u and the scalar y represent the system state, control input and output (measurement), respectively.

Assumption 2.2. *f and g are twice differentiable on non-empty set $S \subset \mathbb{R}^n$.*

Assumption 2.3. *System (2.13) is locally uniformly observable. As introduced in **Definition 2.7**, "uniformly" means that the control input u is completely accessible.*

Consider a strongly observable (2.13) system, an interval $I_0 := [0,T]$ and the output of the system $y(\cdot)$ on this interval. The goal is to estimate an initial value x^0 for $x^{0,*}$ (real value), such that $y(t;0,x^0) = y(t;0,x^{0,*})$ for all $t \in I_0$.

The cost function $\mathscr{N}$ is defined by:

$$\mathscr{N}(x^0,x^{0,*}) := \frac{1}{2}\int_0^T \left(y(t;0,x^0) - y(t;0,x^{0,*})\right)^2 \mathrm{d}t \tag{2.14}$$

here, x^0 is an estimate of $x^{0,*}$. Since the system (2.13) is observable, so x^0 and $x^{0,*}$ are distinguishable, namely,

$$\mathscr{N}(x^0,x^{0,*}) = 0 \quad \Leftrightarrow \quad x^0 = x^{0,*} \tag{2.15}$$

Take the partial derivative of (2.14) with respect to x^0, we have

$$\begin{aligned} D_1\mathscr{N}(x^0,x^{0,*}) &= \int_0^T \left(y(t;0,x^0) - y(t;0,x^{0,*})\right) \frac{\partial y(t;0,x^0)}{\partial x^0}\,\mathrm{d}t \\ &= \int_0^T \left(y(t;0,x^0) - y(t;0,x^{0,*})\right) \left(\frac{\partial g\left(x(t;0,x^0)\right)}{\partial x}\frac{\partial x(t;0,x^0)}{\partial x^0}\right)^{\mathrm{T}}\,\mathrm{d}t \end{aligned} \tag{2.16}$$

If $\mathscr{N}(x^0,x^{0,*})$ is convex near $x^{0,*}$, the following equivalence is then valid:

$$\mathscr{N}(x^0,x^{0,*}) = 0 \quad \Leftrightarrow \quad D_1\mathscr{N}(x^0,x^{0,*}) = 0 \tag{2.17}$$

The common way to check the convexity of $\mathscr{N}(x^0,x^{0,*})$ near $x^{0,*}$ is to examine whether the Hessian matrix

$$D_1^2\mathscr{N}(x^0,x^{0,*}) := \frac{\partial^2\mathscr{N}(x^0,x^{0,*})}{(\partial x^0)^2} \tag{2.18}$$

is positive-definite at $x^0 = x^{0,*}$. Fortunately, **Lemma** 2.1 below gives a necessary and sufficient condition such that $D_1^2\mathscr{N}(x^0, x^{0,*})$ is a Hilbert matrix and thus positive-definite (see Zimmer [1994] for details).

Lemma 2.1. *Given $x_1 \in S$, the Hessian matrix $D_1^2\mathscr{N}(x^1, x^1)$ is said to be positive define if and only if the following linearized system is observable in $I_0 := [0, T]$*

$$\begin{cases} \dot{z} = \dfrac{\partial f(x(t;0,x_1))}{\partial x} z \\ v = \dfrac{\partial g(x(t;0,x_1))}{\partial x} z \end{cases} \tag{2.19}$$

Then, Newton's method is applied to approximate $x^{0,*}$. Recall that Newton's method generates a sequence of x^0 using recursion as

$$x^0_{\text{new}} = x^0_{\text{old}} - \left(D_1^2\mathscr{N}(x^0_{\text{old}}, x^{0,*})\right)^{-1} D_1\mathscr{N}(x^0_{\text{old}}, x^{0,*}) \tag{2.20}$$

Note that before applying Newton's method, one can always check whether $D_1^2\mathscr{N}(x^0, x^{0,*})$ is invertible and by Lemma 2 (omitted here) in Zimmer [1994].

The conditions for terminating the iteration are

$$\mathscr{N}(x^0_{\text{new}}, x^{0,*}) < \kappa\mathscr{N}(x^0_{\text{old}}, x^{0,*}) \tag{2.21}$$

Now all the state estimations $x(\cdot)$ over the interval $I_0 := [0, T]$ can be calculated with the initial value x^0_{new} obtained by (2.20) and (2.21) as follows:

$$x(t) := X(t; 0, x^0_{\text{new}}) \qquad t \in I_0 \tag{2.22}$$

here $X(\cdot; 0, x^0)$ represents the solution of system (2.13) by the four-order Runge-Kutta (RK4) method with the initial value x^0.

Notation: Given $T > 0$, for all $k \in \mathbb{N}_0$, define

$$I_k := [t_k, t_k + T] \qquad t_k := kT$$

Without loss of generality, Zimmer's method can be carried out over an arbitrary interval $I_k, k \in \mathbb{N}_0$. Let

$$\eta(x^k, x^{k,*}) = x^k - \left(D_1^2\mathscr{N}(x^k, x^{k,*})\right)^{-1} D_1\mathscr{N}(x^k, x^{k,*}) \tag{2.23}$$

where x^k represents the final estimate of $x^{k,*}$ at time t_k after terminating of iteration. Also

$$x^{k,*} := X(kT;0,x^{0,*})) \qquad k \in \mathbb{N}_0$$

Repeat the above procedure for each interval $I_k, k \in \mathbb{N}_0$, a sequence of x^k is generated recursively by:

$$\begin{aligned} x^k &:= X(kT;(k-1)T,\eta(x^{k-1},x^{k-1,*})) \\ &= X(T;0,\eta(x^{k-1},x^{k-1,*})) \qquad k \in \mathbb{N} \end{aligned} \tag{2.24}$$

These sequences yield

$$\begin{cases} \lim\limits_{k\to\infty} \|x^k - x(t_k;0,x^{0,*})\| = 0 \\ \lim\limits_{k\to\infty} \|\eta(x^k,x^{k,*}) - x(t_k;0,x^{0,*})\| = 0 \end{cases} \tag{2.25}$$

if x^0 and $x^{0,*}$ are close enough.

Finally, the sequence $\{\eta(x^k,x^{k,*})\}_{k\in\mathbb{N}}$ will be completed towards a piecewise differentiable function by:

$$\begin{cases} \mathbb{R}^+ \to \mathbb{R}^n \\ t \mapsto x_{\mathscr{N}}(t) := X(t;kT,\eta(x^k,x^{k,*})) \qquad t \in [kT,(k+1)T) \end{cases} \tag{2.26}$$

The true state $x(\cdot)$ is approximated by (2.26) in the following norm sense:

$$\lim_{t\to\infty} \|x(t) - x(t;0,x^{0,*})\| = 0 \tag{2.27}$$

if x^0 and $x^{0,*}$ are close enough. Figure 2.1 illustrates the idea described above

This method shows a great performance for nonlinear system (2.13) when there is no control inputs. However, with the presence of control input u, the convergence has only been proven for special control input functions [Zimmer 1993b]. Meanwhile, this approach has already been successfully applied to systems with multiple outputs as well in Zimmer [1993c], where the cost function in (2.14) need to be defined in a quadratic form like

$$\mathscr{N}(x^0,x^{0,*}) := \frac{1}{2}\int_0^T \left(y(t;0,x^0) - y(t;0,x^{0,*})\right)^{\mathrm{T}} \left(y(t;0,x^0) - y(t;0,x^{0,*})\right) \mathrm{d}t$$

Note that the Hessian matrix (2.18) of the cost function (2.14) is required in order to perform the Newton step of this method, this may be hard to realize in practical or be

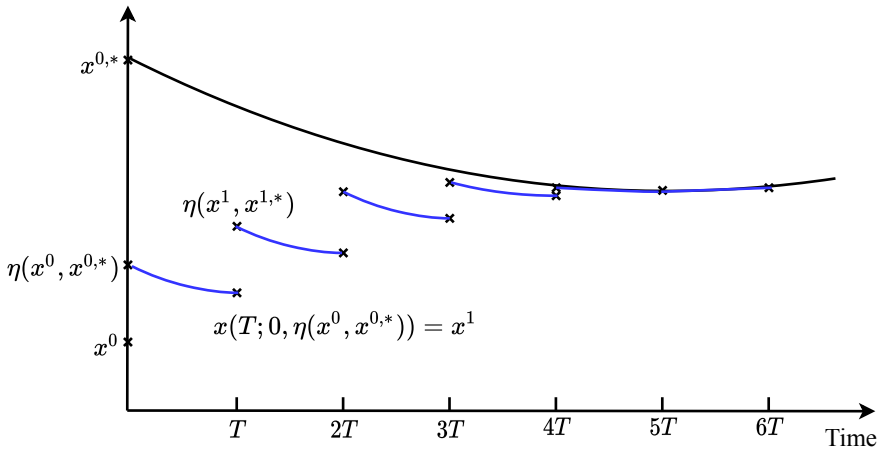

Figure 2.1: The illustration of Zimmer's method [Zimmer 1994]

impossible to perform when the nonlinear functions f and g are not twice differentiable. This method is not in general used even though it shows great theoretical significance.

So far, we've learned that the cost function in gradient descent method is minimized by updating the parameter in the steepest-descent direction which can be computationally expensive if the curvature in different directions is very distinct for the given function. Meanwhile, the (quasi-) Newton's methods remedy this problem but show more complexity due to the calculation of Hessian matrix and performs much worse when the parameters are far from their optimal values. Is there a method that can acts more like a gradient descent method when the parameters are far from their optimal value, and acts more like the (quasi-) Newton's methods when parameters are close to their optimal value? This brings us to the Levenberg-Marquardt algorithm in next subsection.

2.3.3 Nonlinear observers based on Levenberg-Marquardt algorithm

Levenberg-Marquardt (L-M) algorithm was first developed by K. Levenberg [Levenberg 1944] in the early 1940's and then was rediscovered in 1960s by D. Marquardt [Marquardt 1963], which the L-M algorithm adaptively updates the parameter between the gradient descent method and the Gauss-Newton method. Although many variations of L-M algorithm have been published during these years [Kanzow et al. 2004, Pujol 2007, Wilamowski and Yu 2010, Transtrum and Sethna 2012, Bellavia et al. 2018], the observer-related one in Abdelhedi et al. [2016] is what we are going to discussed in this section.

The nonlinear system (2.1) is considered in Abdelhedi et al. [2016], rewritten here

$$\begin{aligned} \dot{x}(t) &= f(x,u) \\ y(t) &= h(x) \end{aligned} \tag{2.28}$$

let us consider L bounded observations collected at regular time interval T_e such that the length of horizon $lh = (L-1)T_e$. Then the optimization problem can be stated as the minimization of the following cost function:

$$J(x) = \frac{1}{2}\sum_{k=1}^{L}(y_{t_k} - \hat{y}_{t_k})^2 \tag{2.29}$$

where y is the measured output and $\hat{y}$ is the estimated one. t_k is the beginning of the horizon so that $t \in [t_k, t_k + lh]$. We know that (2.29) has an optimum at x if the the following condition is verified:

$$\frac{\mathrm{d}J}{\mathrm{d}x} = 0 \tag{2.30}$$

The function $J(x_k)$ in (2.29) may be locally approximated through a second-order Taylor series expansion as

$$J(x_{k+1}) = J(x_k + \mathrm{d}x_k) \approx J(x_k) + \nabla J \cdot \mathrm{d}x_k + \frac{1}{2}\mathrm{d}x_k^{\mathrm{T}} \cdot \mathrm{Hess}(i,j) \cdot \mathrm{d}x_k \tag{2.31}$$

that is

$$\mathrm{d}J(x_k) \approx \nabla J \cdot \mathrm{d}x_k + \frac{1}{2}\mathrm{d}x_k^{\mathrm{T}} \cdot \mathrm{Hess}(i,j) \cdot \mathrm{d}x_k \tag{2.32}$$

with

$$\nabla J = \left.\frac{\partial J}{\partial x}\right|_{x=x_k} = -2\sum_{k=1}^{L}(y_{t_k} - \hat{y}_{t_k})\frac{\partial \hat{y}_{t_k}}{\partial x_k} \tag{2.33a}$$

$$\mathrm{Hess}(i,j) = \frac{\partial^2 J}{\partial x_i \partial x_j} = 2\sum_{k=1}^{L}\left(\frac{\partial \hat{y}_{t_k}(x_i)}{\partial x_j}\right)^2 - 2\sum_{k=1}^{L}(y_{t_k} - \hat{y}_{t_k})\frac{\partial \hat{y}_{t_k}}{\partial x_i \partial x_j} \tag{2.33b}$$

Apply the condition in (2.30) to (2.32), we get

$$\nabla J + \mathrm{Hess}(i,j) \cdot \mathrm{d}x_k = 0 \tag{2.34}$$

then we straightly have the state variation $\mathrm{d}x_k$ as

$$\mathrm{d}x_k = x_{k+1} - x_k = -\mathrm{Hess}(i,j)^{-1}\nabla J \tag{2.35}$$

It is easy to see that the second term of Hessian matrix in (2.33b) can make the Hessian matrix negative. Therefore, the main idea of L-M method is to replace the second term of Hessian matrix by a diagonal matrix, namely

$$x_{k+1} = x_k - [\text{Hess}^*(i,j) + \lambda_k I]^{-1} \nabla J \tag{2.36}$$

with

$$\text{Hess}^*(i,j) = 2\sum_{k=1}^{L} \left(\frac{\partial \hat{y}_{t_k}(x_i)}{\partial x_j} \right)^2 \tag{2.37}$$

represents the Hessian matrix in (2.33b) without the second term. λ_k is called damping parameter or relaxation coefficient, which actually adjusts the eigenvalues of Hessian matrix. When λ_k is a small value, L-M works like Gauss-Newton method while large value of λ_k results in a gradient descent like method. The choice of λ_k in each iteration is simply by multiplying or dividing a certain multiples of the last iteration in Abdelhedi et al. [2016]. For more information about the best choice for the damping parameter, see Transtrum and Sethna [2012].

2.4 Nonlinear Observers with Continuous-Discrete Model

As we know, the dynamics of most engineering systems are naturally in continuous time (CT), such as trajectories of vehicles, flow of electric current etc. It is therefore more convenient and accurate to modeling the physical processes in continuous time by nonlinear ordinary differential equations (ODEs). However, observations or measurements are usually taken by sampling at discrete time (DT) instants since digital sensors are commonly used for engineering systems in practice. For this reason, a significant amount of observer designs has been investigated in the literature based on continuous-discrete (CD) modeling over the past few decades, where the dynamic for systems is expressed based on CT model and the measurement is described through DT modeling.

Early years, Jazwinski [Jazwinski 1970] presented a CD Kalman filter to deal with the filtering problem for CT stochastic nonlinear systems with discrete measurements. Then, Deza et al [Deza et al. 1992] developed the CD high-gain observer with a corrected gain obtained through the integration of CD Riccati equation. Inspired by these earlier works, a large number of papers have been published in recent decades, focusing on CD model based nonlinear observer design subject in both theoretical and practical applied aspects. For instance, a CD observer is designed in Ali et al. [2016] for the Electro-Hydraulic Actuators (EHA) system subject to mechanical and hydraulic disturbances. Ling and Kravaris [Ling

and Kravaris 2019] developed a robust nonlinear CD observer to deal with the multi-rate sampling measurements by building an inter-sample predictor, which has been proved robust with respect to perturbations and inherits all the good properties of the CT implementation as long as the maximum sampling period does not exceed a certain threshold. An efficient linear matrix inequalities (LMIs)-based tool was built in Dinh et al. [2015] to solve the problem of observer synthesis for a class of globally Lipschitz systems in small dimensions. In addition, it is worth mentioning here that there are several research scholars in France whose works have been realized on observer synthesis based on CD model over years. Their relative researches widely include from interval observer design [Mazenc and Dinh 2014], nonlinear observer design [Farza et al. 2014, Mazenc et al. 2015, Farza et al. 2018] to system stabilization [Mazenc and Fridman 2014, Mazenc and Fridman 2016], observer synthesis for systems with delayed inputs or measurements [M'Saad and Farza 2009, Tréangle et al. 2019, Mazenc and Malisoff 2020].

Based upon the aforementioned researches of CD nonlinear observer synthesis and taking into consideration our intention of diagnostic application, there is no doubt that our interests in this thesis will be focused on the CD model as well, more precisely, the mathematical model of the systems considered in our work will be represented by CD model.

2.5 Fault Diagnosis

There are countless literatures and surveys focusing on fault diagnosis [Isermann 1984, Frank 1987; 1990, Frank and Ding 1997, Isermann 2005, Blanke et al. 2006, Ding 2008, Wang et al. 2013, Termeche et al. 2018]. In this section, we intend to introduce some basic but necessary definitions and notations of fault diagnosis, as well as the general diagnostic steps. However, one may immediately realize by examining the literatures that the notations or terminology of this domain is not coherent. The definitions and notations about fault diagnosis given in this thesis are suggested by the IFAC (International Federation of Automatic Control) SAFEPROCESS[1] Technical Committee [Van Schrick 1997, Isermann and Ballé 1997]. Without being exhaustive, the generalized fault detection and isolation (FDI) method based on analytical redundancy will also be briefly presented, together with some observer-based diagnosis approaches at the end of this section.

[1] https://tc.ifac-control.org/6/4/terminology/terminology-in-the-area-of-fault-management

2.5.1 Basic definitions / notations and general diagnostic procedure

According to Isermann and Ballé [1997], the engineering terminology *fault* is defined as "An unauthorized deviation of at least one characteristic property or parameter of the system from the acceptable / usual / standard condition".

As shown in Figure 2.2, one of the most common fault classification is given by the aim of fault tolerant control [Blanke et al. 2006] as

- **Actuator faults:** faults that affect (interrupt or modify) the system control inputs.
- **Sensor faults:** such faults introduce substantial errors to sensor readings.
- **Plant faults:** faults that change the dynamical I/O properties of systems.

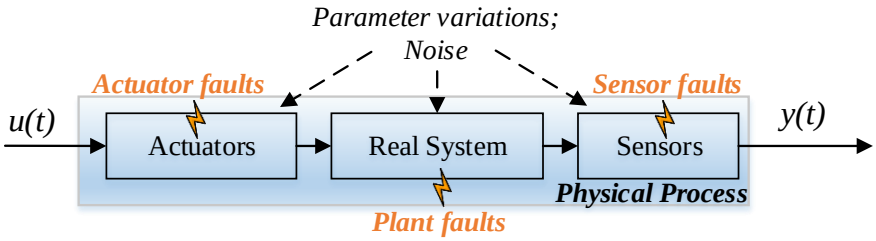

Figure 2.2: Distinctions of different faults types

Note that a fault modifies or changes the performance (for example: operation mode) of the component in an unacceptable way. It is worth knowing that through certain fault-tolerant control, the faulty system may be able to stay operational even with the presence of fault. In the meantime, another notation *failure*, which is easily confused with *fault*, is defined in Isermann and Ballé [1997] as: A permanent interruption of a system's ability to perform a required function under specified operating conditions. Unlike a fault, a failure interprets the incapability in functional level, which means a system or component is not able to achieve its function and then must be shut off. Apparently, a failure is an irrecoverable event. In order to understand the two notations better, it may be useful to recall that one important role of fault tolerant control is to prevent a fault from causing a failure at the system level.

Let us continue to see what the general diagnostic steps are in order to perform fault diagnosis. As Isermann stated in Isermann and Ballé [1997], fault diagnosis consists of determining the type, amplitude, location and occur time of the fault. The diagnostic procedure follows with fault detection, isolation and identification:

- **Fault detection:** determine whether there occurs a fault or not; if yes, determine the time instant of fault occurrence. This step is very important since early fault detection can possibly prevent the system from a catastrophic failure.

- **Fault isolation:** determine in which component the fault is. This step aims to locating the fault, which means to find out the possible fault candidate(s) that can explain the undesired behavior of system. Sometimes there is only one unique fault candidate, unfortunately this case is not always possible. Then the objective of this step need to get a possible fault set.
- **Fault identification and estimation:** identify the fault type and maybe estimate the fault magnitude. This step is also used to see how severe the fault is, then decide whether to perform fault accommodation or to replace the faulty component directly.

Based upon the above general diagnosis procedure, various approaches and researches have been proposed then developed during the last two decades. All these fault diagnosis methods can be broadly categorized into two classes: model-based methods and data driven methods [Wang et al. 2013]. With no doubt, our contribution lies in the first class, more specifically, observer-based FDI approach using analytical redundancy, which is going to be detailed in next subsection.

2.5.2 Generalized fault diagnosis methods using analytical redundancy

As interpreted in Venkatasubramanian et al. [2003], the model-based diagnostic methods can still be classified into two categories: qualitative and quantitative. We currently show no interest to the former category in this thesis. On the contrary, the quantitative one is what we will focus on. Moreover, as most of the quantitative model-based approaches have used, the general input-output state-space model will be investigated in this thesis.

In the domain of automatic control, different FDI methods may use different kinds of dynamical models or might have different assumptions regarding the available measurement information. However, these approaches all follow one common principle: consistency check [Blanke et al. 2006]. The inconsistency between the actual system behavior and the expected nominal behavior might show a fault potential. Therefore, some form of redundancy is required in order to check for consistency. Actually, hardware redundancy and analytical redundancy are two kinds of redundancies that have been usually used in practical. The former one asks for multiple hardware equipments (mostly sensors), which has been applied in mission and safety-critical systems such as digital fly-by-wire flight systems and nuclear reactors [Kratz 1991, Goupil 2011, Hao and Kinnaert 2017]. The analytical redundancy on the other hand utilize a mathematical model of the targeted system in cooperate with certain estimation techniques [Hwang et al. 2010]. The generalized architecture of FDI methods based on analytical redundancy is shown in Figure 2.3, which is inherited from Isermann [1984] and Frank [1990]. Note that there are two major techniques within the framework of

model-based FDI methods: state estimation (parity space approach, observer or filter) and parameter estimation. Eventually, these methods all end up by generating an "indicator", either a residual or the parity. This indicator is exactly the result of the inconsistency check that we have mentioned before.

The path where our contributions will go through is noted in blue in Figure 2.3, the related fault diagnosis procedures is equivalently remarked in green on the right side of Figure 2.3. Observer-based FDI methods will be briefly but accordingly summarized in the next subsection. As for the rest of approaches such as parity space method, parameter estimation and filter, please refer to Chow and Willsky [1984], Isermann [1991], Kinnaert [2003], Almasri et al. [2020] and the references therein.

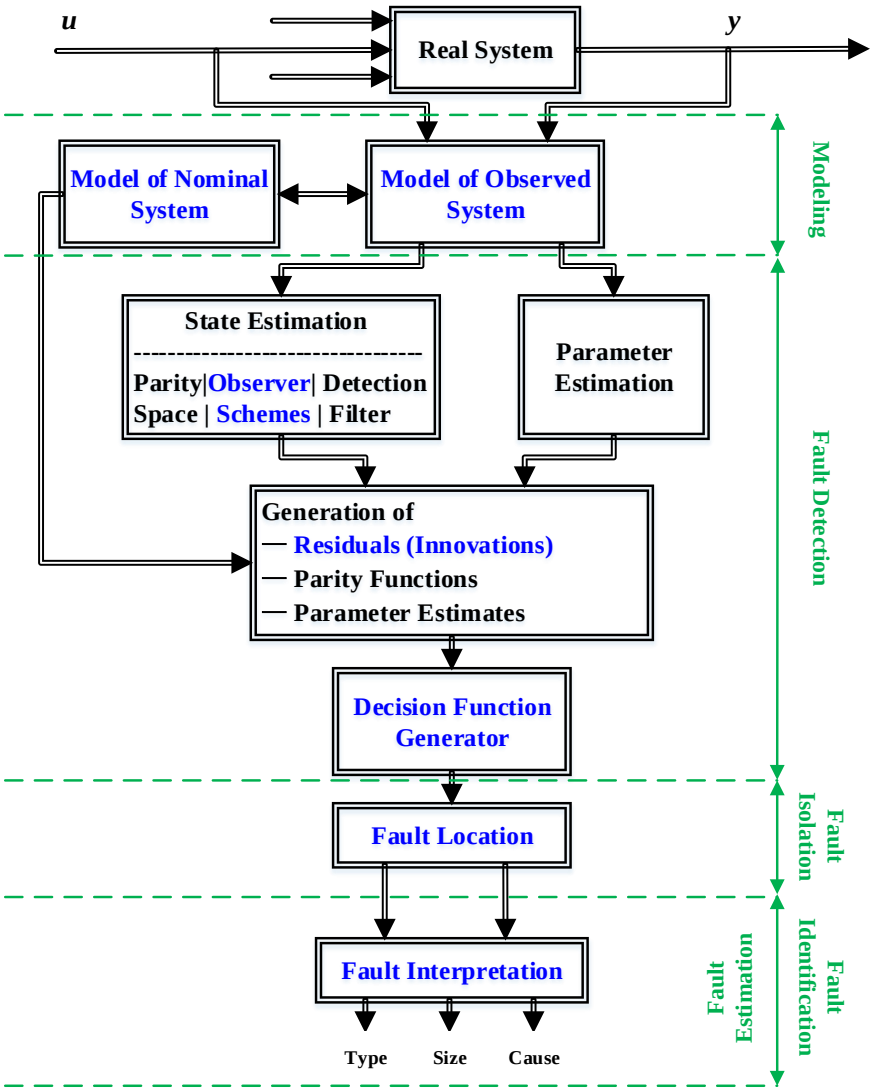

Figure 2.3: Generalized architecture of FDI by analytical redundancy [Isermann 1984]

2.5.3 Observer-based fault diagnosis methods

As model-based FDI methods received considerable attention, observer-based approach is the most extensively used one among model-based fault diagnosis for decades [Chen et al. 1996, Hammouri et al. 1999, Shields 2005, Zhang et al. 2013]. The consistency check indicator in this case is what we usually called *residual*, which represents the difference between estimate measurements and the real ones collected through the output of real system. Observer-based FDI method has been widely used in many fields such as PEM fuel cell [Bougatef et al. 2020], heat-exchanger/reactor system [Han et al. 2019], continuous stirred tank reactor (CSTR) [Li et al. 2018], induction motor [Toumi et al. 2012, El Merraoui et al. 2020] etc. Among all these observer-based applications, there includes unknown-input observer (UIO)-based fault diagnosis, adaptive observer (AO)-based fault diagnosis, sliding-mode observer (SMO)-based fault diagnosis etc [Zhang et al. 2016a].

UIO-based fault diagnosis methods play a significant role since the unknown input (UI) can represent modeling uncertainties, perturbations, faults, etc [Marx et al. 2019], which a physic system may commonly include. Over past decades, UIOs design for *linear* systems has been developed and applied to fault diagnosis by a lot of researchers or scientific group [Hou and Muller 1994, Johnson et al. 2018, Zhang et al. 2016b, Tan et al. 2008]. As for *nonlinear* UIO-based fault diagnosis, Yang et al. presented an approach for actuator FDI by a designed nonlinear UIO with linearized error dynamics [Yang and Saif 1996]. A new development based on decomposition techniques are introduced in Koshkouei et al. [2011], which is constrained by certain conditions. L. Meyer et al. propose in Meyer et al. [2018] an interval UIO by using the derivative of the output vector under some existence assumptions, which also intends to separate the UI from interval error bounds. Meanwhile, Zhang et al. [Zhang et al. 2014] have managed to designed a full-order and reduced-order UIO for one-side Lipschitz system by the Lyapunov-based linear matrix inequality (LMI) method, which the asymptotic convergence is guaranteed. In Koenig [2006], an algebraic method is used to design an observers for nonlinear descriptor systems in presence of UI. As summarized in Alenezi et al. [2019], the existing UIO design methods can be divided into two categories: (1) perform state estimation despite the existence of UI (structural decoupling techniques); (2) estimate both state and UI simultaneously via an augmented observer with some assumptions on the dynamics of UI. In this thesis, our contribution will take a place in the latter category in order to perform actuator fault estimation.

As examined in [Heffes 1966, Toda and Patel 1978], observer-based (all model-based methods) diagnosis method will be affected to divergence due to the accumulation of modeling uncertainties. Furthermore, state estimation based on infinite memory (i.e. all the process history) may result in the insensitivity to recent measurements which might have the clues

of a fault in incipient stage [Graton et al. 2014]. Thus, the corresponding researches like fading filter [Sorenson and Sacks 1971] and finite memory observer are naturally explored. Finite memory observer (FMO) was first proposed by Medvedev [Medvedev and Toivonen 1992] for linear system in the deterministic framework, which indicates that this observer is extremely efficient for state estimation. Afterwards, the robustness and sensitivity of this approach were addressed by Nuninger [Nuninger et al. 1998] and Graton [Graton et al. 2014]. Researchers in Kratz's team have then continued to synthesize this observer in fault diagnosis of linear system [Thuillier et al. 2018] and hybrid system [Kajdan et al. 2006]. All these previous researches of finite memory observer for linear systems reveal that this specific moving horizon technique provides a great potential in state estimation as well as in fault diagnosis. Well, this is how this moving horizon technique has successfully attracted our attention and then became the foundation of our contribution in this thesis.

2.6 Conclusion

In this chapter, after briefly recalling the observation problems of nonlinear systems followed by different observability definitions and observability rank condition, we then passed to present some typical optimization-based observer synthesis for continuous-time nonlinear systems using moving horizon techniques, such as Newton's method based and least square method based. However, it should be noted that this bibliography review is not exhaustive but accordingly introduced. Meanwhile, the researches on nonlinear observer design with continuous-discrete model are being reviewed in order to see which type of model is commonly used for the application-oriented observer synthesis. At the end part of this chapter, the basic but necessary definitions and procedures of fault diagnosis are established together with a brief review of the observer-based fault diagnosis methods.

Through the studies of different types (algorithm-wise or application-wise) of nonlinear observers, we realize that among these existing methods, "half" of them have a theoretical significance but are really hard to apply in practical while the other "half" are ale to be well applicable but show no theoretical significance. Indeed, the nonlinear observer design still has a long way to go and luckily we are going to begin our first step on this road in next chapter. It may be a small step, at least we have already begun.

Chapter 3

Nonlinear Continuous-Discrete Finite Memory Observer (CD-FMO) Design

"If we knew what it was we were doing, it would not be called research, would it?"
- Albert Einstein

Contents of chapter

Résumé en français :

Nous venons de voir au chapitre précédent que l'observateur joue un rôle important dans la réalisation d'un diagnostic performant. L'évolution technologique et numérique permet des communications et des interactions de plus en plus nombreuses entre les différents composants constituant les processus industriels, ou systèmes industriels, qui deviennent ainsi de plus en plus complexes. Il est aujourd'hui très important de pouvoir assurer un fonctionnement efficace à ces processus, c'est-à-dire assurer le diagnostic de défaut. Ce besoin de diagnostic sûr est devenu un problème important pour les processus industriels ainsi que un sujet de recherche à la mode. Inspiré d'approches existantes, nous allons concevoir dans ce chapitre un observateur non linéaire pour une classe de systèmes non linéaires modélisés par un modèle continu-discret (CD) en présence de bruit de processus et de bruit de mesures. L'observateur développé sera construit sur la méthodologie réalisée pour le système linéaire ayant abouti à la conception de l'observateur à mémoire finie (FMO) [Nuninger et al. 1998]. Nous démontrerons les propriétés de l'erreur d'estimation dans le cas déterministe alors que les mêmes études pour le cas stochastique seront réalisées par simulations de Monte Carlo (MC). La stratégie du choix de la longueur de la fenêtre d'observateur sera également donnée en fonction de la variance de l'erreur d'estimation. Concernant l'application, les *résidus* classiques sont générés pour implémenter la détection des défauts par l'algorithme de la somme cumulée (CUSUM), qui permet de détecter efficacement de petites dérives sur la moyenne. Finalement, un banc d'observateur est utilisé pour réaliser la localisation des défauts capteurs et/ou défauts actionneurs pour un bras robotique. Les résultats des simulations montreront que la méthode proposée fournit une détection de défaut assez efficace. La robustesse de cet observateur non linéaire vis-à-vis des bruit de mesure est également étudiée dans ce chapitre.

3.1 Introduction

We can see from the previous chapter that state observer plays an important role in fault diagnosis over the past decades. As the real engineering systems turn into more and more complex, not only the corresponding demand of observer design is growing but also the fault diagnosis for complex nonlinear systems have gained increasing consideration. Inspired by these existing approaches, we aim in this chapter to develop a continuous-discrete finite memory observer (CD-FMO) for a class of nonlinear dynamical systems modeled by ordinary differential equations (ODEs) with discrete measurements. The nonlinear systems under consideration are at least *locally* Lipschitz, which guarantees the existence and uniqueness of solution at each time instant. The proposed nonlinear CD-FMO uses a finite number of

collected measurements to estimate the system state in the presence of measurement noise. Besides, a one-step prediction algorithm incorporated with an iterative-update scheme is performed to solve the integral problem caused by system nonlinearity, and an analysis of the numerical integration approximation error is given. The properties of estimation performance have been further proved in deterministic case and been analyzed by Monte Carlo (MC) simulation in stochastic cases. It's worth noting that the presented method has a finite-time convergence while most nonlinear observers are usually asymptotically convergent. Another advantage is that the proposed CD-FMO has no initial value problem. For the application purpose, residuals are generated to implement fault detection cooperated with Cumulative Sum (CUSUM) algorithm, while a bank of CD-FMOs is adopted to realize fault isolation for different sensor and actuator faults of the considered nonlinear robotic arm. The robustness and effectiveness of the proposed approach are illustrated via the simulation results.

3.2 Nonlinear CD-FMO Design

At first, a description of the nonlinear system is made, then the design of the proposed nonlinear CD-FMO together with an iterative update algorithm for numerically approximating integration due to the nonlinearity of system. In addition, we also give a detailed proof of the finite-time convergence. The criteria of how to choose the window length is also stated in the end of this section.

3.2.1 Problem statement

We consider a class of continuous-discrete nonlinear systems described by the following state-space equations:

$$\dot{x}(t) = Ax(t) + Bu(t) + \Phi(x) + G\omega(t) \tag{3.1a}$$

$$y(k) = Cx(k) + v(k) \tag{3.1b}$$

where $x \in \mathbb{R}^n$, $y \in \mathbb{R}^p$ and $u \in \mathbb{R}^q$ are continuous state vector, discrete measurement vector and continuous input vector, respectively. T_s is the sampling period of measurement (i.e. $\exists k \in \mathbb{N} \mid t = k \times T_s$). $A \in \mathbb{R}^{n\times n}$, $B \in \mathbb{R}^{n\times q}$, $G \in \mathbb{R}^{n\times n}$ and $C \in \mathbb{R}^{p\times n}$ are known matrices. The nonlinearity $\Phi(x)$ is a nonlinear function with respect to state x. $\Phi(x)$ is at least *locally* Lipschitz, i.e.

$$\|\Phi(a) - \Phi(b)\| \leq \kappa \|a - b\| \tag{3.2}$$

where Lipschitz constant $\kappa > 0$. Vectors v and ω represent Gaussian measurement noise and Gaussian process noise, respectively, and v and ω are independent with the following properties:

$$\mathbb{E}[\omega(t)] = 0 \tag{3.3a}$$
$$\mathbb{E}[\omega(t_1)\omega^{\mathrm{T}}(t_2)] = Q \cdot \delta(t_1 - t_2) \tag{3.3b}$$
$$\mathbb{E}[v(k)] = 0 \tag{3.3c}$$
$$\mathbb{E}[v(k_1)v^{\mathrm{T}}(k_2)] = R \cdot \delta_{k_1,k_2} \tag{3.3d}$$

here $\delta(\cdot)$ is *Dirac delta function* and $\delta_{i,j}$ is *Kronecker delta function*. It should be noted that the continuous-discrete systems like (3.1) naturally exist when continuous process are measured via digital sensors. Without loss of generality, we are going to present a nonlinear observer design where the estimation instant is synchronized[1] with the measurements instant since it is exactly what is needed under the background of diagnosis. The proposed CD-FMO will be detailed in next subsection. Before we start, we introduce the following remark first:

Remark 3.1. *The authors in [Kou et al. 1973] have proven that the observability of a nonlinear dynamical system is a necessary condition that there exists a finite-time observer for the system.*

We are able to conclude from this remark that if we can build a finite-time observer for a nonlinear system, then this nonlinear system is observable.

3.2.2 Formulation of CD-FMO

Suppose that at each frozen time instant t, the discrete measurements are collected in the interval $[t-\tau_i, t]$, where $\tau_i = i \times T_s$, and $i = 0, 1, ..., L-1$. Here L is called window length.

Use the square matrix exponential e^{-At} as a factor and integrating (3.1a), we can give the relation between the states in two different time instant t and $t-\tau_i$ as:

$$x(t) = e^{A\tau_i}x(t-\tau_i) + \int_{t-\tau_i}^{t} e^{A(t-\theta)}Bu(\theta)\,\mathrm{d}\theta + \int_{t-\tau_i}^{t} e^{A(t-\theta)}\Phi(x(\theta))\,\mathrm{d}\theta + \int_{t-\tau_i}^{t} e^{A(t-\theta)}G\omega(\theta)\,\mathrm{d}\theta \tag{3.4}$$

[1] The proposed nonlinear CD-FMO also works well for the case that the estimation instant is not synchronized with measurement instant.

Then, pre-multiply (3.4) by the matrix $Ce^{-A\tau_i}$ and taking into account the measurement equation (3.1b) at time instant $t-\tau_i$, we obtain:

$$Ce^{-A\tau_i}x(t) = y(t-\tau_i) - v(t-\tau_i) + \alpha_{t-\tau_i,t} + \beta_{t-\tau_i,t} + \gamma_{t-\tau_i,t} \tag{3.5}$$

with

$$\alpha_{t-\tau_i,t} = \int_{t-\tau_i}^{t} Ce^{A(t-\tau_i-\theta)}Bu(\theta)\,\mathrm{d}\theta \tag{3.6a}$$

$$\beta_{t-\tau_i,t} = \int_{t-\tau_i}^{t} Ce^{A(t-\tau_i-\theta)}\Phi(x(\theta))\,\mathrm{d}\theta \tag{3.6b}$$

$$\gamma_{t-\tau_i,t} = \int_{t-\tau_i}^{t} Ce^{A(t-\tau_i-\theta)}G\omega(\theta)\,\mathrm{d}\theta \tag{3.6c}$$

Applying (3.5) with (3.6) for each measurement in the time window $[t-\tau_{L-1},t]$, then a finite number of augmented measurements can be expressed in terms of system state $x(t)$ as following linear equation:

$$Y_L - V_L = W_L x(t) \tag{3.7}$$

where

$$Y_L = \begin{pmatrix} y(t-\tau_0)+\alpha_{t-\tau_0,t}+\beta_{t-\tau_0,t} \\ y(t-\tau_1)+\alpha_{t-\tau_1,t}+\beta_{t-\tau_1,t} \\ \vdots \\ y(t-\tau_{L-1})+\alpha_{t-\tau_{L-1},t}+\beta_{t-\tau_{L-1},t} \end{pmatrix};$$

$$W_L = \begin{pmatrix} Ce^{-A\tau_0} \\ Ce^{-A\tau_1} \\ \vdots \\ Ce^{-A\tau_{L-1}} \end{pmatrix}; \qquad V_L = \begin{pmatrix} v(t-\tau_0)-\gamma_{t-\tau_0,t} \\ v(t-\tau_1)-\gamma_{t-\tau_1,t} \\ \vdots \\ v(t-\tau_{L-1})-\gamma_{t-\tau_{L-1},t} \end{pmatrix}.$$

It is straightforward that the noise component V_L has zero mean, i.e. $\mathbb{E}(V_L)=0$. Then the variance matrix P (see Appendix A for detailed presentation) is block symmetric as

$$\begin{aligned} P &= \mathbb{E}\left((V_L-\mathbb{E}(V_L))(V_L-\mathbb{E}(V_L))^{\mathrm{T}}\right) = \mathbb{E}\left(V_L V_L^{\mathrm{T}}\right) \\ &= \begin{pmatrix} S_0 & S_0 & \cdots & S_0 \\ S_0 & S_1 & \cdots & S_1 \\ \vdots & \vdots & \ddots & \vdots \\ S_0 & S_1 & \cdots & S_{L-1} \end{pmatrix} + \begin{pmatrix} R & 0 & \cdots & 0 \\ 0 & R & \ddots & \vdots \\ \vdots & \ddots & \ddots & 0 \\ 0 & \cdots & 0 & R \end{pmatrix} \end{aligned} \tag{3.8}$$

where the block elements S_k ($k \triangleq \min[i,j] = 0,1,...,L-1$) represent the following integral calculation [Medvedev 1994]:

$$S_k = \int_{-\tau_k}^{0} Ce^{As} GQG^{\mathrm{T}} e^{A^{\mathrm{T}}s} C^{\mathrm{T}} \, \mathrm{d}s$$

Now, the state estimation $\hat{x}(t)$ at time instant t can be obtained by minimizing the following cost function for (3.7):

$$J(x) = \frac{1}{2} \|Y_L - W_L x(t)\|^2_{P^{-1}} \tag{3.9}$$

with the solution in the sense of least-squares as:

$$\begin{aligned} \hat{x}(t) &= \arg\min \; J(x) = \left(W_L^{\mathrm{T}} P^{-1} W_L\right)^{-1} W_L^{\mathrm{T}} P^{-1} \hat{Y}_L \\ &= \Omega_L^{-1} W_L^{\mathrm{T}} P^{-1} \hat{Y}_L \qquad \left(\Omega_L \triangleq W_L^{\mathrm{T}} P^{-1} W_L\right) \end{aligned} \tag{3.10}$$

where

$$\hat{Y}_L = \begin{pmatrix} y(t-\tau_0) + \alpha_{t-\tau_0,t} + \hat{\beta}_{t-\tau_0,t} \\ y(t-\tau_1) + \alpha_{t-\tau_1,t} + \hat{\beta}_{t-\tau_1,t} \\ \vdots \\ y(t-\tau_{L-1}) + \alpha_{t-\tau_{L-1},t} + \hat{\beta}_{t-\tau_{L-1},t} \end{pmatrix} \tag{3.11a}$$

$$\hat{\beta}_{t-\tau_i,t} = \int_{t-\tau_i}^{t} Ce^{A(t-\tau_i-\theta)} \Phi(\hat{x}(\theta)) \, \mathrm{d}\theta \tag{3.11b}$$

It can be seen that the existence condition of $\hat{x}(t)$ in (3.10) is given by the existence of matrix Ω_L^{-1}. This condition is then given by the rank of matrix W_L, i.e., $\mathrm{rank}(W_L) = n = \dim(x)$, which is guaranteed by the following assumption:

Assumption 3.1. *The pair (A,C) is observable.*

According to (3.10)-(3.11), we obtain the analytical form of state estimation $\hat{x}(t)$ for considered nonlinear systems (3.1). The calculation of two integral terms $\alpha_{t-\tau_i,t}$ and $\hat{\beta}_{t-\tau_i,t}$ in (3.11a) are then detailed afterward.

3.2.2.1 Analytical calculation of the integral $\alpha_{t-\tau_i,t}$

It is obvious to see from (3.6a) that all the elements contained inside the integral are known and it is easy to have an analytical solution by some useful softwares with symbolic computation such as Maple, Mathematica, etc. If the mathematical expression of input $u(t)$ at

each instant is unknown, we can still get the solution by putting the element $u(t)$ as a factor of integral under the assumption that $u(t)$ is sampled as zero-order hold and thus remains to be constant between two consecutive sampling instants, which is usually true since most controllers of actual systems are digital computers in practice.

3.2.2.2 Iterative algorithm for solving the integral $\hat{\beta}_{t-\tau_i,t}$

In order to compute $\hat{\beta}_{t-\tau_i,t}$, we might note that it is impossible to have an exact analytical solution. Since we can see from (3.11b) that there is the term "$\Phi(\hat{x}(\theta))$" in the integral. In order to analytically calculate $\hat{\beta}_{t-\tau_i,t}$, we must know the exact trajectory of "$\hat{x}(\theta)$" between instant $t-\tau_i$ and t, which unfortunately is what we seek to know (via the estimation $\hat{x}(t)$ in (3.10)). Hence, a one-step prediction together with iterative-update algorithm is designed to obtain the approximate solution of $\hat{\beta}_{t-\tau_i,t}$ by Newton-Cotes formulas [Atkinson 1989].

In each time window $[t-\tau_{L-1},t]$, we define the measurement set $\mathbb{Z}_L = \{y(t-\tau_i); i = 0,1,\cdots,L-1\}$ and estimation set $\mathbb{X}_L = \{\hat{x}(t-\tau_j); j = 1,\cdots,L-1\}$. It should be noted here that there is no case $j=0$ since all the elements in $\hat{X}_L$ are obtained by previous window and $\hat{x}(t-\tau_0) = \hat{x}(t)$ is exactly what we aim to estimate by current window. Therefore, a one-step prediction of state x at instant t, noted as $\hat{x}^*(t)$, has been performed by using the tangent slope $\dot{\hat{x}}(t-\Delta t)$ with a small time interval $\Delta t = T_s$ as:

$$\begin{aligned}\hat{x}^*(t) &= \hat{x}(t-\Delta t) + \dot{\hat{x}}(t-\Delta t)\Delta t \\ &= \hat{x}(t-T_s) + \dot{\hat{x}}(t-T_s)T_s \\ &= \hat{x}(t-\tau_1) + \left[A\hat{x}(t-\tau_1) + Bu(t-\tau_1) + \Phi(\hat{x}(t-\tau_1))\right]T_s\end{aligned} \tag{3.12}$$

$\hat{x}^*(t)$ is then iteratively updated by (3.10) - (3.11), which makes the final estimation $\hat{x}(t)$ after all iterations. The iterations are stopped when there is no significant change between two consecutive iterations or the maximum iteration numbers $N_{\max}$ has been reached, namely

$$\hat{x}(t) - \hat{x}^*(t) \leq \varepsilon \qquad \text{or} \qquad m \geq N_{\max} \text{ (with acceptable error)}$$

Furthermore, the first-order Newton-Cotes formulas, which yields *trapezoidal rule*, is employed in this paper to numerically approximate the integral term $\hat{\beta}_{t-\tau_i,t}$ in (3.11a). For the purpose of reducing the massive computing burden in each iteration, we notice from (3.11b) that $\hat{\beta}_{t-\tau_i,t}$ can be divided as follows by the Segment Addition Postulate [Nomizu and Sasaki 1994] for integral calculus:

$$\hat{\beta}_{t-\tau_i,t} = \hat{\beta}_{t-\tau_i,t-\tau_1} + \hat{\beta}_{t-\tau_1,t} \tag{3.13}$$

with

$$\hat{\beta}_{t-\tau_i,t-\tau_1} = \int_{t-\tau_i}^{t-\tau_1} Ce^{A(t-\tau_i-\theta)}\Phi(\hat{x}(\theta))\,\mathrm{d}\theta \tag{3.14a}$$

$$\hat{\beta}_{t-\tau_1,t} = \int_{t-\tau_1}^{t} Ce^{A(t-\tau_1-\theta)}\Phi(\hat{x}(\theta))\,\mathrm{d}\theta \tag{3.14b}$$

let

$$g(\hat{x}(\theta)) = Ce^{A(t-\tau_i-\theta)}\Phi(\hat{x}(\theta)) \tag{3.15}$$

we know that the previous estimation set $\{\hat{x}(t-\tau_j)\}(j=1,\cdots,L-1)$ is unchanged during each iteration of updating $\hat{x}^*(t)$, which leads to $g(\hat{x}(t-\tau_j))$ by (3.15) unchanged. As a consequence, $\hat{\beta}_{t-\tau_i,t-\tau_1}$ by (3.14a) also remains the same at each iteration. Therefore, as it is shown in Figure 3.1, we only need to recalculate the term $\hat{\beta}_{t-\tau_1,t}$ in (3.13) at each iteration. In this way, the unnecessary calculation burden caused by iteration can be dramatically reduced when using Newton-Cotes formulas to calculate the numerical integration.

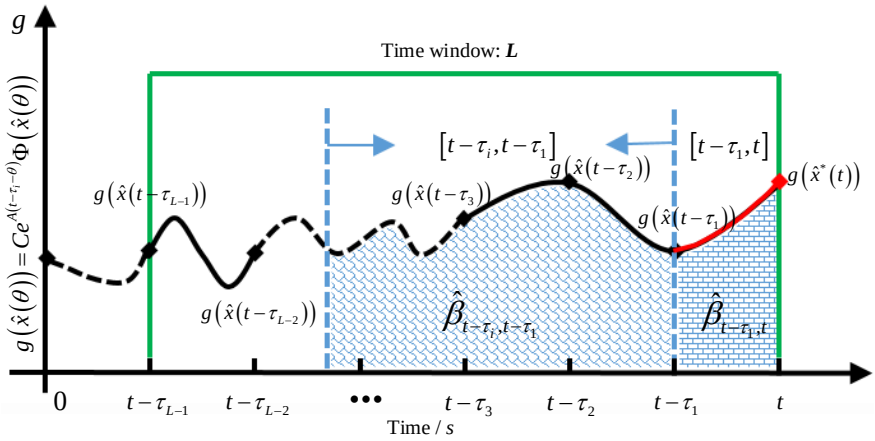

Figure 3.1: Calculation framework of $\hat{\beta}_{t-\tau_i,t}$ in each interval $[t-\tau_i, t]$

For the sake of overall understanding, the summarized algorithm of the proposed nonlinear observer CD-FMO is shown in **Algorithm 1**.

3.2.3 Estimation property of CD-FMO

Theorem 3.1. *If nonlinear system (3.1) satisfies Assumption 3.1, in the case of noise-free and fault-free, the property of estimation by presented CD-FMO are unbiased*

$$\hat{x}(t) = x(t) \qquad t \in [L \times T_s, +\infty)$$

Algorithm 1 The implementation of nonlinear CD-FMO algorithm

1: **Initialization:** at each time instant t, given the iteration threshold ε, the maximum number of iteration $N_{\max}$, the measurement set $\mathbb{Z}_L = \{y(t-\tau_i)\}$ with $i = 0, 1, \cdots, L-1$ and the previous estimation set $\mathbb{X}_L = \{\hat{x}(t-\tau_j)\}$ with $j = 1, \cdots, L-1$.
2: Calculate $g(\hat{x}(t-\tau_j))$ for each member in $\mathbb{X}_L$ by (3.15).
3: Compute integral $\hat{\beta}_{t-\tau_j,t-\tau_1}$ in (3.14a) by Newton Cotes.
4: **One-step prediction:** using $\hat{x}(t-\tau_1)$ to perform a one-step prediction of $x(t)$ via (3.12), noted as $\hat{x}^*(t)$.
5: **Updating by iteration:**
6: **for** each iteration $m = 1 : N_{\max}$ **do**
7: Calculate $g(\hat{x}^*(t))$ with the $\hat{x}^*(t)$ predicted in step 3.
8: Calculate $\hat{\beta}_{t-\tau_1,t}$ in (3.14b) by Newton Cotes formulas.
9: Calculate the entire integral $\hat{\beta}_{t-\tau_i,t}$ via (3.13).
10: Update $\hat{x}^*(t)$ to $\hat{x}(t)$ via (3.10):
11: **if** $\hat{x}(t) - \hat{x}^*(t) \leq \varepsilon$ or $m \geq N_{\max}$ **then**
12: Terminate the iteration, go forward to step 17.
13: **else**
14: Reset $m = m+1$, $\hat{x}^*(t) = \hat{x}(t)$, return to step 7.
15: **end if**
16: **end for**
17: **Moving the time window:** reset $t = t + T_s$, and go back to step 1 for next time instant.

Proof. In the case noise-free and fault-free, according to (3.1)-(3.7), the proposed CD-FMO (3.10) can be rewritten for the deterministic case as following:

$$\begin{aligned}\hat{x}(t) &= \left(W_L^{\mathrm{T}} W_L\right)^{-1} W_L^{\mathrm{T}} \hat{Y}_L \\ &= \Lambda_L^{-1} \sum_{i=0}^{L-1} \left\{ e^{-A^{\mathrm{T}}\tau_i} C^{\mathrm{T}} \left(y(t-\tau_i) + \alpha_{t-\tau_i,t} + \hat{\beta}_{t-\tau_i,t} \right) \right\}\end{aligned} \tag{3.16}$$

with

$$\Lambda_L = W_L^{\mathrm{T}} W_L = \sum_{i=0}^{L-1} e^{-A^{\mathrm{T}}\tau_i} C^{\mathrm{T}} C e^{-A\tau_i} \tag{3.17}$$

then, as stated in (3.5) and regardless of noise term $v(t-\tau_i)$, $y(t-\tau_i)$ can be given as:

$$y(t-\tau_i) = C e^{-A\tau_i} x(t) - \alpha_{t-\tau_i,t} - \beta_{t-\tau_i,t} \tag{3.18}$$

by replacing the term $y(t-\tau_i)$ in (3.16) by (3.18) and taking into account (3.17), we have

$$\begin{aligned}\hat{x}(t) &= \Lambda_L^{-1}\sum_{i=0}^{L-1}\left\{e^{-A^{\mathrm{T}}\tau_i}C^{\mathrm{T}}\left(Ce^{-A\tau_i}x(t)-\beta_{t-\tau_i,t}+\hat{\beta}_{t-\tau_i,t}\right)\right\}\\ &= \Lambda_L^{-1}\sum_{i=0}^{L-1}\left\{e^{-A^{\mathrm{T}}\tau_i}C^{\mathrm{T}}Ce^{-A\tau_i}x(t)\right\}+\Lambda_L^{-1}\sum_{i=0}^{L-1}\left\{e^{-A^{\mathrm{T}}\tau_i}C^{\mathrm{T}}\left(\hat{\beta}_{t-\tau_i,t}-\beta_{t-\tau_i,t}\right)\right\}\\ &= x(t)+\Lambda_L^{-1}\sum_{i=0}^{L-1}\left\{e^{-A^{\mathrm{T}}\tau_i}C^{\mathrm{T}}\left(\hat{\beta}_{t-\tau_i,t}-\beta_{t-\tau_i,t}\right)\right\}\end{aligned} \tag{3.19}$$

In order to prove **Theorem 1**, we know that the following equivalence can be obtained directly:

$$\hat{x}(t)=x(t) \quad\Leftrightarrow\quad \|\hat{x}(t)-x(t)\|=0 \qquad t\in[L\times T_s,+\infty) \tag{3.20}$$

from (3.19), the norm of $\hat{x}(t)-x(t)$ can be therefore expressed as follows:

$$\begin{aligned}\|\hat{x}(t)-x(t)\| &= \left\|\Lambda_L^{-1}\sum_{i=0}^{L-1}\left\{e^{-A^{\mathrm{T}}\tau_i}C^{\mathrm{T}}\left(\hat{\beta}_{t-\tau_i,t}-\beta_{t-\tau_i,t}\right)\right\}\right\|\\ &\le \sum_{i=0}^{L-1}\left\|\Lambda_L^{-1}e^{-A^{\mathrm{T}}\tau_i}C^{\mathrm{T}}\left(\hat{\beta}_{t-\tau_i,t}-\beta_{t-\tau_i,t}\right)\right\|\end{aligned} \tag{3.21}$$

then, based upon (3.6b) and (3.11b), by using Lipschitz condition (3.2), the matrix norm properties and the triangle inequality for integrals [Rudin 2015], (3.21) can be further derived as:

$$\begin{aligned}\|\hat{x}(t)-x(t)\| &\le \sum_{i=0}^{L-1}\left\|\Lambda_L^{-1}e^{-A^{\mathrm{T}}\tau_i}C^{\mathrm{T}}\int_{t-\tau_i}^{t}Ce^{A(t-\tau_i-\theta)}\left[\Phi(\hat{x}(\theta))-\Phi(x(\theta))\right]\mathrm{d}\theta\right\|\\ &\le \sum_{i=0}^{L-1}\int_{t-\tau_i}^{t}\left\|\Lambda_L^{-1}e^{-A^{\mathrm{T}}\tau_i}C^{\mathrm{T}}Ce^{A(t-\tau_i-\theta)}\left[\Phi(\hat{x}(\theta))-\Phi(x(\theta))\right]\right\|\mathrm{d}\theta\\ &\le L\int_{t-\tau_{L-1}}^{t}\left\|\Lambda_L^{-1}e^{-A^{\mathrm{T}}\tau_{L-1}}C^{\mathrm{T}}Ce^{A(t-\tau_{L-1}-\theta)}\left[\Phi(\hat{x}(\theta))-\Phi(x(\theta))\right]\right\|\mathrm{d}\theta\\ &\le L\int_{t-\tau_{L-1}}^{t}\left\|\Lambda_L^{-1}e^{-A^{\mathrm{T}}\tau_{L-1}}C^{\mathrm{T}}Ce^{A(t-\tau_{L-1}-\theta)}\right\|\|\Phi(\hat{x}(\theta))-\Phi(x(\theta))\|\mathrm{d}\theta\\ &\le L\int_{t-\tau_{L-1}}^{t}\left\|\Lambda_L^{-1}e^{-A^{\mathrm{T}}\tau_{L-1}}C^{\mathrm{T}}Ce^{A(t-\tau_{L-1}-\theta)}\right\|\kappa\|\hat{x}(\theta)-x(\theta)\|\mathrm{d}\theta\\ &\le L\int_{L\times T_s}^{t}\left\|\Lambda_L^{-1}e^{-A^{\mathrm{T}}\tau_{L-1}}C^{\mathrm{T}}Ce^{A(t-\tau_{L-1}-\theta)}\right\|\kappa\|\hat{x}(\theta)-x(\theta)\|\mathrm{d}\theta\\ &\le \mathbf{0}+L\int_{L\times T_s}^{t}\left\|\Lambda_L^{-1}e^{-A^{\mathrm{T}}\tau_{L-1}}C^{\mathrm{T}}Ce^{A(t-\tau_{L-1}-\theta)}\right\|\kappa\|\hat{x}(\theta)-x(\theta)\|\mathrm{d}\theta\end{aligned} \tag{3.22}$$

then, the Gronwall inequality [Bellman 1943] yields

$$\begin{aligned}\|\hat{x}(t)-x(t)\| &\leq \mathbf{0}\cdot e^{\int_{L\times T_s}^{t} L\left\|\Lambda_L^{-1}e^{-A^{\mathrm{T}}\tau_{L-1}}C^{\mathrm{T}}Ce^{A(t-\tau_{L-1}-\theta)}\right\|\kappa\,\mathrm{d}\theta}\\ &\leq 0\end{aligned} \tag{3.23}$$

hence,

$$\|\hat{x}(t)-x(t)\|\leq 0 \;\Rightarrow\; \|\hat{x}(t)-x(t)\|=0 \;\Rightarrow\; \hat{x}(t)=x(t)$$

The proof is completed. ■

Remark 3.2. ***Theorem*** *3.1 states that $\hat{x}(t)=x(t)$ is always true when $t\geq L\times T_s$, that is*

(1) The proposed CD-FMO is a dead-beat observer in the case of noise-free and fault-free, the finite-time convergence is $L\times T_s$ (one window-size).

(2) There is no estimation when $t<L\times T_s$. In other words, there is no initial value problem (IVP) for the presented nonlinear observer, which gives us another advantage for application in physics or other sciences.

Remark 3.3. *It is clear that* ***Theorem*** *3.1 shows the unbiased estimation property of the proposed CD-FMO in deterministic case. In stochastic case, namely in the presence of the process noise and measurement noise, the unbiased property*

$$\mathbb{E}\left(\hat{x}(t)-x(t)\right)=0 \quad or \quad \mathbb{E}\left(\hat{x}(t)\right)=x(t) \tag{3.24}$$

can also be demonstrated in the similar manner, see ***Appendix*** *B for more details.*

3.2.4 Analytical choice of the window length L

As it is shown in (3.10) and (3.11), at each time instant t, the state estimation $\hat{x}(t)$ is related to the window length L. Thus, it is necessary to interpret how to select an appropriate window length L. Here we are going to explain this by defining the "minimal length $L_{\min}$" and "maximal length $L_{\max}$", as it has been shown in [Graton et al. 2014].

3.2.4.1 Minimal length $L_{\min}$

The minimal window length $L_{\min}$ is chosen to assure the existence of the proposed CD-FMO by (3.10). As we have already discussed before, this condition is then given by the rank of matrix W_L, i.e., $\operatorname{rank}(W_L)=n=\dim(x)$, which is already guaranteed by **Assumption** 3.1. However, $L_{\min}$ is just used to valid the **Assumption** 3.1, it is definitely not the optimal window length, as showed in the latter subsection.

3.2.4.2 Maximal length $L_{\max}$

Here it should be noticed that, theoretically speaking, there is no maximum window length $L_{\max}$ for CD-FMO. The greater the length L, the better the estimation $\hat{x}(t)$, which is reasonable since the amount of measurement information augments as the window length increases. However, after a certain size, the contribution of additional information by increasing window length is not significant enough to decrease estimation error. Therefore in this chapter, we take "the maximum eigenvalue of covariance matrix $\Sigma_{\tilde{x}}$" of estimation error $\tilde{x} = \hat{x} - x$ as an indicator to select maximum window length $L_{\max}$. Given a selected threshold of estimation error tolerance Υ_{Tol}, $L_{\max}$ is defined as:

$$L_{\max} = \arg\min_{L} \{\max(\text{eig}(\Sigma_{\tilde{x}})) \leq \Upsilon_{\text{Tol}}\} \tag{3.25}$$

which is the smallest window length when the largest eigenvalue of $\Sigma_{\tilde{x}}$ is smaller than error tolerance threshold Υ_{Tol}. This part will be further analyzed in next section with an illustrative example.

3.3 Illustrative Example: a Single-link Robot

In this section, we consider a nonlinear single-link robotic arm, which has an elastic joint rotating in a vertical plane [Zhang et al. 2008]. The nonlinear state-space model is described here as:

$$\begin{aligned} \dot{x}(t) &= Ax(t) + Bu(t) + \Phi(x) + G\omega(t) \\ y(k) &= Cx(k) + v(k) \end{aligned}$$

with $x = [x_1 \quad x_2 \quad x_3 \quad x_4]^{\mathrm{T}}$. Here, components x_1 and x_3 are the displacement of link and rotor respectively while components x_2 and x_4 represent the velocity. The measurement noise $v \sim \mathcal{N}(\mathbf{0}, R)$ and the process noise $\omega(t) = 0$. The initial conditions for the robotic arm system is $x(0) = (1 \quad 1 \quad 1 \quad 1)^{\mathrm{T}}$. The input control $u(t) = 2\sin(2t)$, which is the torque provided by the motor. All the other related matrices are given as:

$$A = \begin{pmatrix} 0 & 1 & 0 & 0 \\ -\frac{k}{J_l} & -\frac{f_l}{J_l} & \frac{k}{J_l} & 0 \\ 0 & 0 & 0 & 1 \\ \frac{k}{J_m} & 0 & -\frac{k}{J_m} & -\frac{f_m}{J_m} \end{pmatrix}; \quad B = \begin{pmatrix} 0 \\ 0 \\ 0 \\ \frac{1}{J_m} \end{pmatrix}; \quad \Phi(x) = \begin{pmatrix} 0 \\ -\frac{mgl}{J_l}\sin x_1 \\ 0 \\ 0 \end{pmatrix};$$

$$C = \begin{pmatrix} 1 & 0 & 0 & 0 \\ 0 & 0 & 1 & 0 \\ 0 & 0 & 0 & 1 \end{pmatrix}; \quad R = \begin{pmatrix} 4\times10^{-4} & 0 & 0 \\ 0 & 4\times10^{-4} & 0 \\ 0 & 0 & 9\times10^{-4} \end{pmatrix}.$$

the simulation scenario is performed according to the parameters shown in Table 3.1.

Table 3.1: Physical parameters (in SI units)

elastic constant $k = 2$	link mass $m = 4$
viscous friction coefficient for motor $f_m = 1$	motor inertia $J_m = 1$
viscous friction coefficient for link $f_l = 0.5$	link inertia $J_l = 2$
mass center $l = 0.5$	link inertia $g_c = 9.8$

3.3.1 Selection of the window length L

As shown in (3.25), we take "$\max(\text{eig}(\Sigma_{\tilde{x}}))$" as an indicator to select $L_{\max}$. It can be seen from Figure 3.2 that the maximum eigenvalue of $\Sigma_{\tilde{x}}$ is asymptotically convergent as window length L increases, which indicates that the estimation performance provided by the presented CD-FMO well improves while the window length augments. After window length $L_1 = 13$, the decrease of the curve is much less significant, which is normal since there is few additional information can be provided by increasing the window length. This is also why the proposed observer is called "*finite memory*". Nevertheless, starting from $L_2 = 20$, the curve shows a slight trend of going up, which is a normal phenomenon because the approximation error of Newton-Cotes formulas (used in (3.11a) for integral term $\hat{\beta}_{t-\tau_i,t}$) will also get bigger as L increases. In order to get a better diagnosis performance, we choose $L = 15$ for all the analysis and diagnosis later in this chapter, which is well between L_1 and L_2.

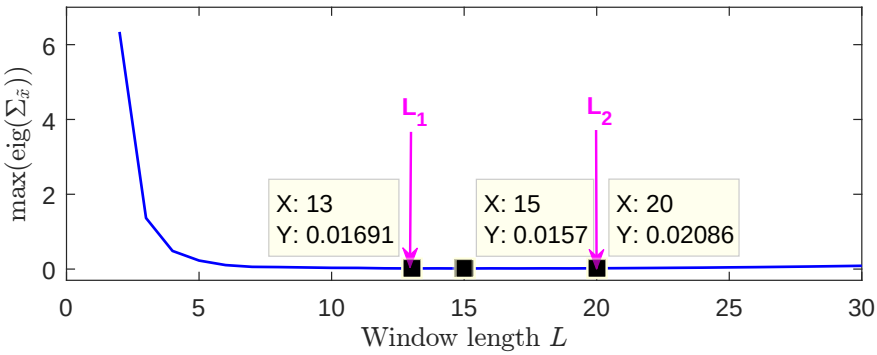

Figure 3.2: Convergence of covariance $\Sigma_{\tilde{x}}$ with window length L increases

3.3.2 Numerical integration approximation error analysis

In order to perform state estimate via (3.10), we choose *trapezoidal rule* to approximate the integral term $\hat{\beta}_{t-\tau_i,t}$ in (3.11a), so it is necessary to give the approximation error bound. We recall the following lemma:

Lemma 3.1. *Given a definite integral* $I = \int_a^b f(x)\,\mathrm{d}x$*, the approximation error of trapezoidal rule is[Atkinson 1989]*

$$\mathscr{O}(I) = -\frac{(b-a)^3}{12} f''(\eta), \quad \eta \in [a,b]$$

We can have the following expression of $\hat{x}(t)$ by rewriting (3.10),

$$\begin{aligned}\hat{x}(t) &= \left(W_L^{\mathrm{T}} P^{-1} W_L\right)^{-1} W_L^{\mathrm{T}} P^{-1} \hat{Y}_L \\ &= \Lambda_L^{-1} \sum_{i=0}^{L-1} e^{-A^{\mathrm{T}}\tau_i} C^{\mathrm{T}} R^{-1} \left(y(t-\tau_i) + \alpha_{t-\tau_i,t} + \hat{\beta}_{t-\tau_i,t}\right)\end{aligned}$$

together with (3.11b) and (3.15), we extract the integral term related to $\hat{\beta}_{t-\tau_i,t}$ and noted as:

$$\mathscr{B}_{t-\tau_i,t} = \Lambda_L^{-1} \sum_{i=0}^{L-1} e^{-A^{\mathrm{T}}\tau_i} C^{\mathrm{T}} R^{-1} \left(\int_{t-\tau_i}^{t} g(\hat{x}(\theta))\,\mathrm{d}\theta\right)$$

we can see from $\mathscr{B}_{t-\tau_i,t}$ that the calculation of approximation error by using trapezoidal rule can be divided into two steps:

1. Calculate the upper approximation error bound $|\mathscr{O}(Int)|$ with $Int = \int_{t-T_s}^{t} g(\hat{x}(\theta))\,\mathrm{d}\theta$.
2. Calculate cumulative error bound Γ_{nc} as i varies in the summation $\sum_{i=0}^{L-1}$.

For Step 1, the bound of approximation error $\mathscr{O}(Int)$ can be given by **Lemme** 3.1 as:

$$|\mathscr{O}(Int)| \leq \frac{T_s^3}{12} \max_{\theta\in[t-T_s,t]} \left|g''(\hat{x}(\theta))\right|$$

from the expression (3.15), we can get the first and second derivatives of g as following:

$$\begin{aligned}g'(\hat{x}(\theta)) =& \frac{\mathrm{d}g(\hat{x}(\theta))}{\mathrm{d}\theta} = -Ce^{A(t-\tau_i-\theta)}A\Phi(\hat{x}(\theta)) + Ce^{A(t-\tau_i-\theta)}\frac{\mathrm{d}\Phi(\hat{x}(\theta))}{\mathrm{d}\hat{x}}\frac{\mathrm{d}\hat{x}(\theta)}{\mathrm{d}\theta} \\ g''(\hat{x}(\theta)) =& \frac{\mathrm{d}^2 g(\hat{x}(\theta))}{\mathrm{d}\theta^2} = \frac{\mathrm{d}g'(\hat{x}(\theta))}{\mathrm{d}\theta} = Ce^{A(t-\tau_i-\theta)}A^2\Phi(\hat{x}(\theta)) \\ & -2Ce^{A(t-\tau_i-\theta)}A\frac{\mathrm{d}\Phi(\hat{x}(\theta))}{\mathrm{d}\hat{x}}\frac{\mathrm{d}\hat{x}(\theta)}{\mathrm{d}\theta} + Ce^{A(t-\tau_i-\theta)}\frac{\mathrm{d}}{\mathrm{d}\theta}\left(\frac{\mathrm{d}\Phi(\hat{x}(\theta))}{\mathrm{d}\hat{x}}\frac{\mathrm{d}\hat{x}(\theta)}{\mathrm{d}\theta}\right)\end{aligned}$$

By calculating the norm of g'' together with the parameters defined at the beginning of this section, we have

$$|\mathscr{O}(Int)| \leq 2.5228 \times 10^{-6} \triangleq \zeta_{t-T_s,t}$$

For Step 2, we can directly get the cumulative error bound Γ_{nc} as i varies in the summation $\sum_{i=0}^{L-1}$ as follows:

$$\begin{aligned}\Gamma_{nc} &\leq 0 + \zeta_{t-T_s,t} + 2\zeta_{t-T_s,t} + \cdots + (L-1)\zeta_{t-T_s,t} \\ &= \frac{L(L-1)}{2}\zeta_{t-T_s,t} \\ &= 2.6489 \times 10^{-4} \qquad (L=15)\end{aligned}$$

meanwhile, the maximum element of standard deviation (SD) σ of measurement noise, noted as $\sigma_{\max}$, is given by:

$$\sigma\sigma^{\mathrm{T}} = R \;\Rightarrow\; \sigma = R^{1/2} = \begin{pmatrix} 2\times10^{-2} & 0 & 0 \\ 0 & 2\times10^{-2} & 0 \\ 0 & 0 & 3\times10^{-2} \end{pmatrix} \;\Rightarrow\; \sigma_{\max} = 3\times10^{-2}$$

It is obvious that $\Gamma_{nc} \ll \sigma_{\max}$, which means that the approximation error for numerical integration is drowned in measurement noise. As a result, we can conclude that our estimation is correct with window length $L = 15$.

3.3.3 State estimation performance

It can be clearly seen from Figure 3.3 that four-dimensional system state x is reconstructed correctly under the presence of measurement noise, the proposed CD-FMO provides great performance of state estimation. Besides, Figure 3.3 also depicts how the accuracy of state estimation getting much better as window length L getting longer, which is another consistent result with respect to Figure 3.2.

3.3.3.1 Unbiased estimation property analysis in stochastic case

The unbiased estimation property of presented CD-FMO in stochastic case is evaluated by root-mean-square error (RMSE) criteria together with monte carlo (MC) simulation, where

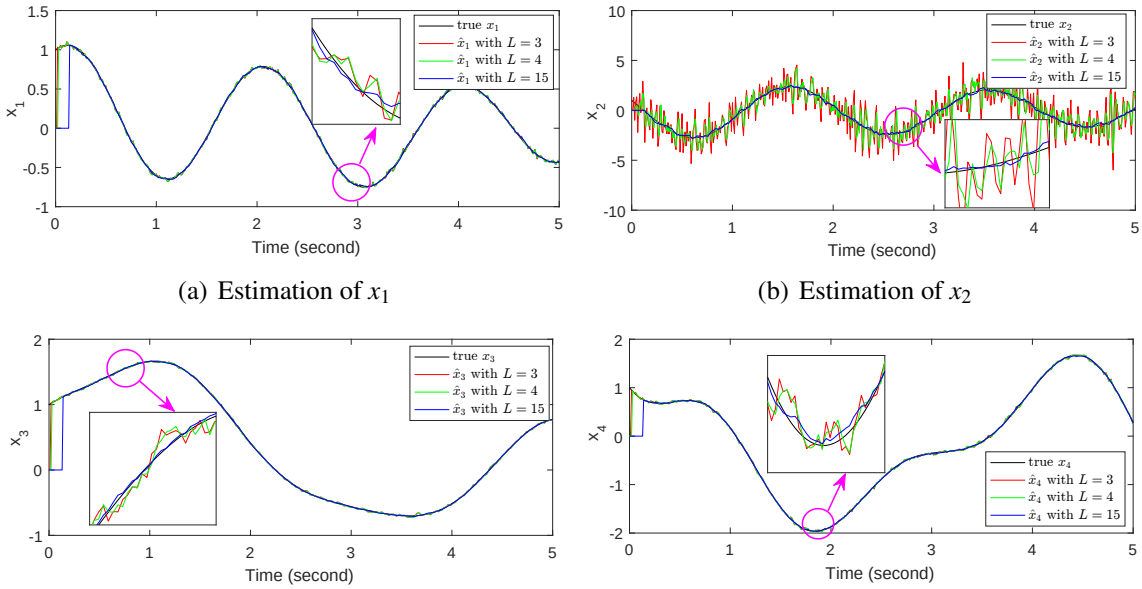

(a) Estimation of x_1 (b) Estimation of x_2

(c) Estimation of x_3 (d) Estimation of x_4

Figure 3.3: State estimation $\hat{x}$ with different window length L

RMSE is defined as:

$$\text{RMSE} = \sqrt{\frac{1}{N_{\text{mc}}} \sum_{i=1}^{N_{\text{mc}}} (\hat{x}^{(i)} - x)^2}$$

here, N_{mc} represents MC simulation times. The state estimation by running multiple MC simulation is therefore defined in the average sense:

$$\mathbb{E}(\hat{x}(t)) \triangleq \hat{x}_{mean} = \frac{1}{N_{\text{mc}}} \sum_{i=1}^{N_{\text{mc}}} \hat{x}^{(i)}$$

Let N_{mc} take the values 100 and 500 respectively. By taking the component x_1 as an example, it can be seen from Figure 3.4 that during the MC simulations, the estimation upper and lower bounds of $\hat{x}$ is quiet small, which means that the state estimation by proposed CD-FMO varies within a small range around real state x in the presence of measurement noise. Moreover, the estimation $\hat{x}_{mean}$ obtained with $N_{\text{mc}} = 500$ is closer to true value than the one by $N_{\text{mc}} = 100$, which is logical since MC simulation performed a series of repeated random sampling of Gaussian measurement noise, the larger the sampling size, the closer the mean value of noise is to zero.

The unbiased estimation property has also been examined by the RMSE with different N_{mc} in Figure 3.5. We can see that the RMSEs are close to zero, meanwhile the RMSE of

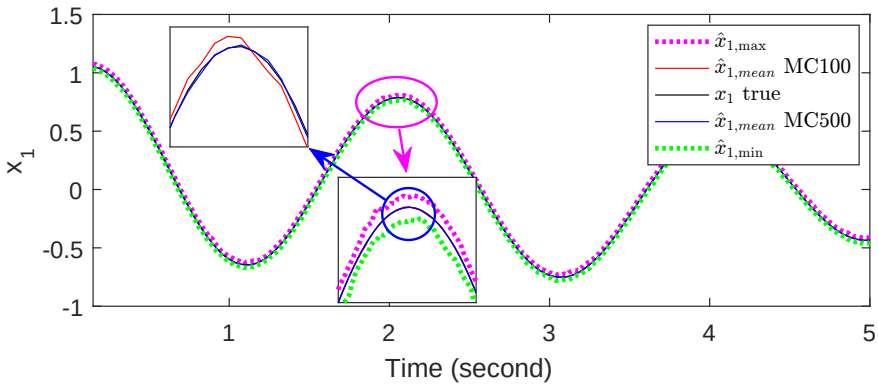

Figure 3.4: Upper (lower) bound and mean of $\hat{x}_1$ between $N_{\text{mc}} = 100$ and $N_{\text{mc}} = 500$

$N_{\text{mc}} = 500$ is smoother than the one $N_{\text{mc}} = 100$. This means that the results obtained by two criteria are consistent.

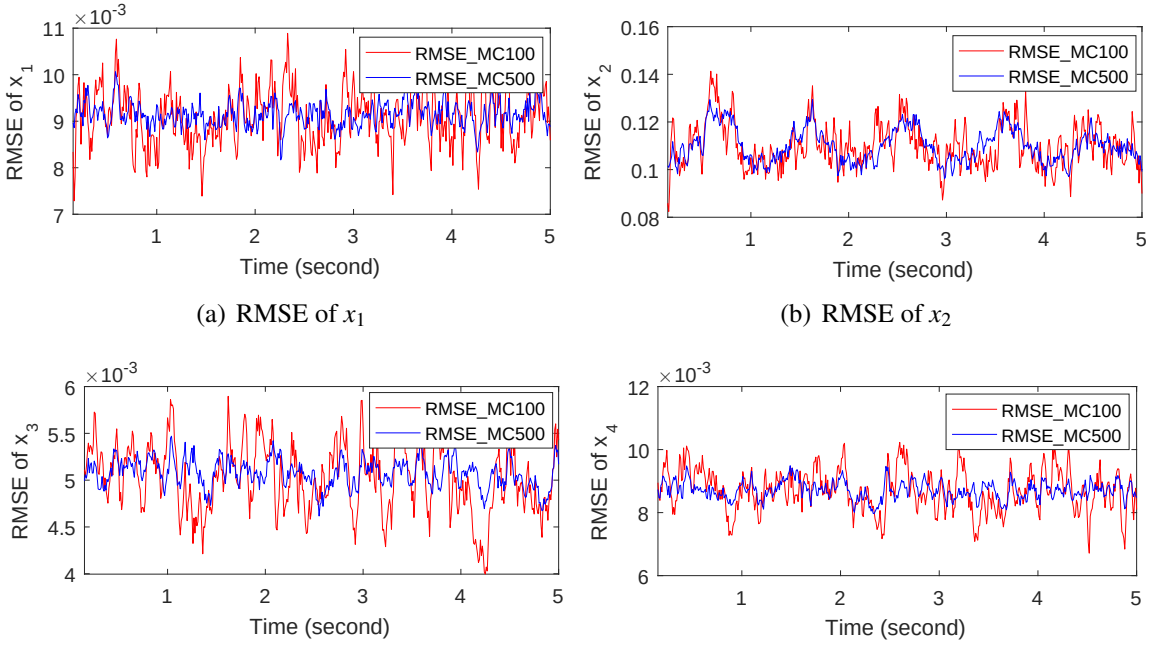

(a) RMSE of x_1

(b) RMSE of x_2

(c) RMSE of x_3

(d) RMSE of x_4

Figure 3.5: RMSE comparison between $N_{\text{mc}} = 100$ and $N_{\text{mc}} = 500$

To summarize what has been mentioned above, we have established by monte carlo simulation that state estimation given by the presented nonlinear observer CD-FMO in the stochastic case is also unbiased, i.e. $\mathbb{E}(\hat{x}(t) - x(t)) = 0$. This property provides a good precondition for the fault diagnosis after-step.

3.3.3.2 Robustness analysis with respect to measurement noise

We are going to analyze the robustness of CD-FMO against measurement noise through three scenarios shown in Table 3.2. Measurement noise varies from σ to 0.5σ and 1.5σ ($\pm 50\,\%$) respectively while the parameter setting of observer doesn't change, which means that the proposed observer (3.10) has an inconsistency between $y(\cdot)$ in (3.11a) and noise parameter P.

Table 3.2: Different scenarios of SD for measurement noise

Measurement noise settings		CD-FMO parameter settings
Scenario 1	SD $= 0.5\sigma$	SD $= \sigma$
Scenario 2	SD $= \sigma$	$R = \sigma^2$
Scenario 3	SD $= 1.5\sigma$	$P = \mathrm{diag}(R, R, \cdots, R)$

By taking x_1 as an example, it can be seen from Figure 3.6(a) that the state estimations $\hat{x}_1$ can still well follow the trajectory of true state x_1 even if the measurement noise has $\pm 50\,\%$ variations, which shows the robustness of CD-FMO with respect to measurement noise. In addition, we can see from the RMSEs in Figure 3.6(b) that state estimation of Scenario 1 is better than Scenario 2. It is logical because of the following reason: we have chosen $L = 15$ for the considered robotic arm system.

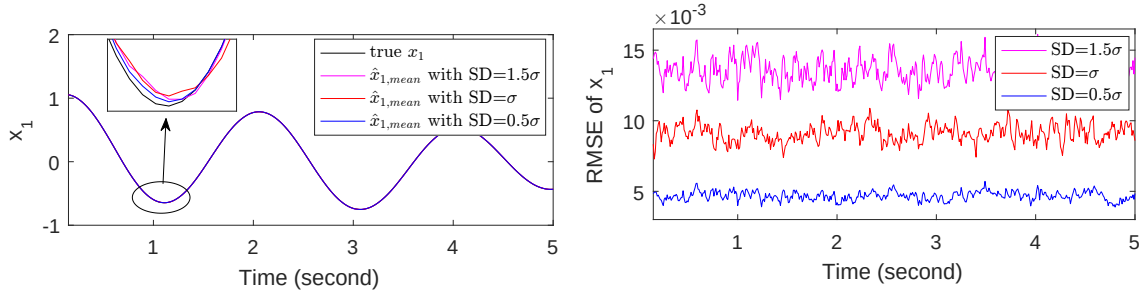

(a) Estimation of x_1 in different noise scenarios

(b) RMSE in different noise scenarios

Figure 3.6: Robustness analysis in different measurement noise scenarios

In fact, CD-FMO with $L = 15$ in Scenario 2 has already performed a little bit role of "*filter*" for this nonlinear system. As shown in Figure 3.2, when $L = 15$, $\max(\mathrm{eig}(\Sigma_{\tilde{x}})) = 0.0157$, while the minimum noise level in this case (minimum non-zero value of σ) is 0.02, i.e. $\sigma_{\min} = 0.02$. The fact of $\max(\mathrm{eig}(\Sigma_{\tilde{x}})) \leq \sigma_{\min}$ means that the largest dispersion of estimation is still smaller than the minimum noise level, which is the performance of a filter. Accordingly,

when we use the same window length for an even more lower noise level, i.e. Scenario 1, the presented CD-FMO will still perform as a filter, maybe filter even more. That is why we get a better estimation even when CD-FMO "over-estimate" the real noise level.

3.4 Application to Fault Diagnosis

In this section, we are going to apply the proposed CD-FMO to perform the fault diagnosis of the considered nonlinear single-link robotic arm system. In order to deal with all faults in the same simulation launch, we suppose that each fault only occurs during certain period $[T_{\text{fs}}, T_{\text{fe}}]$, therefore we use the following function to characterize the fault duration:

$$\Pi(t, T_{\text{fs}}, T_{\text{fe}}) = H(t - T_{\text{fs}}) - H(t - T_{\text{fe}})$$

where $H(\cdot)$ is *Heaviside step function*. In this paper, we injected two kinds of typical faults:

1. *Sensor bias:* a sudden bias is one of the abrupt sensor faults, which is modeled as: $y_{\text{f}} = y + \Pi(t, T_{\text{fs}}, T_{\text{fe}}) I\Delta$
   - *A bias on* y_1 (**F1**): $I = I_{y_1} = [1 \quad 0 \quad 0]^{\text{T}}$; $\Delta = \Delta_{y_1} = 0.15$; fault period $[T_{\text{fs}}, T_{\text{fe}}] = [0.5s, 1.0s]$.
   - *A bias on* y_2 (**F2**): $I = I_{y_2} = [0 \quad 1 \quad 0]^{\text{T}}$; $\Delta = \Delta_{y_2} = 0.15$; fault period $[T_{\text{fs}}, T_{\text{fe}}] = [2.0s, 2.5s]$.
   - *A bias on* y_3 (**F3**): $I = I_{y_3} = [0 \quad 0 \quad 1]^{\text{T}}$; $\Delta = \Delta_{y_3} = -0.15$; fault period $[T_{\text{fs}}, T_{\text{fe}}] = [3.5s, 4.0s]$.
2. *Actuator fault:* the actuator fault is modeled as: $u_{\text{f}} = \Pi(t, T_{\text{fs}}, T_{\text{fe}})(1 - \rho)u$ where $\rho \in [0, 1]$ describes control loss level. $\rho = 0$ means there is no actuator fault whereas $\rho = 1$ signifies that the control is completely lost.
   - *Actuator fault* (**F4**): $\rho = 0.6$; $[T_{\text{fs}}, T_{\text{fe}}] = [5.0s, 5.5s]$.

3.4.1 Fault detection

In this section, *residuals* are chosen as fault indicators and it is defined as:

$$r(t) = y(t) - C\hat{x}(t)$$

with $t = k \times T_s$, which checks the consistency of real measurements of system and measurements estimated by the proposed CD-FMO. We use both residual r and the Cumulative Sum

(CUSUM) of r for the reason that CUSUM algorithm is well-known as the efficiency of detecting small change in the mean of a sequence. As introduced in [Montgomery 2013] in the case of control chart case, the upper CUSUM $G^+(k)$ and lower CUSUM $G^-(k)$ of residuals sequences $r(k)$ (with mean μ_r and SD σ_r) are defined as:

$$\begin{cases} G^+(k) = \max\{0, G^+(k-1) + r(k) - \mu_r - K\} \\ G^-(k) = \min\{0, G^-(k-1) + r(k) - \mu_r + K\} \end{cases}$$

with the starting value $G^+(0) = G^-(0) = 0$. The detection criterion is:

$$G^+(k) > H \qquad \text{or} \qquad G^-(k) < -H$$

In order to quickly detect the small shift in mean, the parameters of CUSUM algorithm is set as: $K = \frac{1}{2}\sigma_r$ and $H = 3\sigma_r$. In the presence of measurement noise, CUSUM algorithm can improve the performance of diagnosis. For example in Figure 3.7(a), the change of residual r_1 is not very obvious during fault **F3** occurs, but it can be clearly seen from the CUSUM of r_1 in Figure 3.7(b). CUSUM can also help to detect the incipient fault such as **F4** more quickly, as shown in Figure 3.7(a) and Figure 3.7(b). Fault signature of residual r and fault detection instant T_d with respect to different faults are therefore given in Table 3.3. These results reveal that the proposed CD-FMO has a good and effective performance in both sensor and actuator fault detection for the single-link robotic arm.

Table 3.3: Fault signature for different faults

Different Faults	**Start Instant** T_{fs} (vertical dash line)	**End Instant** T_{fe} (vertical solid line)	**Signature**			**Detect Instant** T_{d}
			r_1	r_2	r_3	
F1	$0.5s$	$1.0s$	1	0	1	$0.5s$
F2	$2.0s$	$2.5s$	0	1	1	$2.0s$
F3	$3.5s$	$4.0s$	1	0	1	$3.5s$
F4	$5.0s$	$5.5s$	1	0	1	$5.05s$

3.4.2 Fault isolation

It can be obviously seen from Table 3.3 that fault **F2** is isolable as it has a unique fault signature $[0, 1, 1]$. On the other hand, the remaining three faults **F1**, **F3** and **F4** can not be

isolated because of the identical fault signature $[1,0,1]$. Hence in this subsection we aim at solving this problem by using Generalized observer scheme (GOS) [Frank 1987] with another additional observer (CD-FMO 2), while CD-FMO 1 is the same as the previous part. The structure of a bank of CD-FMO is illustrated in Figure 3.8. CD-FMO 2 is constructed by

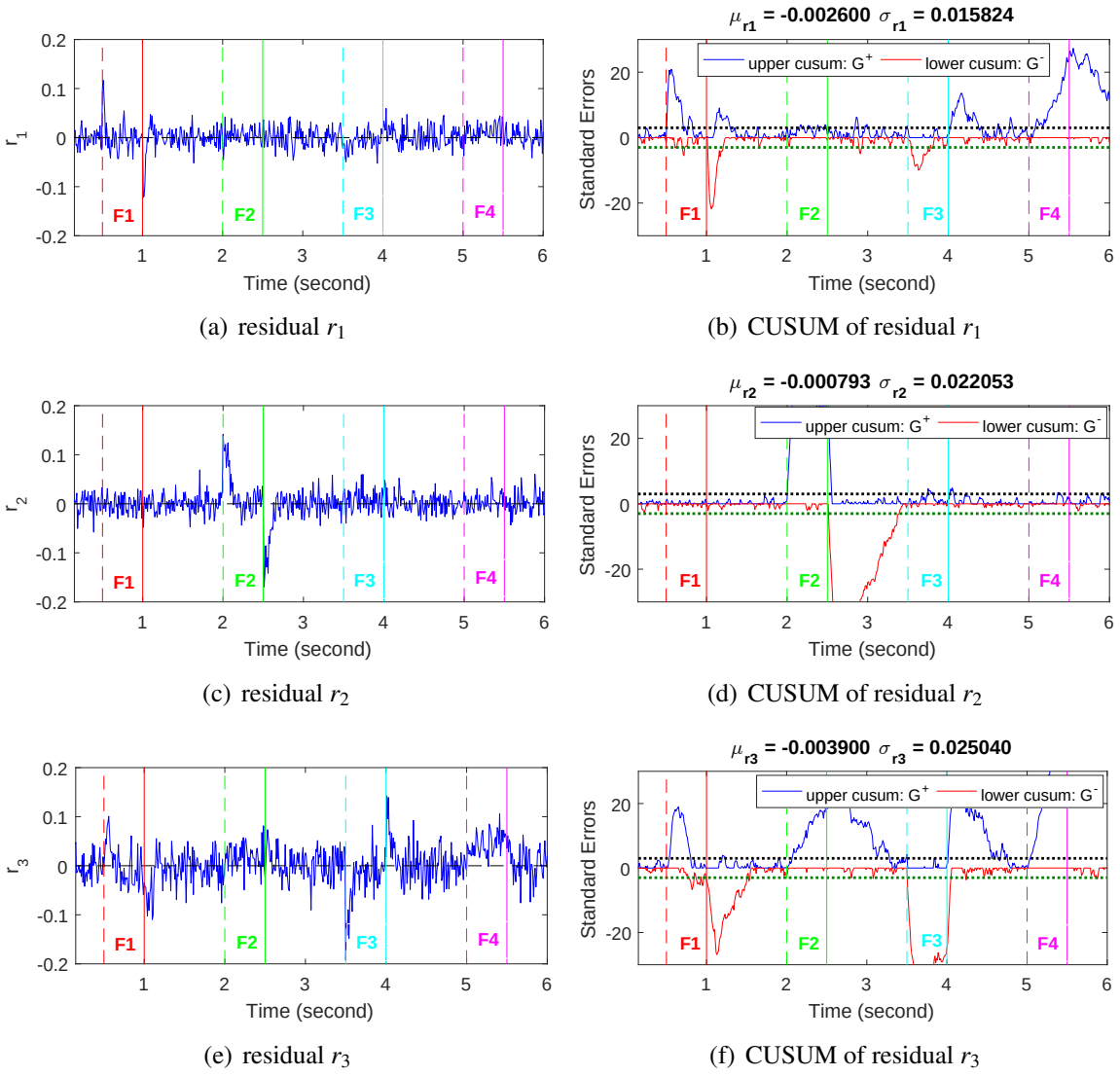

(a) residual r_1 (b) CUSUM of residual r_1

(c) residual r_2 (d) CUSUM of residual r_2

(e) residual r_3 (f) CUSUM of residual r_3

Figure 3.7: Residual r and the CUSUM of r

choosing subset measurements y_1 and y_3, then the corresponding model parameter changes from C to C_{13}, where C_{13} is composed by the first and third rows of C. Here, state estimation provided by CD-FMO 2 is noted as $\hat{x}'$, therefore the residual in this case is

$$r'(t) = y(t) - C\hat{x}'(t)$$

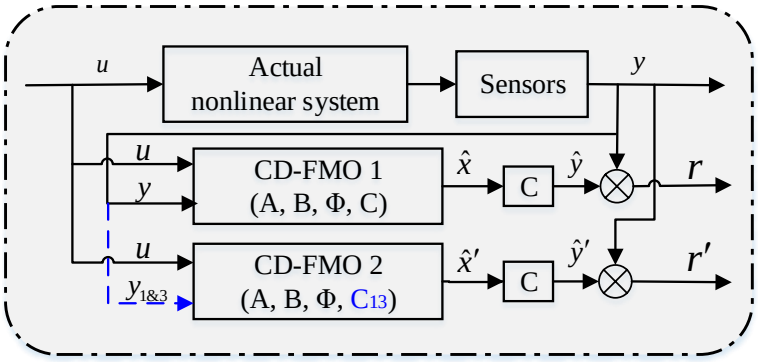

Figure 3.8: The scheme for a bank of CD-FMO

The results of r' are shown in Figure 3.9(a)-3.9(c), respectively. It shows that all the faults can be detected by residual r'_2 while **F1** and **F3** are also detected by r'_1 and r'_3. By comparing

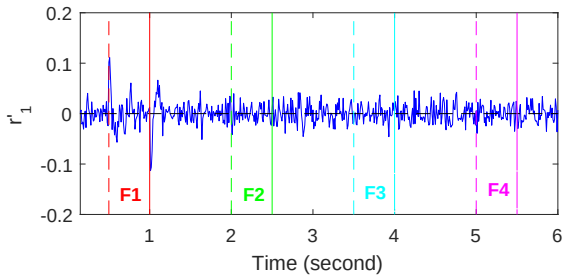

(a) residual r'_1 of CD-FMO 2

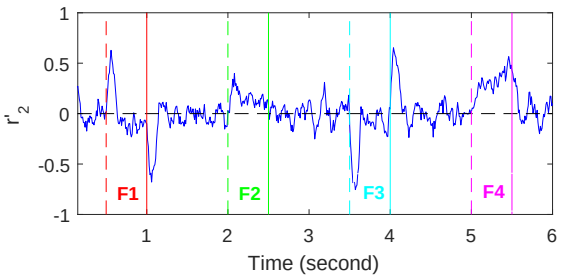

(b) residual r'_2 of CD-FMO 2

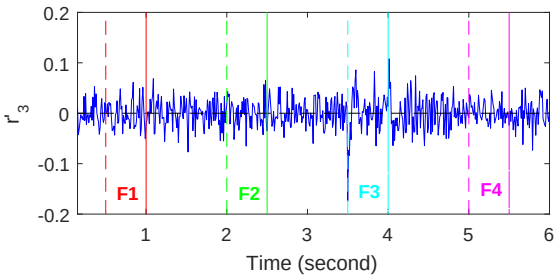

(c) residual r'_3 of CD-FMO 2

Figure 3.9: GOS of CD-FMOs and residual r' of CD-FMO 2

the fault signature obtained by CD-FMO 1 and CD-FMO 2 in Table 3.4, we can obviously see that the three indistinguishable faults **F1**, **F3** and **F4**, which have identical fault signature $[1,0,1]$ by CD-FMO 1, become isolable with $[1,1,0]$, $[0,1,1]$ and $[0,1,0]$ by CD-FMO 2. It means that by applying the GOS structure, the presented CD-FMO can also accomplish the objective of fault isolation effectively.

Table 3.4: Fault signature by CD-FMO 1 and CD-FMO 2

Different Faults	**Fault Signature** CD-FMO 1			**Fault Signature** CD-FMO 2		
	r_1	r_2	r_3	r'_1	r'_2	r'_3
A bias on y_1 (**F1**)	1	0	1	1	1	0
A bias on y_2 (**F2**)	0	1	1	0	1	0
A bias on y_3 (**F3**)	1	0	1	0	1	1
Actuator fault (**F4**)	1	0	1	0	1	0

3.5 Conclusion

In this chapter, a nonlinear observer has been proposed to perform state estimation and fault diagnosis for a class of continuous-discrete nonlinear dynamical systems. The performance of state estimation is excellent and can be significantly improved by choosing a larger window length. Also the presented approach has a finite-time convergence, which is a great advantage from the perspective of FDI. Simulations have illustrated that the proposed method provides a quite effective fault detection for sensor and actuator faults, which can also show the robustness of this nonlinear observer against the measurement noise. Meanwhile, by using the bank of observers, we are able to deal with the isolation of faults with identical fault signature. It is very worth noting that the proposed observer structure can also be apply to the following cases:

- Estimation instant is not synchronized with measurement instant, i.e. we are able to obtain the state estimation $\hat{x}(t)$ with $t \in (kT_s, (k+1)T_s)$;
- The sampling period of measurement is not a constant, i.e. $T_s \neq constant$.

The work in this chapter has been published in Zhang et al. [2020]. During the development and synthesis of CD-FMO in this chapter, the following questions have been also raised in our mind as the perspectives:

1. Can we further perform fault estimation for the actuator fault? Since the actuator serves as the controller of system, where a faulty actuator may make the plant uncontrollable, it is obviously not enough to just detect that there exists an actuator fault.
2. What if a sensor fault and an actuator fault occur at the same time? How can we provide more evidences to help locating or isolating the multiple simultaneous faults.

3. Instead of having a time-invariant system, what if the considered nonlinear system (3.1) is time-varying? It is worth noting that the linearization of a *time-invariant* nonlinear system often (when the nominal solution is not a constant) gives rise to *time-varying* systems, and this is actually one of the chief ways time-varying systems are encountered in system analysis.

As we have always believed, *there are no problems, only solutions*. Let's find the solutions to the above three problems in the rest chapters of this thesis.

Chapter 4

Continuous-Discrete Unknown Input FMO Design: Actuator Fault Estimation

"Any intelligent fool can make things bigger and more complex. It takes a touch of genius and a lot of courage to move in the opposite direction."

- Albert Einstein

Contents of chapter

Résumé en français :

Afin de répondre aux deux premières questions posées à la fin du chapitre précédent, nous allons construire dans ce chapitre un observateur à mémoire finie (CD-UI-FMO) en temps continu et à mesures discrètes pour les systèmes non linéaires dynamiques avec une entrée inconnue. Les systèmes non linéaires considérés sont toujours au moins *localement* Lipschitz et représentés par des équations différentielles ordinaires (ODEs) avec des bruits de processus et des bruits de mesure. Le CD-UI-FMO proposé est conçu par un modèle augmenté dans le but d'estimer simultanément les états du système et les entrées inconnues. La preuve de l'estimation non biaisée dans le cas déterministe est la même que celle dans le chapitre précédent, et elle sera également montrée via des simulations de Monte Carlo (MC) dans le cas stochastique. De plus, les observateurs non linéaires présentés sont appliqués avec succès à la détection et l'estimation de défaut actionneur pour un bras robotique à l'aide de l'algorithme à *moyenne mobile avec pondération exponentielle* (EWMA). Les résultats de la simulation mettent en évidence l'efficacité de l'approche proposée dans ce chapitre.

4.1 Introduction

In order to answer the first two questions raised at the end of the precedent chapter, we intend to design a continuous-discrete unknown input finite memory observer (CD-UI-FMO) for dynamical nonlinear systems with unknown input in this chapter. The nonlinear systems under consideration are still at least *locally* Lipschitz and represented by ordinary differential equations (ODEs) with process noise while measurements are sampled at discrete-time instants with measurement noises. By an augmented model, the proposed CD-UI-FMO is designed with the aim to simultaneously estimate system states and unknown inputs. The unbiased estimation property appears to remain the same as the previous chapter and it will be shown via Monte Carlo (MC) simulations as well in stochastic case. Moreover, the presented nonlinear observer are successfully applied to an actuator fault detection and estimation for a single-link joint robotic arm incorporating with the *exponentially weighted moving average* (EWMA) algorithm. Illustrative simulation results highlight the effectiveness of the proposed approach in this chapter.

4.2 CD-UI-FMO Design

For the sake of clarity, it should be noting that some notations may be changed in this chapter even if they represent the same variables compared to those in the previous chapter.

4.2.1 Problem statement

Let us consider the same class of nonlinear systems (3.1) as in precedent chapter with process noise and measurement noise, while another term is added to represent the *unknown input*. It is therefore modeled by the following state space equation: Consider the original system

$$\begin{aligned} \dot{X}(t) &= A_0 X(t) + B_0 u(t) + \Phi(X) + F\xi(t) + G_0 \omega_X(t) \\ y(k) &= C_0 X(k) + v(k) \end{aligned} \tag{4.1}$$

where $X(t) \in \mathbb{R}^{n_X}$, $u(t) \in \mathbb{R}^{n_u}$ and $y(k) \in \mathbb{R}^{n_y}$ are respectively continuous-time state vector, continuous-time input vector and discrete-time measurement vector, $\exists k \in \mathbb{N} \mid t = k \times T_s$, T_s is the sampling period of measurements. $A_0 \in \mathbb{R}^{n_X \times n_X}$, $B_0 \in \mathbb{R}^{n_X \times n_u}$, $G_0 \in \mathbb{R}^{n_X \times n_{\omega_X}}$ and $C_0 \in \mathbb{R}^{n_y \times n_X}$ are known matrices. The term $\xi(t)$ represents the *unknown input*, $F \in \mathbb{R}^{n_X \times n_\xi}$ is referring as the unknown input distribution matrix. The nonlinearity $\Phi(X)$ is a nonlinear function with respect to state X. Finally, the mutually independent vectors $\omega_X \in \mathbb{R}^{n_{\omega_X}}$ and $v \in \mathbb{R}^{n_y}$ respectively represent process noise and measurement noise, which assume to be zero mean Gaussian noises, namely:

$$\begin{aligned} \mathbb{E}[\omega_X(t)] &= 0 \\ \mathbb{E}[\omega_X(t_1)\omega_X^{\mathrm{T}}(t_2)] &= Q_X \cdot \delta(t_1 - t_2) \\ \mathbb{E}[v(k)] &= 0 \\ \mathbb{E}[v(k_1)v^{\mathrm{T}}(k_2)] &= R \cdot \delta_{k_1,k_2} \end{aligned}$$

here, $\delta(\cdot)$ is *Dirac delta function* and $\delta_{i,j}$ denotes *Kronecker delta function*. The proposed CD-UI-FMO for nonlinear systems (4.1) will be detailed under the following assumptions:

Assumption 4.1. *The nonlinear function $\Phi(X)$ satisfies the Lipschitz condition with Lipschitz constant κ as follow:*

$$\|\Phi(a) - \Phi(b)\| \leq \kappa \|a - b\|$$

Assumption 4.2. *The dynamic of unknown input $\xi(t)$ is given as:*

$$\dot{\xi}(t) = D_\xi \omega_\xi(t)$$

where $D_\xi \in \mathbb{R}^{n_\xi \times n_{\omega_\xi}}$ is the noise distribution matrix and $\omega_\xi(t) \in \mathbb{R}^{n_{\omega_\xi}}$, which is also independent of v, is zero mean Gaussian process noise for ξ with properties as follows:

$$\begin{aligned} \mathbb{E}[\omega_\xi(t)] &= 0 \\ \mathbb{E}[\omega_\xi(t_1)\omega_\xi^T(t_2)] &= Q_\xi \cdot \delta(t_1 - t_2) \end{aligned}$$

4.2.2 Mathematical model for CD-UI-FMO

Based on (4.1) and the dynamic of unknown input $\xi(t)$ in **Assumption** 4.2, an augmented model can be built as follows:

$$\dot{x}(t) = Ax(t) + Bu(t) + \phi(x) + G\omega(t) \tag{4.2a}$$
$$y(k) = Cx(k) + v(k) \tag{4.2b}$$

with

$$x(t) = \begin{bmatrix} X(t) \\ \xi(t) \end{bmatrix};\ A = \begin{bmatrix} A_0 & F \\ 0 & 0 \end{bmatrix};\ B = \begin{bmatrix} B_0 \\ 0 \end{bmatrix};\ \phi(x) = \begin{bmatrix} \Phi(X) \\ 0 \end{bmatrix}$$
$$\omega(t) = \begin{bmatrix} \omega_X(t) \\ \omega_\xi(t) \end{bmatrix};\ G = \begin{bmatrix} G_0 & 0 \\ 0 & D_\xi \end{bmatrix};\ C = \begin{bmatrix} C_0 & 0 \end{bmatrix};\ Q = \begin{bmatrix} Q_X & q^{\mathrm{T}} \\ q & Q_\xi \end{bmatrix}.$$

where the Lipschtiz condition in **Assumption** 4.1 is well-preserved for $\phi(x)$ according to the definition of the *norm*. The augmented process noise $\omega(t)$ is also Gaussian with the covariance Q, i.e.

$$\mathbb{E}[\omega(t)] = 0$$
$$\mathbb{E}[\omega(t_1)\omega^{\mathrm{T}}(t_2)] = Q \cdot \delta(t_1 - t_2)$$

Note that the covariance term q in matrix Q equals to zero when the UI process noise ω_ξ is uncorrelated with the state process noise ω_X, i.e. when correlation coefficient $\rho_{\omega_\xi \omega_X} = 0$.

The proposed CD-UI-FMO will be designed based upon the mathematical model (4.2) in next subsection. Before we start, the remark and assumption of observability are recalled again as follows:

Remark 4.1 ([Kou et al. 1973])**.** *The observability of a nonlinear system is a necessary condition that there exists a finite-time observer.*

Assumption 4.3. *The pair* (A, C) *is observable.*

4.2.3 Formulation of CD-UI-FMO

At each frozen time instant t, suppose that the discrete measurements are collected at L time instants $t - \tau_i$ with $i = 0, 1, ..., L-1$. It is evident that $[t - \tau_{L-1}, t]$ determines a time window where window length is L.

Firstly, both side of (4.2a) are pre-multiplied by an matrix exponential integrating factor e^{-At}. Then, by directly integrating and rearranging, the relation of states between two

different time instant t and $t-\tau_i$ can be given as:

$$x(t) = e^{A\tau_i}x(t-\tau_i) + \int_{t-\tau_i}^{t} e^{A(t-\theta)}Bu(\theta)\,\mathrm{d}\theta + \int_{t-\tau_i}^{t} e^{A(t-\theta)}\phi(x(\theta))\,\mathrm{d}\theta + \int_{t-\tau_i}^{t} e^{A(t-\theta)}G\omega(\theta)\,\mathrm{d}\theta \tag{4.3}$$

then, we obtain the following equation via left multiplying the matrix $Ce^{-A\tau_i}$ to (4.3) and taking into account the measurement equation (4.2b) at time instant $t-\tau_i$:

$$Ce^{-A\tau_i}x(t) = y(t-\tau_i) - v(t-\tau_i) + \alpha_{t-\tau_i,t} + \beta_{t-\tau_i,t} + \gamma_{t-\tau_i,t} \tag{4.4}$$

with

$$\alpha_{t-\tau_i,t} = \int_{t-\tau_i}^{t} Ce^{A(t-\tau_i-\theta)}Bu(\theta)\,\mathrm{d}\theta \tag{4.5a}$$

$$\beta_{t-\tau_i,t} = \int_{t-\tau_i}^{t} Ce^{A(t-\tau_i-\theta)}\phi(x(\theta))\,\mathrm{d}\theta \tag{4.5b}$$

$$\gamma_{t-\tau_i,t} = \int_{t-\tau_i}^{t} Ce^{A(t-\tau_i-\theta)}G\omega(\theta)\,\mathrm{d}\theta \tag{4.5c}$$

By applying equation (4.4) for every instant within the time window $[t-\tau_{L-1}, t]$, a finite number of concatenated measurements can be denoted with respected to the system state $x(t)$ as the following linear equation:

$$Y_L = W_L x(t) + V_L \tag{4.6}$$

where

$$Y_L = \begin{pmatrix} y(t-\tau_0) + \alpha_{t-\tau_0,t} + \beta_{t-\tau_0,t} \\ y(t-\tau_1) + \alpha_{t-\tau_1,t} + \beta_{t-\tau_1,t} \\ \vdots \\ y(t-\tau_{L-1}) + \alpha_{t-\tau_{L-1},t} + \beta_{t-\tau_{L-1},t} \end{pmatrix};$$

$$V_L = \begin{pmatrix} v(t-\tau_0) - \gamma_{t-\tau_0,t} \\ v(t-\tau_1) - \gamma_{t-\tau_1,t} \\ \vdots \\ v(t-\tau_{L-1} - \gamma_{t-\tau_{L-1},t} \end{pmatrix};\quad W_L = \begin{pmatrix} Ce^{-A\tau_0} \\ Ce^{-A\tau_1} \\ \vdots \\ Ce^{-A\tau_{L-1}} \end{pmatrix}.$$

It is evident that the noise term V_L has zero mean, i.e. $\mathbb{E}(V_L) = 0$. According to the properties of $\omega(t)$ and $v(k)$, together with *Fubini's theorem* and the shifting property of the *Dirac delta function*, the covariance matrix P, which is block symmetric, may be computed

as the following form (see Appendix A for more details):

$$\begin{aligned} P &= \mathbb{E}\left((V_L - \mathbb{E}(V_L))\,(V_L - \mathbb{E}(V_L))^{\mathrm{T}} \right) \\ &= \begin{pmatrix} S_0 & S_0 & \cdots & S_0 \\ S_0 & S_1 & \cdots & S_1 \\ \vdots & \vdots & \ddots & \vdots \\ S_0 & S_1 & \cdots & S_{L-1} \end{pmatrix} + \begin{pmatrix} R & 0 & \cdots & 0 \\ 0 & R & \ddots & \vdots \\ \vdots & \ddots & \ddots & 0 \\ 0 & \cdots & 0 & R \end{pmatrix} \end{aligned} \tag{4.7}$$

where the block elements S_k ($k \triangleq \min[i,j] = 0,1,...,L-1$) represent the following integral [Medvedev 1994]:

$$S_k = \int_{-\tau_k}^{0} C e^{As} G Q G^{\mathrm{T}} e^{A^{\mathrm{T}} s} C^{\mathrm{T}}\, \mathrm{d}s$$

Using the method of least-squares, the state estimation $\hat{x}(t)$ at time instant t is obtained from the solution of (4.6) as follows:

$$\hat{x}(t) = \left(W_L^{\mathrm{T}} P^{-1} W_L \right)^{-1} W_L^{\mathrm{T}} P^{-1} \hat{Y}_L \tag{4.8}$$

with

$$\hat{Y}_L = \begin{pmatrix} y(t-\tau_0) + \alpha_{t-\tau_0,t} + \hat{\beta}_{t-\tau_0,t} \\ y(t-\tau_1) + \alpha_{t-\tau_1,t} + \hat{\beta}_{t-\tau_1,t} \\ \vdots \\ y(t-\tau_{L-1}) + \alpha_{t-\tau_{L-1},t} + \hat{\beta}_{t-\tau_{L-1},t} \end{pmatrix} \tag{4.9a}$$

$$\hat{\beta}_{t-\tau_i,t} = \int_{t-\tau_i}^{t} C e^{A(t-\tau_i-\theta)} \phi(\hat{x}(\theta))\, \mathrm{d}\theta \tag{4.9b}$$

4.2.4 Unbiased estimation property of CD-UI-FMO

Note that the formulation of CD-UI-FMO from (4.3) to (4.9) is very similar to CD-FMO in the previous chapter. Therefore, for the sake of brevity, please refer to section 3.2.3 and Appendix B for the theoretical proofs of unbiased estimation property in deterministic case and in stochastic case.

4.3 Application to a Single-link Flexible Joint Robotic Arm

The dynamics (4.1) cover a broad class of systems with unknown input, and the proposed CD-UI-FMO is validated in this section through a single-link flexible joint robotic arm.

4.3.1 Nonlinear augmented continuous-discrete state-space model

The state-space model is described by (4.1) where components X_1 and X_3 are the displacement of link and rotor respectively while components X_2 and X_4 represent the velocity. The control input $u(t) = 2\sin(t)$, which represents the torque provided by the motor. The unknown input, $\xi(t) = -0.5\sin(t)$, represents two different kinds of actuator fault in this example, which is injected during $0.15s \sim 0.35s$. The standard derivation (SD) for all the process noise are set as $\sigma_{p_X} = \sigma_{p_\xi} = 0.01$, i.e. $Q_X = 0.01^2 \cdot \mathbf{I_4}$ and $Q_\xi = 0.01^2$. The noise distribution matrices G_0 and D_ξ are set to the identity matrix with proper dimensions. The matrices and parameters are set as follows with the physical parameters shown in Table 4.1:

$$A_0 = \begin{pmatrix} 0 & 1 & 0 & 0 \\ -\frac{k}{J_l} & -\frac{f_l}{J_l} & \frac{k}{J_l} & 0 \\ 0 & 0 & 0 & 1 \\ \frac{k}{J_m} & 0 & -\frac{k}{J_m} & -\frac{f_m}{J_m} \end{pmatrix}; \ \Phi(X) = \begin{pmatrix} 0 \\ -\frac{mlg_c}{J_l}\sin X_1 \\ 0 \\ 0 \end{pmatrix}; \ B_0 = F = \begin{pmatrix} 0 \\ 0 \\ 0 \\ \frac{1}{J_m} \end{pmatrix};$$

$$Q_X = \sigma_{p_X}^2 \cdot \mathbf{I_4} = \begin{pmatrix} 0.01^2 & 0 & 0 & 0 \\ 0 & 0.01^2 & 0 & 0 \\ 0 & 0 & 0.01^2 & 0 \\ 0 & 0 & 0 & 0.01^2 \end{pmatrix}; \ Q_\xi = \sigma_{p_\xi}^2 = 0.01^2; \ G_0 = \begin{pmatrix} 1 & 0 & 0 \\ 0 & 1 & 0 \\ 0 & 0 & 1 \end{pmatrix};$$

$$D_\xi = 1; \ C_0 = \begin{pmatrix} 1 & 0 & 0 & 0 \\ 0 & 0 & 1 & 0 \\ 0 & 0 & 0 & 1 \end{pmatrix}; \ R = \sigma_m \sigma_m^{\mathrm{T}} = \begin{pmatrix} 0.0002^2 & 0 & 0 \\ 0 & 0.0002^2 & 0 \\ 0 & 0 & 0.0003^2 \end{pmatrix}.$$

Table 4.1: Physical parameters (in SI units)

elastic constant $k = 2$	link mass $m = 4$
viscous friction coefficient for motor $f_m = 1$	motor inertia $J_m = 1$
viscous friction coefficient for link $f_l = 0.5$	link inertia $J_l = 2$
mass center $l = 0.5$	link inertia $g_c = 9.8$

Then, an augmented model can be constructed for CD-UI-FMO according to (4.2) as

$$\text{Augmented Model: } \begin{cases} \dot{x}(t) = Ax(t) + Bu(t) + \phi(x) + G\omega(t) \\ y(k) = Cx(k) + v(k) \end{cases}$$

with

$$x(t)=\begin{bmatrix}X(t)\\ \xi(t)\end{bmatrix};\ A=\begin{bmatrix}A_0 & F\\ 0 & 0\end{bmatrix};\ B=\begin{bmatrix}B_0\\ 0\end{bmatrix};\ \phi(x)=\begin{bmatrix}\Phi(X)\\ 0\end{bmatrix};\ \omega(t)=\begin{bmatrix}\omega_X(t)\\ \omega_\xi(t)\end{bmatrix};$$

$$G=\begin{bmatrix}G_0 & 0\\ 0 & D_\xi\end{bmatrix};\ Q\triangleq\sigma_p\sigma_p^{\mathrm{T}}=\begin{bmatrix}Q_X & q^{\mathrm{T}}\\ q & Q_\xi\end{bmatrix};\ C=\begin{bmatrix}C_0 & 0\end{bmatrix};\ R\triangleq\sigma_m\sigma_m^{\mathrm{T}}.$$

In next subsection, we will evaluate by simulations the performances of CD-UI-FMO on the unbiased state estimation property, the actuator fault (unknown input) detection and estimation based upon this augmented model in stochastic case, which includes the presence of measurement noise and process noise.

4.3.2 Optimal window length selection

As shown in Figure 4.1, with the augmented model, the variance of the estimation error $\tilde{x}=x-\hat{x}$ by the proposed CD-UI-FMO decreases asymptotically as the window length increasing. Meanwhile, it can also be seen in Figure 4.1 that the speed of the convergence became slower compared to the estimation error with the nominal model described as follows

$$\text{Nominal Model:}\begin{cases}\dot{X}(t)=A_0X(t)+B_0u(t)+\Phi(X)+G_0\omega_X(t)\\ y(k)=C_0X(k)+v(k)\end{cases}$$

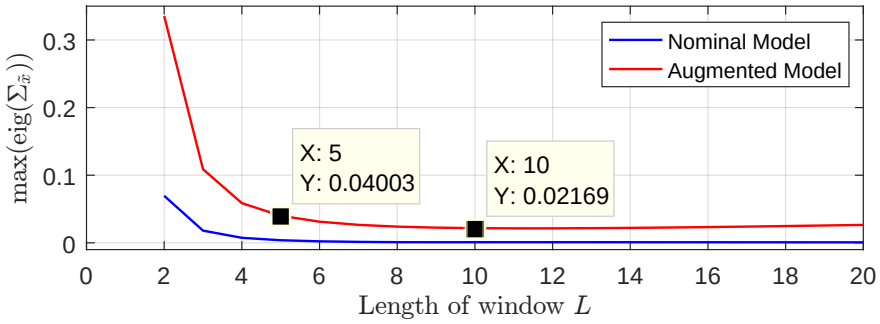

Figure 4.1: Convergence of the estimation error as window length L increasing

Since the nominal model does not need to deal with the unknown input during the state estimation while the CD-UI-FMO by the augmented model perform the state estimation and UI estimation in the same time, it seems logical that the convergence speed of the estimation error slows down. $L=10$ will be chosen in the rest of this chapter if it is not indicated.

4.3.3 Residuals comparison between different models

Give the notation of residual as $r(t) = y(t) - C\hat{x}(t)$, the residuals obtained by the nominal model and the augmented model are shown in Figure 4.2 - Figure 4.4 in the presence of the unknown input. By examining the figures, we can see that the unknown input injected during

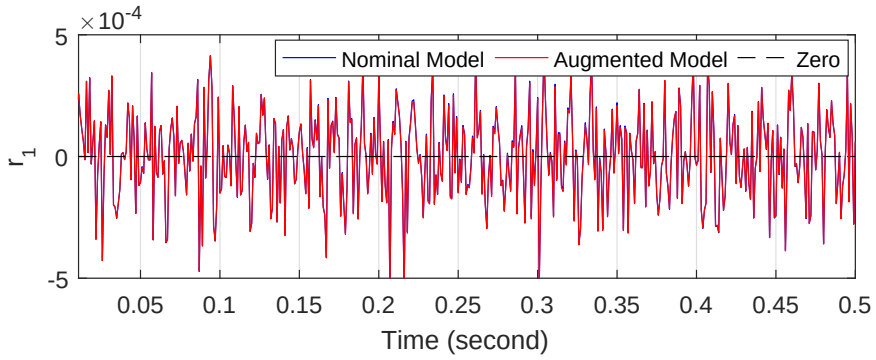

Figure 4.2: Residual r_1 comparison between nominal model and augmented model

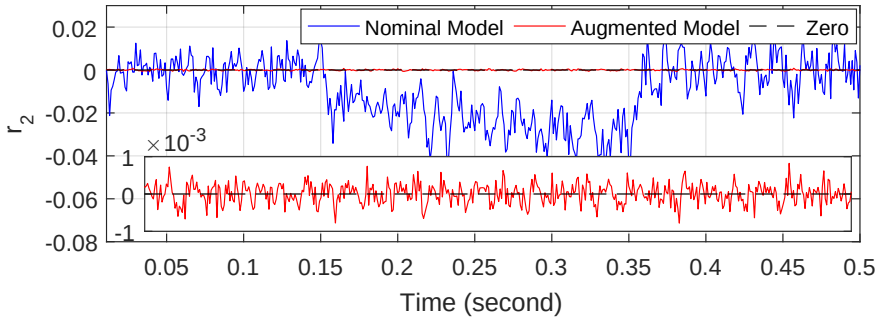

Figure 4.3: Residual r_2 comparison between nominal model and augmented model

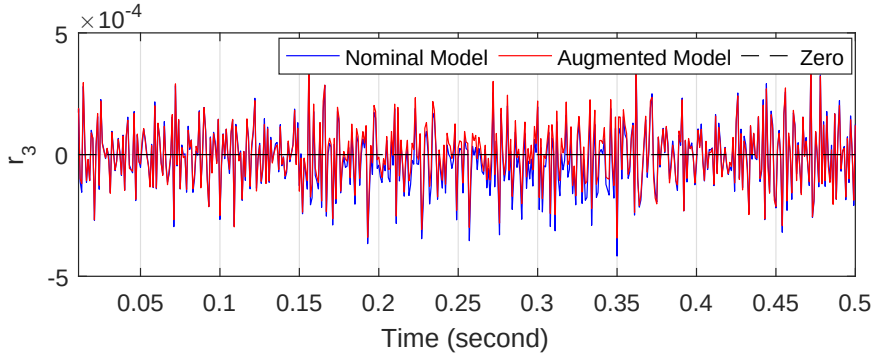

Figure 4.4: Residual r_3 comparison between nominal model and augmented model

$0.15s \sim 0.35s$ causes a significant bias on r_2, a slight mean shift on r_3 and no influence at all on r_1 when using the nominal model. According to the given UI distribution matrix F, we can see that the unknown input ξ has only been distributed to the fourth component $\dot{x}_4$. Then

through the matrices A_0 and C_0, we know that r_1 is not sensible to the UI injection in this example. The different influence level on r_2 and r_3 is caused by the numerical sensitivity coefficient, which will be theoretically studied in the future work. On the other hand, it is shown that the residuals are well centered around zero when using the proposed CD-UI-FMO, which appears to be normal since the UI is simultaneously estimated by the augmented state.

4.3.4 Unbiased estimation performance in stochastic case

The unbiased estimation performance will be illustrated in two aspects: using one single Monte Carlo (MC) run to show the convergence of estimation accuracy through different window length L; using multiple Monte Carlo simulations show the unbiased performance of both system state and unknown input estimations.

4.3.4.1 State and UI estimations by different window length

Let us firstly see the state estimations of x_2 in Figure 4.5 and UI estimations in Figure 4.6, it is quite obvious that the estimation performance has been significantly improved as the window length L increases, which means that the estimation accuracies converge with the

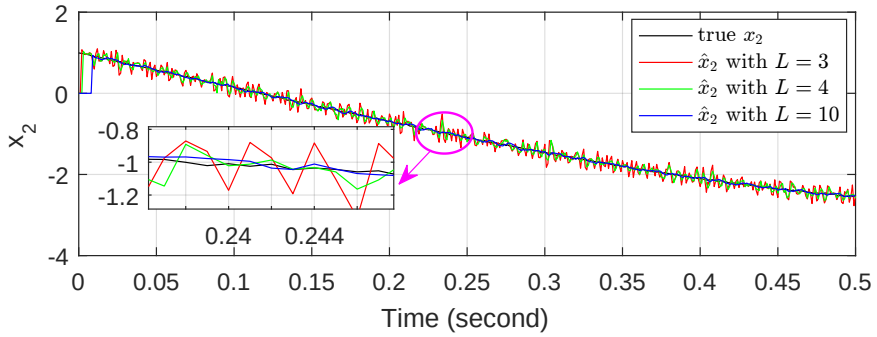

Figure 4.5: State estimations of x_2 through different window length L

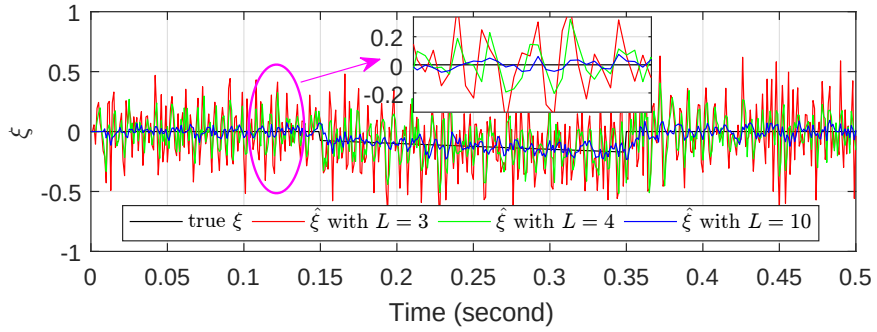

Figure 4.6: UI estimations through different window length L

augment of window length L, as depicted in Figure 4.1. This is only logical since the longer the window length L is, the more amount of information it will contain in each horizon, and therefore the better estimations we will obtain. Indeed, "information amount" can be said as the key essence of the moving horizon techniques introduced in previous chapter.

On the other hand, it seems that the same conclusions can not been straightforwardly drawn to the state estimations of components x_1, x_3 and x_4 shown in Figure 4.7 - Figure 4.9. As a matter of fact, it is necessary to notice that these three components (x_1, x_3 and x_4) are exactly the states we measured (see matrices C and C_0). This means that the informations of

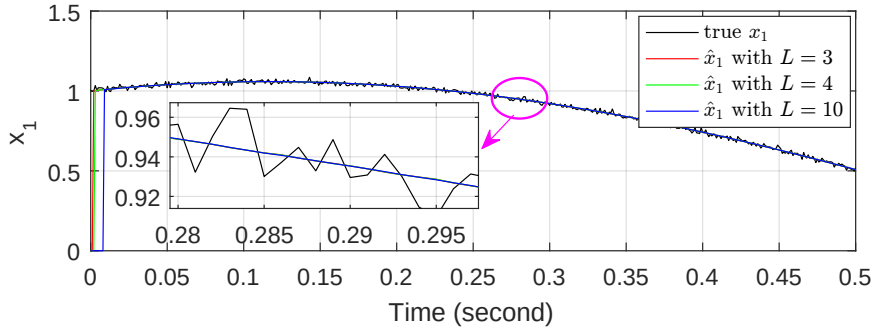

Figure 4.7: State estimations of x_1 through different window length L

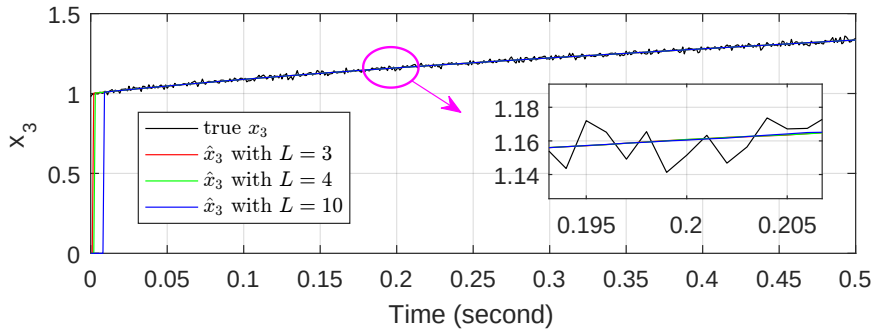

Figure 4.8: State estimations of x_3 through different window length L

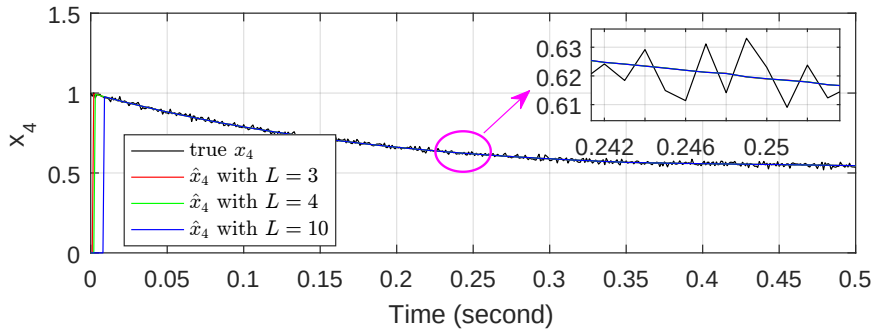

Figure 4.9: State estimations of x_4 through different window length L

these three states can be obtained at all sampling instants, and it is absolutely normal to have a good estimation performance on these three components even if the window length is set as $L = 1$. Moreover, since $L = 1$ is "long" enough to have good estimations on x_1, x_3 and x_4, when we employ $L \geq 1$, the *filter* role with respect to the noises can be seen as well by examining Figure 4.7 - Figure 4.9 (see subsection 3.3.3.2 of Chapter 3).

4.3.4.2 Unbiased state and UI estimations by MC simulations

As studied in previous chapter, we are going to perform multiple Monte Carlo simulations in this subsection to illustrate the unbiased estimation property of the proposed CD-UI-FMO in stochastic case, namely

$$\bar{\hat{x}} \triangleq \mathbb{E}(\hat{x}(t)) = x(t) \quad t \in [L \times T_s, +\infty)$$

with

$$\mathbb{E}(\hat{x}(t)) = \frac{1}{N_{\text{mc}}} \sum_{i=1}^{N_{\text{mc}}} \hat{x}^{(i)}$$

here, N_{mc} represents Monte Carlo simulation times. $N_{\text{mc}} = 500$ runs of Monte Carlo simulations have been performed to the nonlinear system with unknown input and the state estimation results are shown in Figure 4.10 - Figure 4.13. It can be seen by examining the figures that the original system states, with the presence of both noises (process and measurement) and unknown input, are well estimated around the true value with no bias after performing 500 runs of MC simulations.

Among the 500 different state estimations obtained by 500 runs of MC simulation, let us take the one with maximum dispersion *above* true state value as the *upper bound* of the estimations while the one with the maximum dispersion *below* the true state value is taken as the *lower bound*. In stochastic case, these two bounds happen to define an state estimation *envelope* where all the possible estimations are supposed to be within this envelope.

Now let us examine Figure 4.10 - Figure 4.13 again, it can be seen that the estimation upper and lower bounds of the proposed CD-UI-FMO are within a very small range, which means that even with the noises and UI, all the possible state estimations by CD-UI-FMO vary within a small range around real state x. This might be another verification of sufficient estimation precision of the proposed observer.

Finally, the unbiased estimation performance of the unknown input (actuator fault) $\xi = -0.5\sin(t)$ can be seen from Figure 4.14. The expectation of $\hat{\xi}$ with 500 runs of MC simulation is well located around the true value.

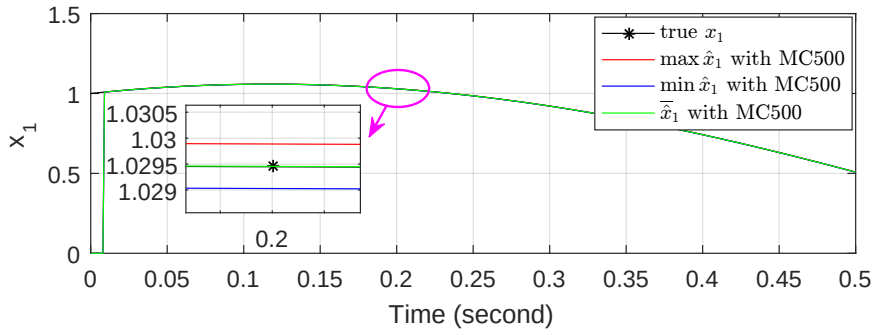

Figure 4.10: Expectation $\bar{\hat{x}}_1$ and upper and lower bound of $\hat{x}_1$ with $N_{\text{mc}} = 500$

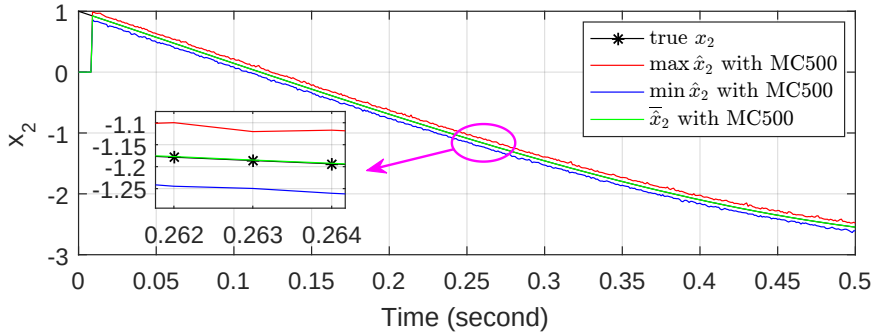

Figure 4.11: Expectation $\bar{\hat{x}}_2$ and upper and lower bound of $\hat{x}_2$ with $N_{\text{mc}} = 500$

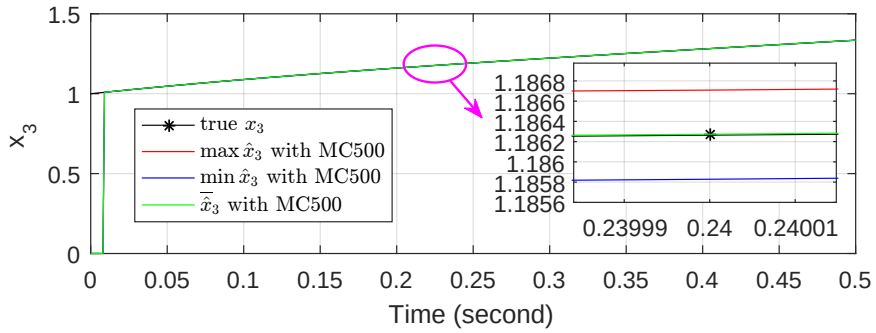

Figure 4.12: Expectation $\bar{\hat{x}}_3$ and upper and lower bound of $\hat{x}_3$ with $N_{\text{mc}} = 500$

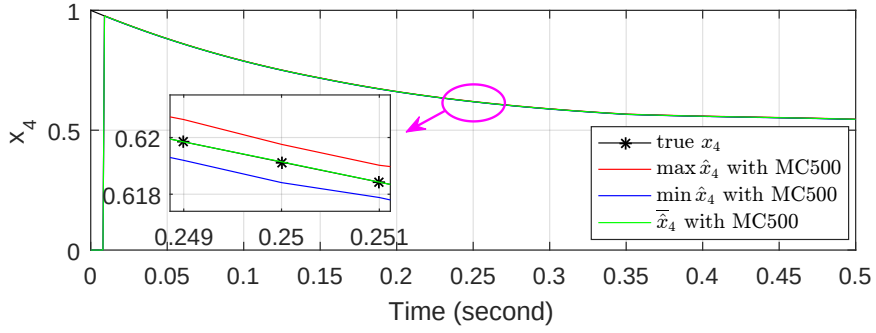

Figure 4.13: Expectation $\bar{\hat{x}}_4$ and upper and lower bound of $\hat{x}_4$ with $N_{\text{mc}} = 500$

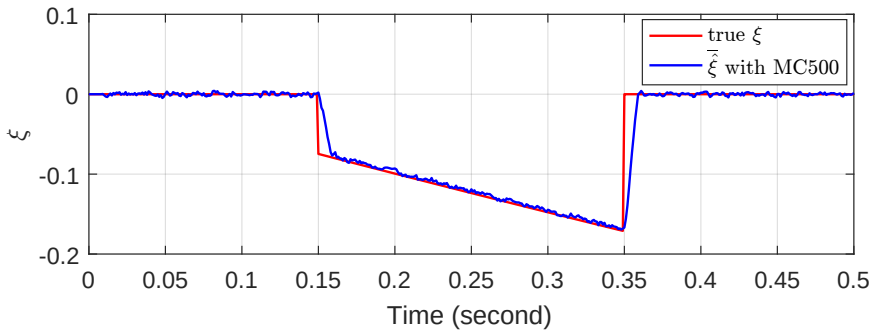

Figure 4.14: Expectation $\bar{\hat{\xi}}$ with $N_{\text{mc}} = 500$

4.3.5 Robustness with respect to measurement and process noises

In this section, the robustness of CD-UI-FMO with respect to measurement noise and process noise is analyzed through different scenarios in Table 4.2, which the standard derivation of measurement noise (SD_m) and process noise (SD_p) vary $\pm 50\,\%$ while the noise configurations of CD-UI-FMO doesn't change. The robustness analysis intends to see whether the proposed CD-UI-FMO has the ability to resist noise variations without adapting its noise configuration.

Table 4.2: Different scenarios of process noise and measurement noise

Noises scenarios of actual system		CD-UI-FMO parameter settings
Scenario 0 (S0)	$\text{SD}_m = \sigma_m$; $\text{SD}_p = \sigma_p$	$\text{SD}_m = \sigma_m$; $R = \sigma_m \sigma_m^{\text{T}}$ $\text{SD}_p = \sigma_p$; $Q = \sigma_p \sigma_p^{\text{T}}$
Scenario 1 (S1)	$\text{SD}_m = 0.5\sigma_m$; $\text{SD}_p = 0.5\sigma_p$	
Scenario 2 (S2)	$\text{SD}_m = 1.5\sigma_m$; $\text{SD}_p = 0.5\sigma_p$	
Scenario 3 (S3)	$\text{SD}_m = 0.5\sigma_m$; $\text{SD}_p = 1.5\sigma_p$	
Scenario 4 (S4)	$\text{SD}_m = 1.5\sigma_m$; $\text{SD}_p = 1.5\sigma_p$	

By performing $N_{\text{mc}} = 500$ runs of MC simulations with $L = 10$, the state estimation performance as well as the RMSEs are respectively shown in Figure 4.15 and Figure 4.16. The robustness of CD-UI-FMO can be well validated by examining these figures. Furthermore, it can be seen from the RMSEs in Figure 4.16 that estimation performance of Scenario S1 is always better than Scenario S4 since "overestimate" the real noises level is always better than "underestimate" the noises level for CD-UI-FMO. In the meantime, the RMSEs amplitudes also decrease one by one from "top" to "bottom" due to the filter performance explicated in subsection 3.3.3.2 of Chapter 3.

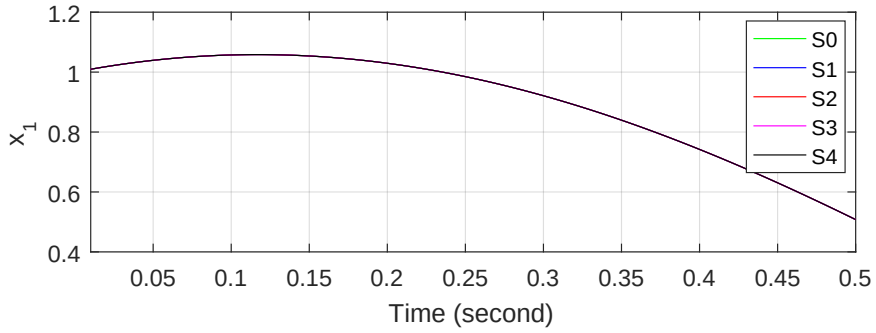

(a) $\hat{x}_1$ via different noise scenarios

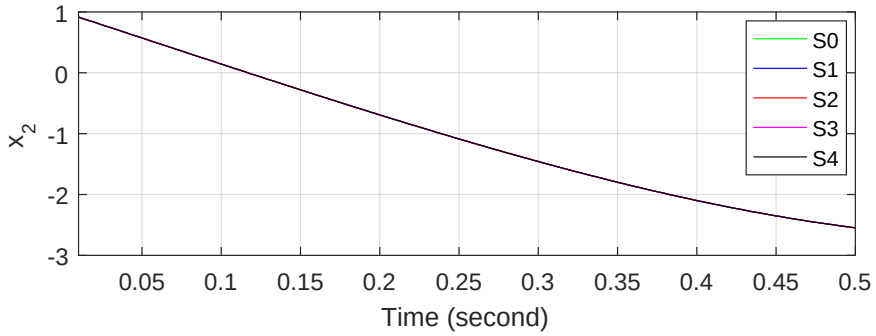

(b) $\hat{x}_2$ via different noise scenarios

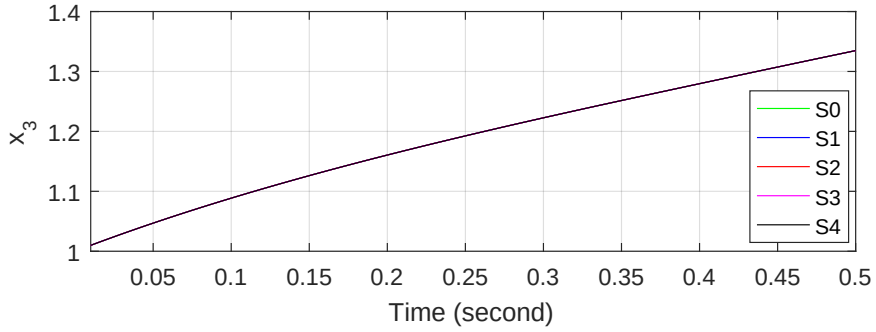

(c) $\hat{x}_3$ via different noise scenarios

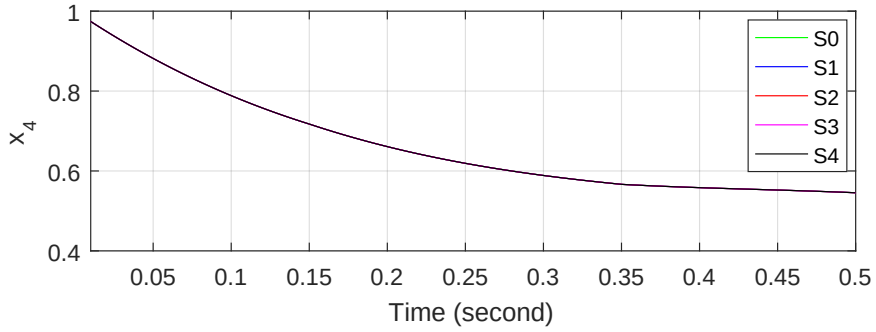

(d) $\hat{x}_4$ via different noise scenarios

Figure 4.15: Robustness analyses of $\hat{x}$ via different noise scenarios

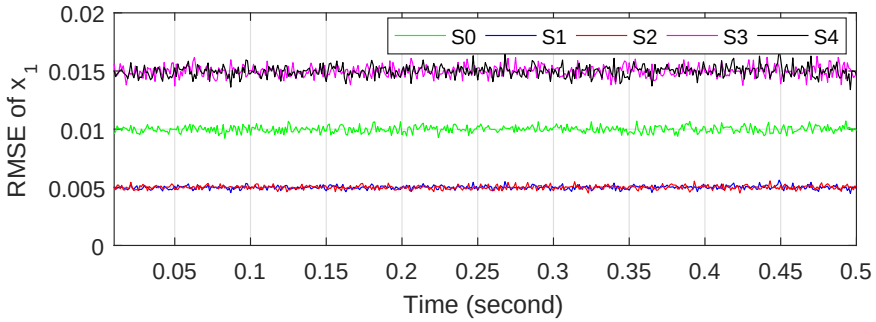

(a) RMSE of $\hat{x}_1$ via different noise scenarios

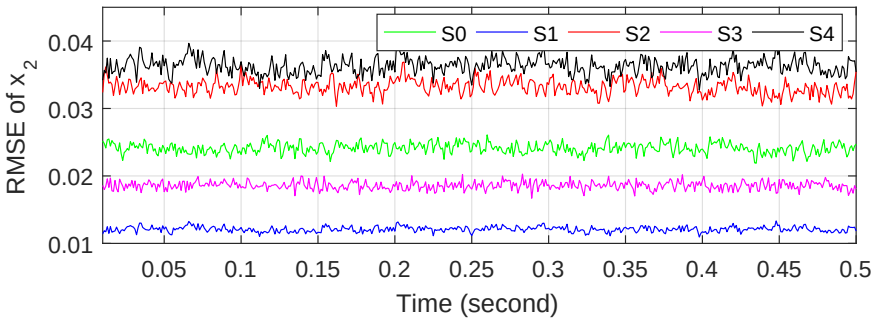

(b) RMSE of $\hat{x}_2$ via different noise scenarios

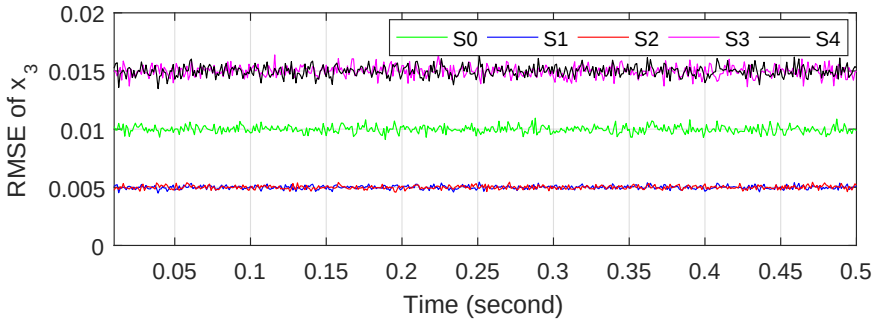

(c) RMSE of $\hat{x}_3$ via different noise scenarios

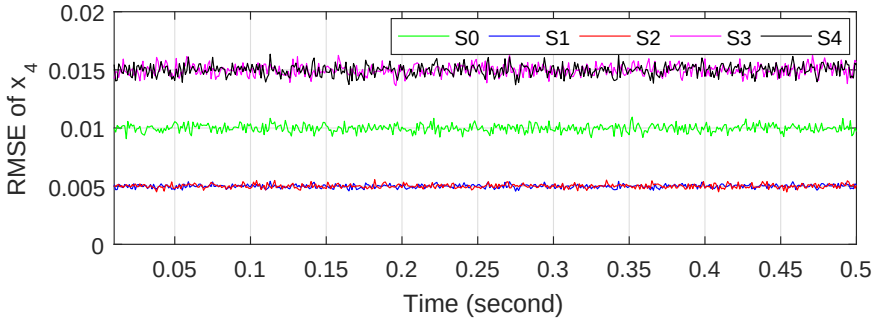

(d) RMSE of $\hat{x}_4$ via different noise scenarios

Figure 4.16: RMSE of $\hat{x}$ via different noise scenarios

It can be seen from Figure 4.17 that the unknown input estimation by CD-UI-FMO is robust as well facing different noise scenarios.

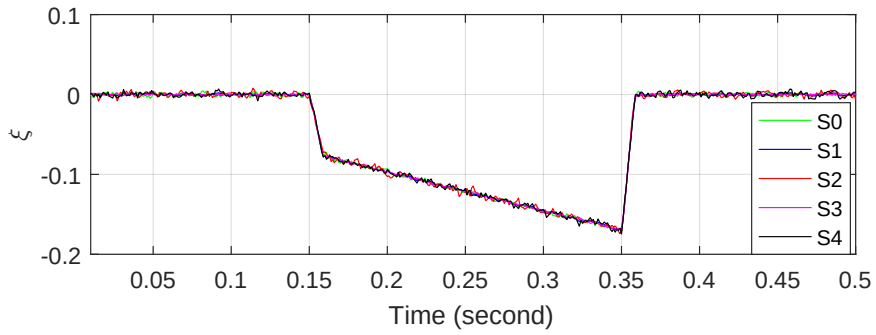

Figure 4.17: Robustness analyses of UI $\hat{\xi}$ via different noise scenarios

4.3.6 Performance with correlation coefficient $\rho_{\omega_\xi \omega_X} \neq 0$

The above analyses is performed when the state process noise ω_X and unknown input process noise ω_ξ are uncorrelated, i.e. $\rho_{\omega_\xi \omega_X} = 0$. What will happen when $\rho_{\omega_\xi \omega_X} \neq 0$?

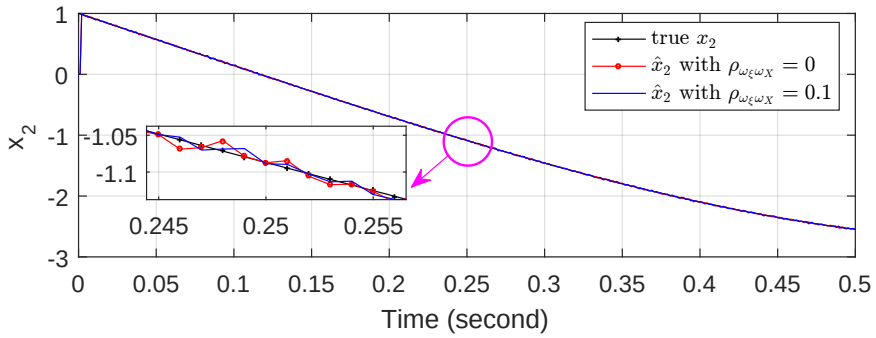

Figure 4.18: State estimation with correlated process noise

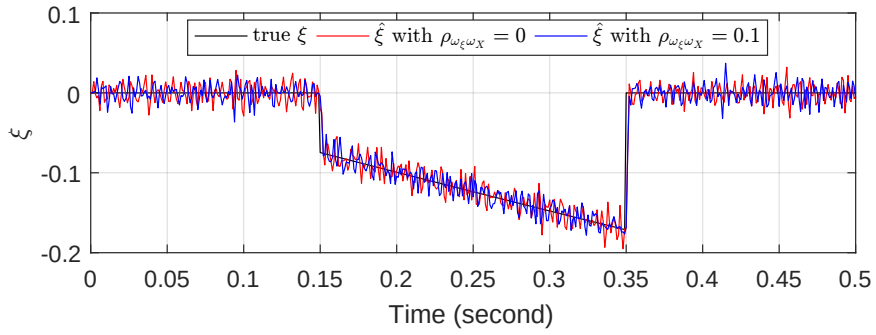

Figure 4.19: UI estimation with correlated process noise

Let us take $\rho_{\omega_\xi \omega_X} = 0.1$, in which case the process noise covariance matrix Q is no longer diagonal. Take the unmeasured component x_2 as a representative of state estimation, the performance of both state and UI estimations are shown in Figure 4.18 and Figure 4.19 with $L = 3$ and $N_{\text{mc}} = 500$. It seems that the performance of CD-UI-FMO remains good even with the correlated process noises, which can be consider as another efficient performance.

Now, let us only see Figure 4.6 and Figure 4.14 for the UI estimations obtained by the proposed CD-UI-FMO. On the one hand, the UI estimation in Figure 4.6 based on just one single run of MC simulation turns out to be a little bit noisy. Even though it can be improved by augmenting the window length L, the compute time and calculation burdens will augmented as well. On the other hand, the UI estimation performance in Figure 4.14 is indeed great due to the multiples runs of Monte Carlo simulations, however one of the major disadvantages of MC simulation is also the computer time. In addition, the UI in this thesis represents an actuator fault (without loss of generality). As previously introduced in Chapter 2 (see subsection 2.5.1), the first step of fault diagnosis procedure is fault detection, which is required to be as *quick* as possible. Apparently in this case, we do not want to perform fault detection neither after "multiple MC simulations" nor "with a super large window length L". This brings us to the exponentially weighted moving average (EWMA) algorithm introduced in next part, which trades off between fault estimation and fault detection effectiveness.

4.3.7 Actuator fault diagnosis by the EWMA algorithm

The exponentially weighted moving average (EWMA) [Cisar et al. 2010] algorithm is employed in this subsection to perform fault detection and estimation thanks to its well-known efficiency and filtering ability when facing small shifts. Compared to the previously used Cumulative Sum (CUSUM) algorithm, which is the sum of the entire process history, a weighted sum of the *recent* history would be more meaningful for the purpose of fault estimation (filtering). Furthermore, it might be worth noting that CUSUM algorithm uses the cumulative sum of the shift signal to detect the fault while EWMA uses directly the fault signal itself to perform the fault detection.

The following notations of EWMA are firstly defined: the upper control limit (UCL), center line (CL) and lower control limit (LCL) are defined as follows:

$$\begin{cases} \text{UCL} = \mu_{\text{target}} + n \cdot \sigma_{\text{target}} \sqrt{\dfrac{\lambda}{2-\lambda}\left[1-(1-\lambda)^{2i}\right]} \\ \text{CL} = \mu_{\text{target}} \\ \text{LCL} = \mu_{\text{target}} - n \cdot \sigma_{\text{target}} \sqrt{\dfrac{\lambda}{2-\lambda}\left[1-(1-\lambda)^{2i}\right]} \end{cases} \tag{4.10}$$

where i represent the sampling numbers (observations), the mean and SD values of the target data are respectively noted as μ_{target} and σ_{target}. n is used to represent the control limits (with respect to σ_{target}) of the target data while the weighted constant is represented by λ.

4.3.7.1 Actuator fault detection and estimation

Without the loss of generality, the target data is shown in Figure 4.20, which is the estimated actuator fault $\hat{\xi}$ obtained by CD-UI-FMO. Under the usual three-sigma rule, the detection by CUSUM is also shown in Figure 4.21. However, as mentioned before, CUSUM performs the fault detection by the cumulative sum of mean deviations and does not directly process the target data (actuator fault), we are going to use EWMA algorithm in next step.

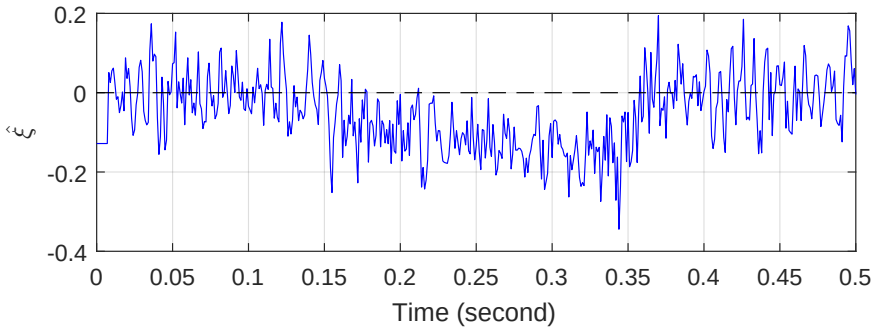

Figure 4.20: Actuator fault estimate by CD-UI-FMO

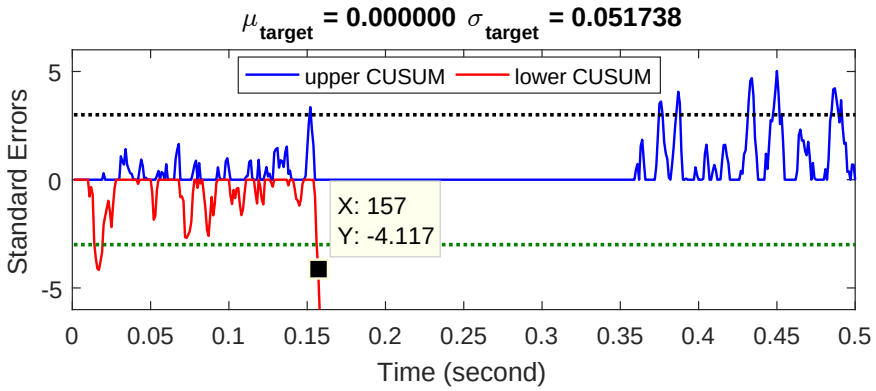

Figure 4.21: Actuator fault detection by CUSUM

In order to use the EWMA algorithm to deal with the estimated actuator fault $\hat{\xi}$ with $i = 500$ data, the target mean and SD values are set as $\mu_{\text{target}} = 0$ and $\sigma_{\text{target}} = 0.0517$, which obtains by CD-UI-FMO under the same parameter configuration as in Figure 4.20 but fault-free ($\xi = 0$). The control limits $n = 3$ (three-sigma rule), the weighted constant $\lambda = 0.2$.

It is shown in Figure 4.22 that the detection of actuator fault starting instant is $0.157s$ with a delay of $0.007s$ since the real fault occurring instant is $0.15s$. It is worth mentioned here that in this example five consecutive alarm points is used as decision rule for detecting pattern, "less than five consecutive points" is said to be a *false alarm*. It should be noted that the detecting pattern of false alarm can be adapted accordingly for actual physical systems [Montgomery 2013].

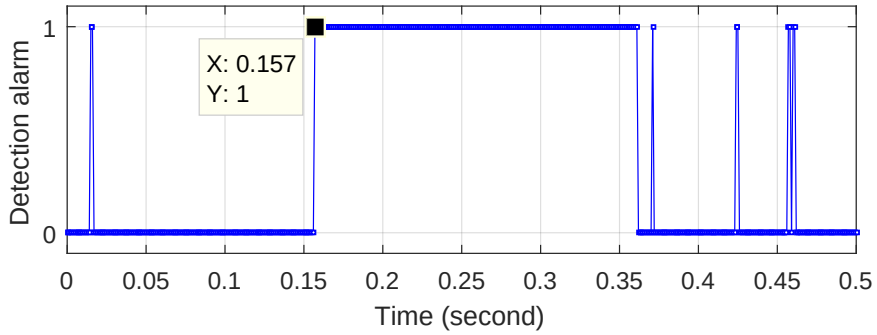

Figure 4.22: EWMA detection alarm of actuator fault $\xi = -0.5\sin(t)$

Compared to CUSUM in Figure 4.21, the fault starting instant seems the same, however, with EWMA, we also get the processed (filtered) fault estimation shown in Figure 4.23 thanks to the smooth factor λ. The examination of Figure 4.20 and Figure 4.23 makes it

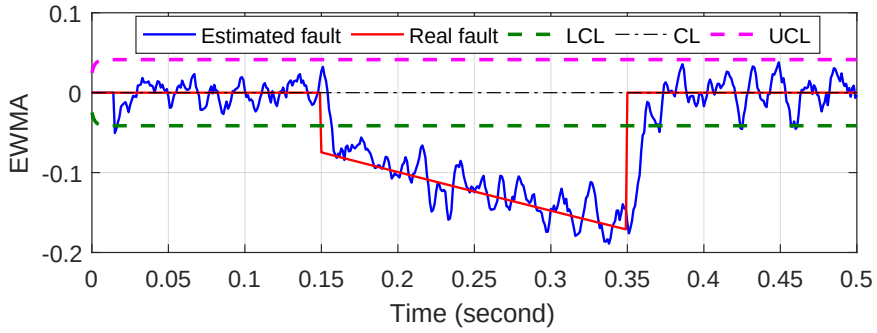

Figure 4.23: Estimation of actuator fault $\xi = -0.5\sin(t)$ via EWMA

clear that the proposed CD-UI-FMO in cooperation with the EWMA algorithm performs a great fault estimation of the unknown actuator fault ξ in noisy environments thanks to the efficiency and robustness of EWMA algorithm and CD-UI-FMO.

4.3.7.2 Minimum detection amplitude analyses

A ramp-shape actuator fault is injected to find out the minimum actuator fault amplitude for EWMA to detect with $n = 3$ and $\lambda = 0.2$ while $\mu_{\text{target}} = 0$ and $\sigma_{\text{target}} = 0.0517$. The detection

alarm by EWMA is shown in Figure 4.24, in which the detection instant is $t = 0.168s$. Meanwhile, as shown in Figure 4.25, the corresponding actuator fault estimated via EWMA at $t = 0.168s$ is $\hat{\xi}_{\min} = 0.0504$, which is said to be the minimal detection amplitude. As a

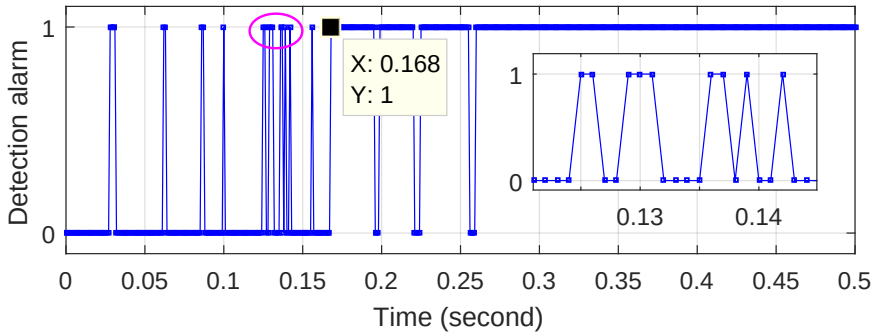

Figure 4.24: EWMA detection alarm of ramp-shape actuator fault

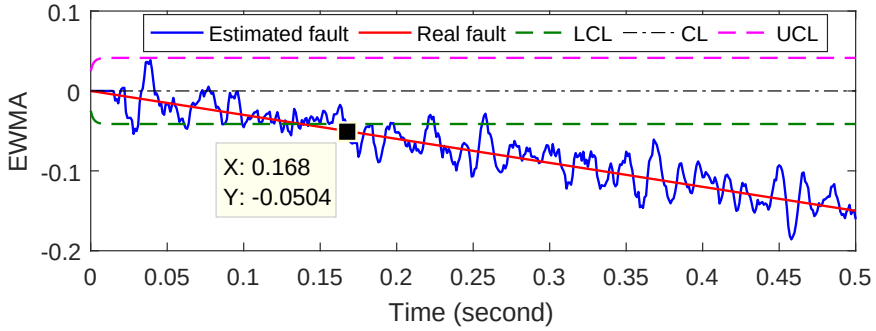

Figure 4.25: Minimal amplitude estimate by EWMA

matter of fact, if we substitute the parameter configuration value into the UCL and LCL defined in (4.10), we can calculate the detection bound as

$$\begin{aligned}
\xi_{\text{bound}}^{\lambda=0.2} &= \mu_{\text{target}} \pm n \cdot \sigma_{\text{target}} \sqrt{\frac{\lambda}{2-\lambda}\left[1-(1-\lambda)^{2i}\right]} \\
&= 0 \pm 3 \cdot 0.0517 \sqrt{\frac{0.2}{2-0.2}\left[1-(1-\lambda)^{2\times 500}\right]} \\
&= \pm 3 \cdot 0.0517 \sqrt{\frac{1}{9}} \\
&= 0.0517
\end{aligned}$$

it is straightforward that

$$\hat{\xi}_{\min} \approx \xi_{\text{bound}}^{\lambda=0.2} = 1 \cdot \sigma_{\text{target}}$$

Let us inject a constant actuator fault $\xi_{\min} = 0.055$ during $0.15s \sim 0.35s$ to test the obtained minimal amplitude. The fault detection results are shown in Figure 4.26 and Figure

4.27. We can see that the detection instant has a delay of $0.013s$ and also the detection alarm is not "steady", it all seems normal since it is the minimal fault amplitude.

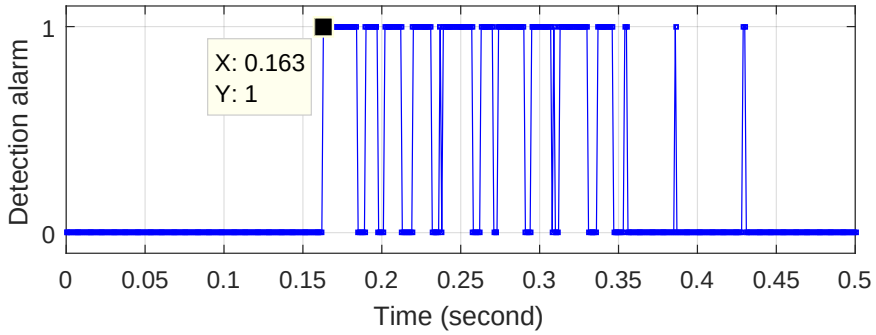

Figure 4.26: EWMA detection alarm of minimum amplitude ($\lambda = 0.2$)

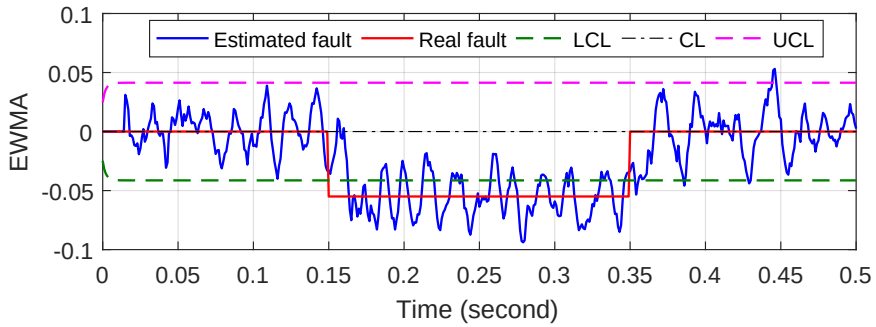

Figure 4.27: Minimal amplitude validation by EWMA ($\lambda = 0.2$)

Note that the parameter λ determines the rate at which "older" data enter into the calculation of the EWMA statistic. By the choice of weighting factor λ, the EWMA algorithm can be designed sensitive to a even small fault. For instant, if we take $\lambda = 0.1$ for actuator fault $\xi_{\min} = 0.055$, the detection alarm is shown in Figure 4.28, which becomes very "neat". However, the detection instant has a $1ms$ more delay which appears logical since a smaller value of λ gives more weight to older data.

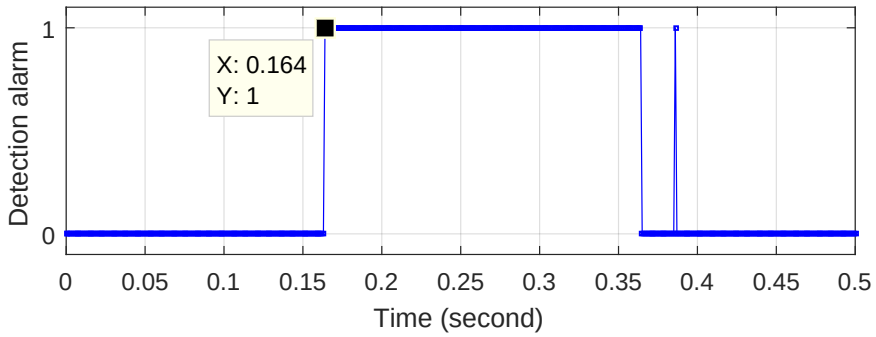

Figure 4.28: EWMA detection alarm of minimum amplitude ($\lambda = 0.1$)

In fact, when $\lambda = 0.1$, the detection bound becomes as

$$\begin{aligned}
\xi_{\text{bound}}^{\lambda=0.1} &= \mu_{\text{target}} \pm n \cdot \sigma_{\text{target}} \sqrt{\frac{\lambda}{2-\lambda}\left[1-(1-\lambda)^{2i}\right]} \\
&= 0 \pm 3 \cdot 0.0517 \sqrt{\frac{0.1}{2-0.1}\left[1-(1-\lambda)^{2\times 500}\right]} \\
&= \pm 3 \cdot 0.0517 \sqrt{\frac{1}{19}} \\
&= 0.0356 < \xi_{\text{min}} = 0.055
\end{aligned}$$

that's why the detection alarm in Figure 4.28 is much more better than Figure 4.26 for actuator fault $\xi_{\text{min}} = 0.055$. In order to further prove this, an actuator fault $\xi^* = 0.04$ is used as

$$\xi_{\text{bound}}^{\lambda=0.1} < \xi^* < \xi_{\text{bound}}^{\lambda=0.2}$$

It can be clearly seen from Figure 4.29 and Figure 4.30 that a detection alarm with $0.011s$ delay is provided when $\lambda = 0.1$ while there is no detection with $\lambda = 0.2$ as the alarms are always followed immediately by no alarms.

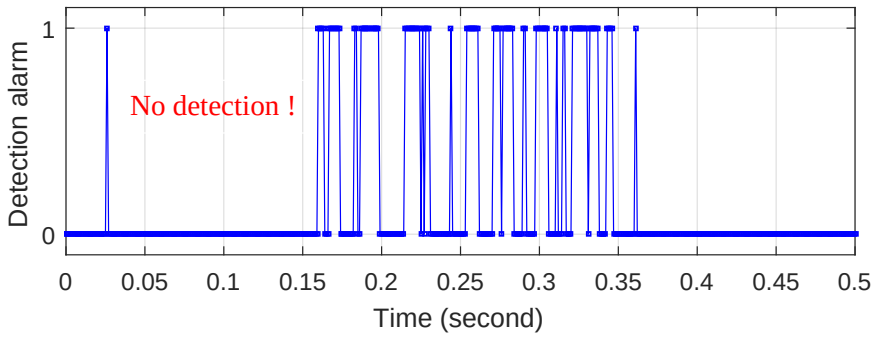

Figure 4.29: Detection alarm of $\xi^* = 0.04$ with $\lambda = 0.2$

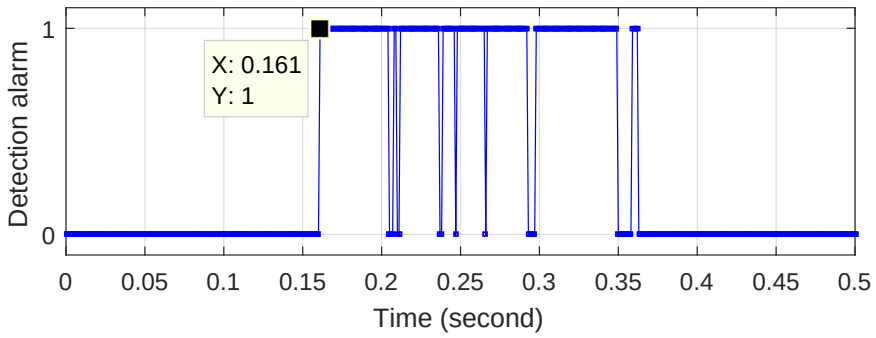

Figure 4.30: Detection alarm of $\xi^* = 0.04$ with $\lambda = 0.1$

Note that the EWMA control chart is very effective and can be designed by the configuration of the value of λ as well as control limit n, which there is no explicit formula of the best λ for a specific fault. It is possible to choose these parameters differently according to the practical requirements, such as noise level or fault-tolerant criteria.

4.4 Simultaneous actuator and sensor faults diagnosis

The proposed CD-UI-FMO in this chapter can also be used to provide more evidences for locating or isolating the simultaneous sensor and actuator faults. In order to show this performance, the following different multiple simultaneous faults (MSF) and single fault (SF) scenarios are used during $0.15s \sim 0.35s$:

1. **MSF1**: Sensor fault $\Delta_{y_1} = 0.01$ (a bias on y_1) & Actuator fault $\xi = -0.4$;
2. **MSF2**: Sensor fault $\Delta_{y_2} = 0.01$ (a bias on y_2) & Actuator fault $\xi = -0.4$;
3. **MSF3**: Sensor fault $\Delta_{y_3} = -0.01$ (a bias on y_3) & Actuator fault $\xi = -0.4$;
4. **SF1**: Sensor fault $\Delta_{y_1} = 0.01$ (a bias on y_1);
5. **SF2**: Sensor fault $\Delta_{y_2} = 0.01$ (a bias on y_2) ;
6. **SF3**: Sensor fault $\Delta_{y_3} = -0.01$ (a bias on y_3);
7. **SF4**: Actuator fault $\xi = -0.4$.

In the meantime, the following two fault patterns are defined according to the fault shape reflected on residuals $r(t) = y(t) - \hat{y}(t)$:

- **Peak** (p): the fault is reflected on residuals as the form of a peak;
- **Bias** (b): the fault is reflected on residuals as the form of a bias or shift.

CD-FMO (proposed in Chapter 3) with nominal model and CD-UI-FMO with augmented model are used to perform the fault diagnosis for the above three MSF scenarios, and the residuals $r(t)$ are respectively as

$$r(t) = y(t) - \hat{y}(t) = \begin{cases} y(t) - C_0\hat{X}(t) & \text{CD-FMO (with Nominal Model)} \\ y(t) - C\hat{x}(t) & \text{CD-UI-FMO (with Augmented Model)} \end{cases}$$

The resulting residuals obtained for different scenarios are respectively given from Figure 4.31 to Figure 4.37 and then summarized in Table.4.3.

By examining the residuals of the upper left part of Table.4.3, one may notice that if we only use the fault signature of CD-FMO, the multiple simultaneous faults MSF1 and MFS2 can not at all be isolated from each other since they have the same signature $[1,1,1]$. Let us now take into account the fault pattern as well, with which seems that MSF1 can be distinguished from MSF2 since the fault pattern on r_3 is "p&b" for MSF1 and "b" for MSF2. However, we still need more evidences to answer the following questions: Is it a multiple simultaneous faults? a sensor fault? an actuator fault? This brings us to the proposed CD-UI-FMO in this chapter.

Table 4.3: Multiple Simultaneous Faults Diagnosis by CD-UI-FMO

Scenarios	**Fault Signature (Pattern)** CD-FMO			**Fault Signature (Pattern)** CD-UI-FMO		
	r_1	r_2	r_3	r_1	r_2	r_3
MSF1	**1 (p)**	**1 (p&b)**	**1 (p&b)**	1 (p)	1 (p)	1 (p)
MSF2	**1 (p)**	**1 (p&b)**	**1 (b)**	1 (p)	1 (p)	0
MSF3	**0**	**1 (p&b)**	**1 (p&b)**	0	0	1 (p)
SF1	1 (p)	1 (p)	1 (p)	1 (p)	1 (p)	1 (p)
SF2	1 (p)	1 (p)	0	1 (p)	1 (p)	0
SF3	0	1 (p)	1 (p)	0	0	1 (p)
SF4	0	1 (b)	1 (b)	0	0	0

The residuals obtained by using CD-UI-FMO is given in the upper right part of Table.4.3. It can be seen that all the pattern "b" disappear while there only remains fault pattern "p" for MSF1, MSF2 and MSF3. Since CD-UI-FMO is designed to estimate the unknown input of systems, we can't help but thinking that the pattern "b" might represent an actuator fault while "p" signifies a sensor fault. The reason why pattern "b" disappears on residual is that the actuator fault is estimated and compensated by CD-UI-FMO.

This diagnosis result can be confirmed by the results of using CD-UI-FMO to diagnose the four single faults SF1-SF4, which are in the lower right part of Table.4.3. The signature $[0,0,0]$ for SF4 confirms that the compensated fault by CD-UI-FMO in MSF1-MSF3 is indeed actuator fault. Moreover, the fact that the signatures for SF1-SF3 are the same as MSF1-MSF3 proves there are also sensor faults in MSF1-MSF3. More specifically, according to the distinguished signatures $[1,1,1]$,$[1,1,0]$ and $[0,0,1]$, it can be known that there is sensor fault Δ_{y_1} in MSF1, Δ_{y_2} for MSF2 and Δ_{y_3} for MSF3. So far, the detection and isolation of the multiple simultaneous faults are realized with the aid of proposed CD-UI-FMO.

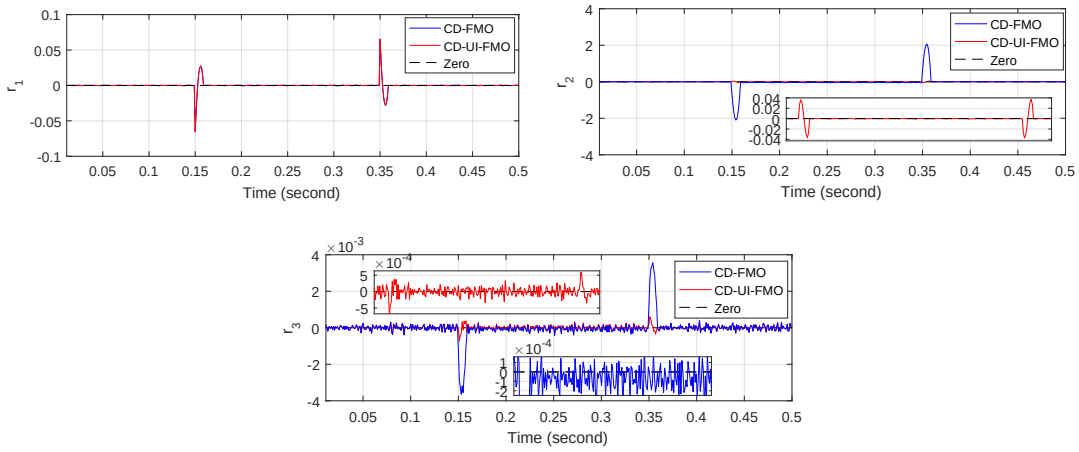

Figure 4.31: Residual *r* under the presence of MSF1

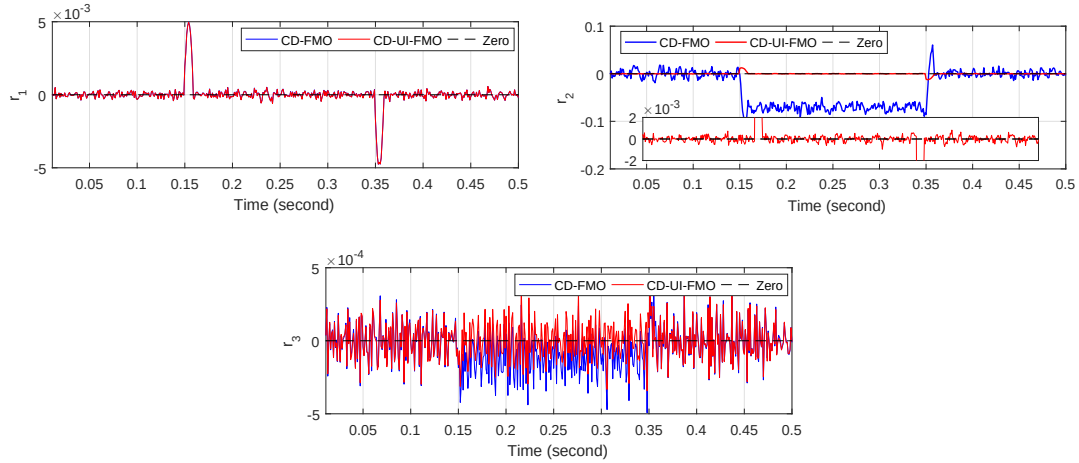

Figure 4.32: Residual *r* under the presence of MSF2

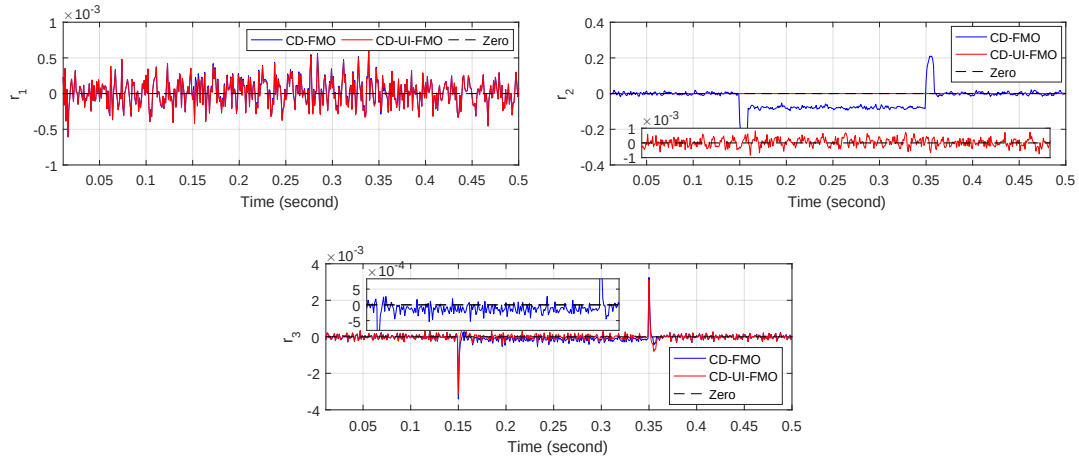

Figure 4.33: Residual *r* under the presence of MSF3

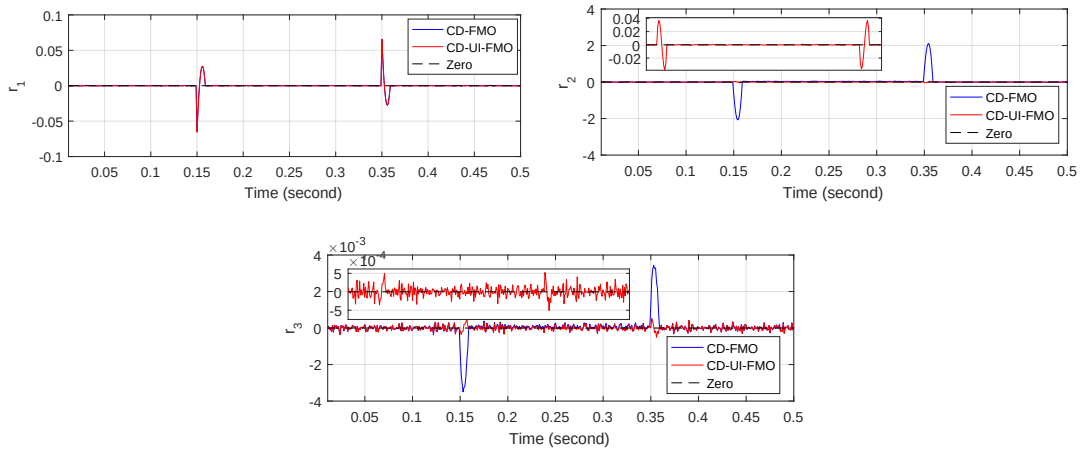

Figure 4.34: Residual r under the presence of SF1

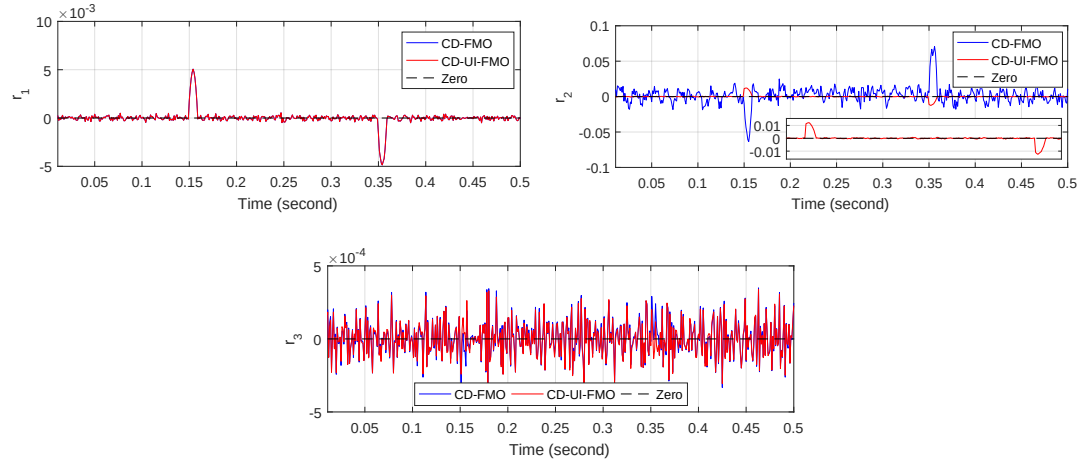

Figure 4.35: Residual r under the presence of SF2

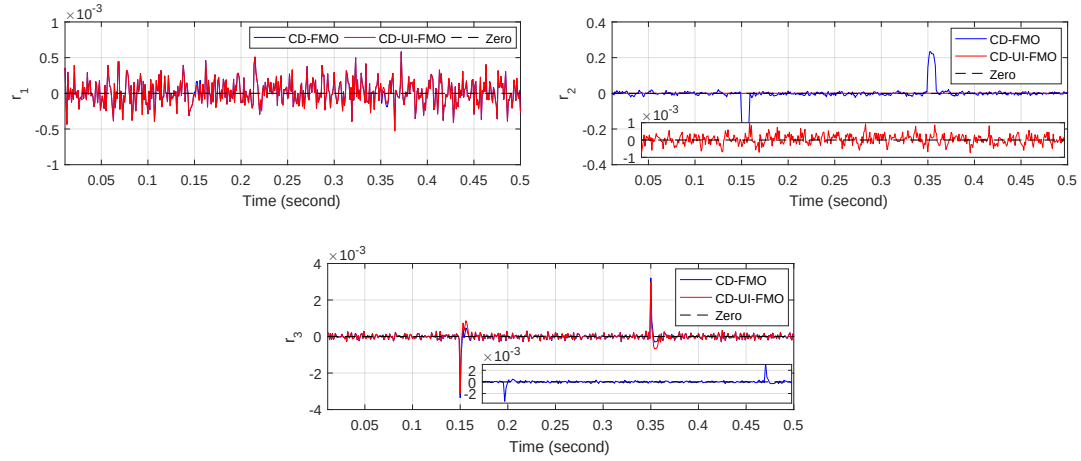

Figure 4.36: Residual r under the presence of SF3

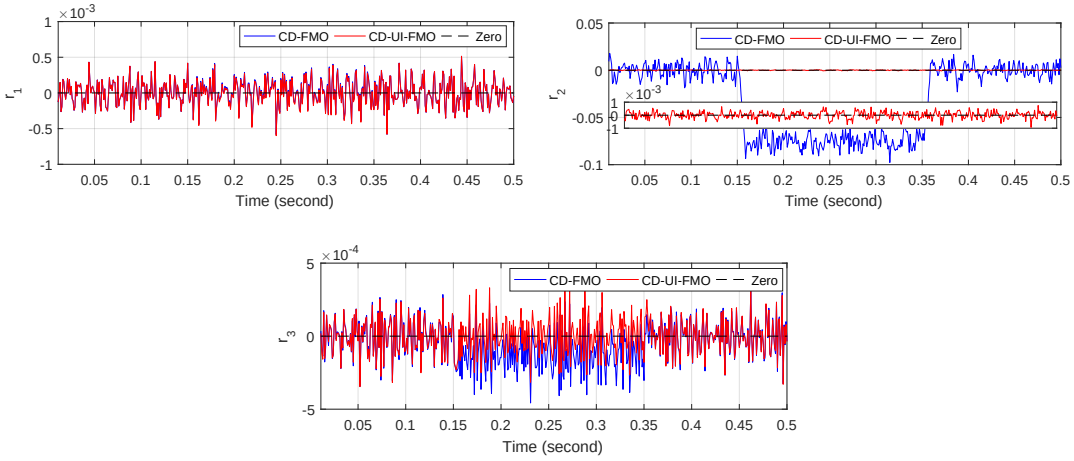

Figure 4.37: Residual r under the presence of SF4

4.5 Conclusion

A nonlinear unknown input finite memory observer has been developed in this chapter for a class of nonlinear Lipschitz systems with the aim of providing simultaneous unknown input and state estimations in the presence of both process and measurement noises. The unbiased estimation property can be proved theoretically and has also been fully verified in detail by Monte Carlo simulations in stochastic case. Additionally, the proposed method has been applied to implement actuator fault detection and estimation for a single-link robotic arm with the aid of the EWMA algorithm. Finally the proposed CD-UI-FMO is successfully used to perform fault diagnosis for multiple simultaneous sensor and actuator faults. The state and unknown input estimations accuracy and the effectiveness of fault diagnosis are well illustrated via the simulation results.

Chapter 5

Continuous-Discrete FMO Design for Nonlinear Time-Varying (NLTV) Systems

"If you thought that science was certain, well, that is just an error on your part."
- Richard P. Feynman

Contents of chapter

Résumé en français :

Dans ce chapitre, nous continuons à répondre à la troisième question posée à la fin du chapitre 3, qui concerne la synthèse d'observateur à mémoire finie pour une classe de systèmes non linéaires variant au cours du temps. À notre connaissance, l'observateur à mémoire finie n'a été conçu pour aucun *système en temps-continu et à temps-variant*, ni pour les systèmes linéaires en temps-continu, ni pour les systèmes non linéaires. Nous allons donc présenter la synthèse d'observateur à mémoire finie en commençant par des systèmes continus linéaires variant au cours du temps, une extension aux systèmes non linéaire sera ensuite réalisée sur la base du cas linéaire et de ce qui a été réalisé dans Chapitre 3.

Un observateur à mémoire finie sera tout d'abord développé pour les systèmes linéaires à temps-variant en présence de bruit de processus et bruit de mesure. Nous démontrerons que l'observateur proposé est *le meilleur estimateur non-biaisé* parmi tous les estimateurs linéaires. De plus, une formulation séquentielle de la variance de l'erreur d'estimation en fonction de la longueur de fenêtre sera également montrée, ce qui conduit naturellement à une stratégie pour sélectionner une longueur optimale. Un exemple numérique sera fourni pour vérifier les démonstrations théoriques dans le cas linéaire. L'observateur proposé sera ensuite étendu aux systèmes non linéaires par une brève démonstration et un exemple numérique à la fin de ce chapitre.

5.1 Introduction

In this chapter, we continue to deal with the third question raised at the end of Chapter 3, which requires to design a finite memory observer for a class of continuous-discrete nonlinear time-varying (CD-NLTV) systems. As far as we know, the finite memory observer (FMO) has not (yet) been designed for any *continuous time-varying* system, neither for continuous linear time-varying (LTV) systems, nor for nonlinear time-varying (NLTV) systems. Therefore, we choose to illustrate our design method by beginning with continuous-discrete linear time-varying (CD-LTV) systems, then a further extension to NLTV systems will be carried out based upon the CD-LTV case and what has been realized in Chapter 3.

A robust finite memory observer will be firstly developed for the CD-LTV systems in the presence of both process and measurement noises. It is going to be theoretically proved that the state estimation is unbiased and has the smallest dispersion among all the linear estimators, namely *best linear unbiased estimator (BLUE)*. In addition, a sequential form of the estimation error variance with respect to window length will be demonstrated as well, which naturally leads to be a theoretical strategy of selecting the window length. A numerical simulation example will be provided to verify the aforementioned theoretical proofs for

CD-LTV systems. Finally, the proposed observer will be extended to the CD-NLTV systems through a brief demonstration and a numerical example at the end of this chapter.

5.2 FMO Design for CD-LTV Systems (CD-LTV-FMO)

5.2.1 Problem statement and preliminaries

Let us consider the following continuous-time LTV systems with discrete measurements:

$$\dot{x}(t) = A(t)x(t) + B(t)u(t) + \omega(t) \tag{5.1a}$$
$$y(k) = C(t_k)x(t_k) + v(k) \tag{5.1b}$$

where $x \in \mathbb{R}^n$, $y \in \mathbb{R}^p$ and $u \in \mathbb{R}^q$ are continuous state vector, discrete measurement vector and continuous input vector, respectively. Without loss of generality, we assume that we have a constant sampling period of measurement T_s, i.e. $\exists k \in \mathbb{N} \mid t_k = k \times T_s$. In the meantime, $A(\cdot) \in \mathbb{R}^{n\times n}$, $B(\cdot) \in \mathbb{R}^{n\times q}$ and $C(\cdot) \in \mathbb{R}^{p\times n}$ are known matrices and are functions of time. Vectors v and ω represent Gaussian measurement noise and Gaussian process noise, respectively. v and ω are independent with the following properties:

$$\mathbb{E}[\omega(t)] = 0 \tag{5.2a}$$
$$\mathbb{E}[\omega(t_1)\omega^{\mathrm{T}}(t_2)] = Q \cdot \delta(t_1 - t_2) \tag{5.2b}$$
$$\mathbb{E}[v(k)] = 0 \tag{5.2c}$$
$$\mathbb{E}[v(k_1)v^{\mathrm{T}}(k_2)] = R \cdot \delta_{k_1,k_2} \tag{5.2d}$$

where $\delta(\cdot)$ is *Dirac delta function* and $\delta_{i,j}$ is *Kronecker delta function*. The proposed observer will be detailed in next section under the following assumptions:

Assumption 5.1. *The matrix $A(\cdot)$ is piecewise continuous or at least satisfies the integral condition (see Coddington and Levinson [1987]).*

Assumption 5.2. *The pair $(A(\cdot), C(\cdot))$ of CD-LTV systems (5.1) is observable.*

Meanwhile, **Definition** 2.8 and **Remark** 2.3 in Chapter 2 are recalled here:

Definition 5.1 (Observability Gramian)**.** *The pair $(A(\cdot), C(\cdot))$ is said to be observable at time t_0 if and only if there exists a finite $t_f > t_0$ such that $\mathbb{O}_{ob}(t_0, t_f) \in \mathbb{R}^{n\times n}$, defined by*

$$\mathbb{O}_{ob}(t_0, t_f) := \int_{t_0}^{t_f} \Phi^T(\theta, t_0) C^T(\theta) C(\theta) \Phi(\theta, t_0)\, \mathrm{d}\theta$$

is nonsingular. Here, $\Phi(\theta,t_0)\in\mathbb{R}^{n\times n}$ *is the state transition matrix from* t_0 *to* θ *with* $\theta\in[t_0,t_f]$*, which satisfies the following differential equation:*

$$\begin{cases}\dfrac{\mathrm{d}\Phi(\theta,t_0)}{\mathrm{d}\theta}=A(\theta)\Phi(\theta,t_0)\\ \Phi(t_0,t_0)=I_n \qquad I_n \text{ is identity matrix of size } n\end{cases}$$

This means that for any unknown initial state $x(0)$, there exists a finite $t_f>t_0$ so that it is possible to determine $x(0)$ by knowing inputs u and outputs y.

Remark 5.1. *It may be worth recalling here some properties of state transition matrix* $\Phi(\cdot,\cdot)$ *as follows [Chen 1999, Kailath 1980] :*

- $\Phi^{-1}(t_2,t_1)=\Phi(t_1,t_2)$ *for any* $t_1,t_2\in[t_0,t_f]$*;*
- $\Phi(t_1,t_3)\Phi(t_3,t_2)=\Phi(t_1,t_2)$ *for any* $t_1,t_2,t_3\in[t_0,t_f]$*;*
- $\Phi(t,t)=I_n$ *holds for all* $t\in[t_0,t_f]$*;*
- $\Phi(\cdot,\cdot)$ *is never singular.*
- *Given* $x(t_0)$ *at any time* t_0*, the state at any other time* t *is given by the mapping:* $x(t)=\Phi(t,t_0)x(t_0)$.

5.2.2 CD-LTV-FMO formulation

At each frozen time instant t, suppose that the discrete measurements are collected at L time instants $t-\tau_i$ with $i=0,1,...,L-1$. It is evident that $[t-\tau_{L-1},t]$ determines a time window.

By using the state transition matrix $\Phi(t,t-\tau_i)$, the state mapping between $x(t)$ and $x(t-\tau_i)$ can be obtained as [Kailath 1980]:

$$x(t)=\Phi(t,t-\tau_i)x(t-\tau_i)+\int_{t-\tau_i}^{t}\Phi(t,\theta)B(\theta)u(\theta)\,\mathrm{d}\theta+\int_{t-\tau_i}^{t}\Phi(t,\theta)\omega(\theta)\,\mathrm{d}\theta \tag{5.3}$$

Then, both sides of (5.3) are left multiplied by a coefficient matrix $C(t-\tau_i)\Phi^{-1}(t,t-\tau_i)$, which gives

$$\begin{aligned}C(t-\tau_i)\Phi^{-1}(t,t-\tau_i)x(t)=&\,C(t-\tau_i)x(t-\tau_i)\\&+\int_{t-\tau_i}^{t}C(t-\tau_i)\Phi^{-1}(t,t-\tau_i)\Phi(t,\theta)B(\theta)u(\theta)\,\mathrm{d}\theta\\&+\int_{t-\tau_i}^{t}C(t-\tau_i)\Phi^{-1}(t,t-\tau_i)\Phi(t,\theta)\omega(\theta)\,\mathrm{d}\theta\end{aligned} \tag{5.4}$$

Take into consideration the measurement equation (5.1b) at time instant $t-\tau_i$, then rearrange with the properties of $\Phi(\cdot,\cdot)$ in **Remark** 5.1, we have

$$C(t-\tau_i)\Phi(t-\tau_i,t)x(t) = y(t-\tau_i) + \alpha_{[t-\tau_i,t]} - \beta_{[t-\tau_i,t]} \tag{5.5}$$

with

$$\alpha_{[t-\tau_i,t]} = \int_{t-\tau_i}^{t} C(t-\tau_i)\Phi(t-\tau_i,\theta)B(\theta)u(\theta)\,\mathrm{d}\theta$$
$$\beta_{[t-\tau_i,t]} = v(t-\tau_i) - \int_{t-\tau_i}^{t} C(t-\tau_i)\Phi(t-\tau_i,\theta)\omega(\theta)\,\mathrm{d}\theta$$

Now we write equation (5.5) for every instant $t-\tau_i$ with $i = 0,1,...,L-1$ in the time window $[t-\tau_{L-1},t]$, a finite number of concatenated measurements can be denoted with respected to the system state at instant t, namely $x(t)$, as the following linear equation:

$$Y_L(t) = W_L(t)x(t) + V_L(t) \tag{5.6}$$

where

$$Y_L(t) = \begin{pmatrix} y(t-\tau_0)+\alpha_{[t-\tau_0,t]} \\ y(t-\tau_1)+\alpha_{[t-\tau_1,t]} \\ \vdots \\ y(t-\tau_{L-1})+\alpha_{[t-\tau_{L-1},t]} \end{pmatrix};$$

$$W_L(t) = \begin{pmatrix} C(t-\tau_0)\Phi(t-\tau_0,t) \\ C(t-\tau_1)\Phi(t-\tau_1,t) \\ \vdots \\ C(t-\tau_{L-1})\Phi(t-\tau_{L-1},t) \end{pmatrix};\ V_L(t) = \begin{pmatrix} \beta_{[t-\tau_0,t]} \\ \beta_{[t-\tau_1,t]} \\ \vdots \\ \beta_{[t-\tau_{L-1},t]} \end{pmatrix}.$$

It is evident that the noise term $V_L(t)$ has zero mean, that's $\mathbb{E}(V_L(t)) = 0$. In a manner similar to the calculation in **Appendix** A, the variance matrix $P_L(t)$ can be computed as follows [Medvedev 1994]:

$$\begin{aligned} P_L(t) &= \mathbb{E}\left((V_L(t) - \mathbb{E}(V_L(t)))\,(V_L(t) - \mathbb{E}(V_L(t)))^{\mathrm{T}} \right) = \mathbb{E}\left(V_L(t)V_L^{\mathrm{T}}(t) \right) \\ &= \begin{pmatrix} S_0(t) & S_0(t) & \cdots & S_0(t) \\ S_0(t) & S_1(t) & \cdots & S_1(t) \\ \vdots & \vdots & \ddots & \vdots \\ S_0(t) & S_1(t) & \cdots & S_{L-1}(t) \end{pmatrix} + \begin{pmatrix} R & 0 & \cdots & 0 \\ 0 & R & \ddots & \vdots \\ \vdots & \ddots & \ddots & 0 \\ 0 & \cdots & 0 & R \end{pmatrix} \end{aligned} \tag{5.7}$$

where the block elements $S_k(t)$ $(k \triangleq \min[i,j] = 0,1,...,L-1)$ represents the following integral:

$$S_k(t) = \int_{t-\tau_k}^{t} C(t-\tau_k)\Phi(t-\tau_k,\theta)Q\Phi^{\mathrm{T}}(t-\tau_k,\theta)C^{\mathrm{T}}(t-\tau_k)\,\mathrm{d}\theta$$

Using the method of least-squares, the state estimation $\hat{x}_L(t)$ at time instant t could be directly obtained from the least-squares solution of (5.6) as follows:

$$\begin{aligned}\hat{x}_L(t) &= \arg\min \frac{1}{2}||Y_L(t) - W_L(t)x(t)||^2_{P_L^{-1}(t)} \\ &= \left[W_L^{\mathrm{T}}(t)P_L^{-1}(t)W_L(t)\right]^{-1} W_L^{\mathrm{T}}(t)P_L^{-1}(t)Y_L(t)\end{aligned} \tag{5.8}$$

so far we obtain the analytical form of the finite memory observer for continuous-time LTV systems with discrete noisy measurements.

5.3 Estimation Error Properties Analyses: “BLUE”

In this section, we are going to theoretically prove by two steps that the proposed CD-LTV-FMO is the *best linear unbiased estimator (BLUE)* for the continuous-discrete linear time-varying systems.

5.3.1 Unbiased estimation proof

Theorem 5.1. *Let $\varepsilon_L(t) = \hat{x}_L(t) - x(t), t \geq L \times T_s$, represents the estimation error of the proposed observer (5.8), then in the case of fault-free, we have:*

$$\begin{aligned}\mathbb{E}[\varepsilon_L(t)] &= 0 \\ Var(\varepsilon_L(t)) &= \left[W_L^T(t)P_L^{-1}(t)W_L(t)\right]^{-1}\end{aligned}$$

Proof. First of all, the following equation can be directly obtained according to (5.5)

$$y(t-\tau_i) = C(t-\tau_i)\Phi(t-\tau_i,t)x(t) - \alpha_{[t-\tau_i,t]} + \beta_{[t-\tau_i,t]} \tag{5.9}$$

Let ρ_i with $i = 1,2,\cdots,L-1$ represents the i-th column of matrix $P_L^{-1}(t)$, namely

$$P_L^{-1}(t) \triangleq [\rho_1(t), \rho_2(t), \cdots, \rho_{L-1}(t)] \tag{5.10}$$

Consider rewriting $\hat{x}(t)$ in (5.8) as follows:

$$\hat{x}_L(t) = \Omega_L^{-1}(t) \sum_{i=0}^{L-1} \left\{ \Phi^{\mathrm{T}}(t-\tau_i,t) C^{\mathrm{T}}(t-\tau_i) \rho_i(t) \left[y(t-\tau_i) + \alpha_{[t-\tau_i,t]} \right] \right\} \tag{5.11}$$

where

$$\Omega_L(t) \triangleq W_L^{\mathrm{T}}(t) P_L^{-1}(t) W_L(t) = \sum_{i=0}^{L-1} \Phi^{\mathrm{T}}(t-\tau_i,t) C^{\mathrm{T}}(t-\tau_i) \rho_i(t) C(t-\tau_i) \Phi(t-\tau_i,t) \tag{5.12}$$

Substitute $y(t-\tau_i)$ in (5.11) with (5.9), then rearrange it with (5.12) as

$$\begin{aligned}
\hat{x}_L(t) &= \Omega_L^{-1}(t) \sum_{i=0}^{L-1} \left\{ \Phi^{\mathrm{T}}(t-\tau_i,t) C^{\mathrm{T}}(t-\tau_i) \rho_i(t) \left[C(t-\tau_i) \Phi(t-\tau_i,t) x(t) + \beta_{[t-\tau_i,t]} \right] \right\} \\
&= \Omega_L^{-1}(t) \Omega_L(t) x(t) + \Omega_L^{-1}(t) \sum_{i=0}^{L-1} \left\{ \Phi^{\mathrm{T}}(t-\tau_i,t) C^{\mathrm{T}}(t-\tau_i) \rho_i(t) \beta_{[t-\tau_i,t]} \right\} \\
&= x(t) + \Omega_L^{-1}(t) \sum_{i=0}^{L-1} \left\{ \Phi^{\mathrm{T}}(t-\tau_i,t) C^{\mathrm{T}}(t-\tau_i) \rho_i(t) \beta_{[t-\tau_i,t]} \right\} \\
&= x(t) + \Omega_L^{-1}(t) W_L^{\mathrm{T}}(t) P_L^{-1}(t) V_L(t)
\end{aligned}$$

which yields

$$\varepsilon_L(t) = \hat{x}_L(t) - x(t) = \Omega_L^{-1}(t) W_L^{\mathrm{T}}(t) P_L^{-1}(t) V_L(t) \tag{5.13}$$

Since only the noise term $V_L(t)$ in $\varepsilon_L(t)$ is stochastic and $V_L(t)$ is independent of the other terms, it is then straightforward that

$$\mathbb{E}[\varepsilon_L(t)] = \Omega_L^{-1}(t) W_L^{\mathrm{T}}(t) P_L^{-1}(t) \mathbb{E}[V_L(t)] = 0 \tag{5.14}$$

we know that $(\Omega_L^{-1}(t))^{\mathrm{T}} = \Omega_L^{-1}(t)$ and $(P_L^{-1}(t))^{\mathrm{T}} = P_L^{-1}(t)$ are symmetric, then

$$\begin{aligned}
Var(\varepsilon_L(t)) &= \mathbb{E}[(\varepsilon_L(t) - \mathbb{E}[\varepsilon_L(t)]) (\varepsilon_L(t) - \mathbb{E}[\varepsilon_L(t)])^{\mathrm{T}}] = \mathbb{E}[\varepsilon_L(t) \varepsilon_L^{\mathrm{T}}(t)] \\
&= \mathbb{E}[\Omega_L^{-1}(t) W_L^{\mathrm{T}}(t) P_L^{-1}(t) V_L(t) V_L^{\mathrm{T}}(t) P_L^{-1}(t) W_L(t) \Omega_L^{-1}(t)] \\
&= \Omega_L^{-1}(t) W_L^{\mathrm{T}}(t) P_L^{-1}(t) \mathbb{E}[V_L(t) V_L^{\mathrm{T}}(t)] P_L^{-1}(t) W_L(t) \Omega_L^{-1}(t) \\
&= \Omega_L^{-1}(t) W_L^{\mathrm{T}}(t) P_L^{-1}(t) P_L(t) P_L^{-1}(t) W_L(t) \Omega_L^{-1}(t) \\
&= \Omega_L^{-1}(t) \Omega_L(t) \Omega_L^{-1}(t) \\
&= \Omega_L^{-1}(t)
\end{aligned} \tag{5.15}$$

The proof is completed. ■

It may be worth to compare the above unbiased proof for time-varying systems with the proof of **Theorem** 3.1 in Chapter 3 and the one in **Appendix** B for nonlinear time-invariant systems, which appears to base on the same “spirit” through different “manners”.

Corollary 5.1. *From **Theorem** 5.1, it can be easily conclude that in the case of noise-free (without process noise and measurement noise) and fault-free, the proposed observer has the following estimation property :*

$$\hat{x}_L(t) = x(t) \qquad t \geq L \times T_s$$

Remark 5.2. *According to **Theorem** 5.1 and **Corollary** 5.1, it may be worth noting that the performance of the proposed observer doesn't depend on the initial condition. The fact of no initial value problem (IVP) gives the presented observer another advantage for real applications.*

Note that the proposed observer (5.8) is the least square solution of linear equation (5.6), which is the linear combination of $Y_L(t)$. We have also proved that it is an unbiased linear estimator in both deterministic and stochastic case. Now we are going to give in the next subsection the variance property of the estimation error.

5.3.2 Smallest variance proof

Theorem 5.2. *The proposed observer has the smallest variance (least dispersion) among all the other unbiased linear estimator. That is to say, if $\hat{x}^*(t)$ is another unbiased linear estimation of linear equation (5.6), let $\varepsilon^*(t) = \hat{x}^*(t) - x(t)$, then*

$$Var(\varepsilon^*(t)) \geq Var(\varepsilon_L(t)) = \Omega_L^{-1}(t)$$

Proof. Since $\hat{x}^*(t)$ is another unbiased linear estimation of (5.6), then let $\hat{x}^*(t) = \mathscr{A}(t)Y_L(t)$ where $\mathscr{A}(t) \in \mathbb{R}^{n \times pL}$ represents the linear combination. $\varepsilon^*(t)$ is then calculated as

$$\begin{aligned}
\varepsilon^*(t) &= \hat{x}^*(t) - x(t) \\
&= \mathscr{A}(t)Y_L(t) - x(t) \\
&= \mathscr{A}(t)\left[W_L(t)x(t) + V_L(t)\right] - x(t) \\
&= \left[\mathscr{A}(t)W_L(t) - I_n\right]x(t) + \mathscr{A}(t)V_L(t)
\end{aligned}$$

since $\mathbb{E}[V_L(t)] = 0$ and $\hat{x}^*(t)$ is another unbiased linear estimation, i.e. $\mathbb{E}(\varepsilon^*(t)) = 0$, then

$$\mathbb{E}(\varepsilon^*(t)) = \left[\mathscr{A}(t)W_L(t) - I_n\right]x(t) = 0 \quad \Rightarrow \quad \mathscr{A}(t)W_L(t) = I_n \tag{5.16}$$

which yields

$$\varepsilon^*(t) = \mathscr{A}(t)V_L(t) \tag{5.17}$$

Now let us suppose the linear combination $\mathscr{A}(t)$ has the following form

$$\mathscr{A}(t) = \Omega_L^{-1}(t)W_L^{\mathrm{T}}(t)P_L^{-1}(t) + \Gamma(t) \tag{5.18}$$

where $\Gamma(t) \in \mathbb{R}^{n\times pL}$ is a non-zero matrix. Then,

$$\begin{aligned}\mathscr{A}(t)W_L(t) &= \Omega_L^{-1}(t)W_L^{\mathrm{T}}(t)P_L^{-1}(t)W_L(t) + \Gamma(t)W_L(t)\\ &= \Omega_L^{-1}(t)\Omega_L(t) + \Gamma(t)W_L(t)\\ &= I_n + \Gamma(t)W_L(t)\end{aligned} \tag{5.19}$$

according to equation (5.16), we obtain

$$\Gamma(t)W_L(t) = 0 \tag{5.20}$$

Calculate the variance of estimation error $\varepsilon^*(t)$ based on (5.17) and (5.20) as follows

$$\begin{aligned}Var(\varepsilon^*(t)) &= \mathbb{E}\left[\varepsilon^*(t)\varepsilon^{*\mathrm{T}}(t)\right]\\ &= \mathscr{A}(t)\mathbb{E}\left[V_L(t)V_L^{\mathrm{T}}(t)\right]\mathscr{A}^{\mathrm{T}}(t)\\ &= \left[\Omega_L^{-1}(t)W_L^{\mathrm{T}}(t)P_L^{-1}(t) + \Gamma(t)\right]P_L(t)\left[\Omega_L^{-1}(t)W_L^{\mathrm{T}}(t)P_L^{-1}(t) + \Gamma(t)\right]^{\mathrm{T}}\\ &= \Omega_L^{-1}(t)W_L^{\mathrm{T}}(t)P_L^{-1}(t)P_L(t)P_L^{-1}(t)W_L(t)\Omega_L^{-1}(t) + \Gamma(t)\Gamma^{\mathrm{T}}(t)\\ &\quad + \Omega_L^{-1}(t)W_L^{\mathrm{T}}(t)P_L^{-1}(t)P_L(t)\Gamma^{\mathrm{T}}(t) + \Gamma(t)P_L(t)P_L^{-1}(t)W_L(t)\Omega_L^{-1}(t)\\ &= \Omega_L^{-1}(t)\Omega_L(t)\Omega_L^{-1}(t) + \Gamma(t)\Gamma^{\mathrm{T}}(t) + 0 + 0\\ &= \Omega_L^{-1}(t) + \Gamma(t)\Gamma^{\mathrm{T}}(t) + 0 + 0\\ &= Var(\varepsilon_L(t)) + \Gamma(t)\Gamma^{\mathrm{T}}(t)\end{aligned} \tag{5.21}$$

we know that $\Gamma(t)\Gamma^{\mathrm{T}}(t)$ is a positive semi-definite matrix, then it is obvious that $Var(\varepsilon^*(t))$ exceeds $Var(\varepsilon_L(t))$ by a positive semi-definite matrix, namely

$$Var(\varepsilon^*(t)) \geq Var(\varepsilon_L(t))$$

The proof is completed. ■

For continuous-time LTV systems (2.4), it is well known that Kalman filter (KF) is also one of the optimal estimators under certain conditions. This means that the variance of estimation error $\Sigma(t)$ by KF described by the following continuous-time Riccati equation

(CT-RE), will converge to Cramér-Rao Lower Bound (CRLB).

$$\text{CT-RE:} \qquad \dot{\Sigma}(t) = A(t)\Sigma(t) + \Sigma(t)A^{\mathrm{T}}(t) - \Sigma(t)C^{\mathrm{T}}(t)R^{-1}C(t)\Sigma(t) + Q(t) \tag{5.22}$$

In the meantime, for continuous-discrete LTV systems like (5.1), we should not include the R term in (5.22) because we are integrating P between measurement times, during which we do not have any measurements. Another way of looking at it is that in between measurement times we have measurements with infinite covariance ($R = \infty$), so the R-related term on the right side of (5.22) goes to zero. This gives us the following CD-RE for the time-update variance equation of CD Kalman filter [Simon 2006]:

$$\text{CD-RE:} \qquad \dot{\Sigma}(t) = A(t)\Sigma(t) + \Sigma(t)A^{\mathrm{T}}(t) + Q(t) \tag{5.23}$$

The variance comparison between the proposed CD-LTV-FMO and KF will be later given in the simulation section by an numerical example of LTV system.

5.4 Optimal Window Length Selection Strategy

There follows the section in which we are going to provide a window length selection strategy by showing how to determine “the minimal length" $L_{\min}$ and “the maximum length" $L_{\max}$, as been also used in Graton et al. [2014].

First of all, let $L_{\min}$ is chosen to guarantee the possibility that the proposed observer (5.8) exists, which depends whether the matrix multiplication term $W_L^{\mathrm{T}}(t)P_L^{-1}(t)W_L(t)$ in (5.8) is invertible. This means that each column of matrix $W_L(t)$ should be linearly independent. Nonetheless, this condition will always been satisfied thanks to **Assumption** 5.2. Therefore, $L_{\min}$ should be chosen to make sure that **Assumption** 5.2 is validated.

Since the variance of state estimation error $Var(\varepsilon_L(t))$ depends on L, we are therefore going to show the idea of selecting $L_{\max}$ by studying how does L has an influence on $Var(\varepsilon_L(t))$, the estimation performance indicator of the proposed observer. Let us note

$$\begin{aligned} \varepsilon_L(t) &= \hat{x}_L(t) - x(t) \\ \varepsilon_{L+1}(t) &= \hat{x}_{L+1}(t) - x(t) \end{aligned} \tag{5.24}$$

where $\hat{x}_L(t)$ and $\hat{x}_{L+1}(t)$, as illustrated in Figure 5.1, respectively represent the estimations with different window length,

Note that the related variances of $\varepsilon_L(t)$ and $\varepsilon_{L+1}(t)$ can be expressed as

$$\begin{aligned} Var(\varepsilon_L(t)) &= \Omega_L^{-1}(t) = \left[W_L^{\mathrm{T}}(t)P_L^{-1}(t)W_L(t)\right]^{-1} \\ Var(\varepsilon_{L+1}(t)) &= \Omega_{L+1}^{-1}(t) = \left[W_{L+1}^{\mathrm{T}}(t)P_{L+1}^{-1}W_{L+1}(t)\right]^{-1} \end{aligned} \tag{5.25}$$

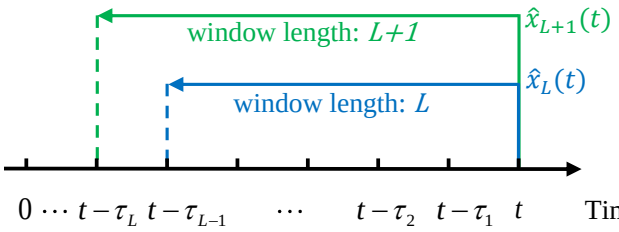

Figure 5.1: Illustration of state estimations $\hat{x}(t)$ with different window length L

In order to give the sequential formulation between $\Omega_L^{-1}(t)$ and $\Omega_{L+1}^{-1}(t)$, decompose the matrices $W_{L+1}(t)$ and $P_{L+1}(t)$ based on (5.6) and (5.7) as follows

$$W_{L+1}(t) = \begin{bmatrix} W_L(t) \\ w(t-\tau_L) \end{bmatrix} \quad P_{L+1}(t) = \begin{bmatrix} P_L(t) & \eta(t) \\ \eta^{\mathrm{T}}(t) & r^{\mathrm{T}}(t)r(t) \end{bmatrix} \tag{5.26}$$

where

$$\begin{aligned} w(t-\tau_L) &= C(t-\tau_L)\Phi(t-\tau_L,t) \\ r^{\mathrm{T}}(t)r(t) &= S_L(t)+R \\ \eta(t) &= [S_0(t),S_1(t),\cdots,S_{L-1}(t)]^{\mathrm{T}} \end{aligned} \tag{5.27}$$

Since $P_{L+1}(t)$ and $P_L(t)$ are positive-definite and invertible, the Schur complement of $P_L(t)$ in $P_{L+1}(t)$, namely

$$\begin{aligned} \mathbb{S}(t) &:= P_{L+1}(t)\backslash P_L(t) \\ &= r^{\mathrm{T}}(t)r(t) - \eta^{\mathrm{T}}(t)P_L^{-1}(t)\eta(t) \end{aligned} \tag{5.28}$$

is positive-definite (see Appendix C) and then invertible. Since $r^{\mathrm{T}}(t)r(t)$ and $\eta^{\mathrm{T}}(t)P_L^{-1}(t)\eta(t)$ in (5.28) are all symmetric matrices, $\mathbb{S}(t)$ is thus symmetric as well. Therefore, the inverse of $\mathbb{S}(t)$ is symmetric positive-definite and it can then be decomposed via *Cholesky decomposition* [Higham 2009] as

$$\mathbb{S}^{-1}(t) = U(t)U^{\mathrm{T}}(t) \tag{5.29}$$

where $U(t)$ is a lower triangular matrix with positive diagonal entries. Use the block-wise inversion [Zhang 2010], the inverse of $P_{L+1}(t)$ can be obtained as

$$P_{L+1}^{-1}(t) = \begin{bmatrix} P_L^{-1}(t) & 0 \\ 0 & 0 \end{bmatrix} + \begin{bmatrix} -P_L^{-1}(t)\eta(t) \\ I \end{bmatrix} U(t)U^{\mathrm{T}}(t) \begin{bmatrix} -\eta^{\mathrm{T}}(t)P_L^{-1}(t) & I \end{bmatrix} \tag{5.30}$$

according to (5.26) and (5.30), we can then write $\Omega_{L+1}(t)$ as

$$\begin{aligned} \Omega_{L+1}(t) &= W_{L+1}^{\mathrm{T}}(t)P_{L+1}^{-1}W_{L+1}(t) \\ &= \begin{bmatrix} W_L^{\mathrm{T}}(t) & w^{\mathrm{T}}(t-\tau_L) \end{bmatrix} \left\{ \begin{bmatrix} P_L^{-1}(t) & 0 \\ 0 & 0 \end{bmatrix} + \begin{bmatrix} -P_L^{-1}(t)\eta(t) \\ I \end{bmatrix} \right. \\ &\qquad \left. U(t)U^{\mathrm{T}}(t) \begin{bmatrix} -\eta^{\mathrm{T}}(t)P_L^{-1}(t) & I \end{bmatrix} \right\} \begin{bmatrix} W_L(t) \\ w(t-\tau_L) \end{bmatrix} \\ &= W_L^{\mathrm{T}}(t)P_L^{-1}(t)W_L(t) + D(t)D^{\mathrm{T}}(t) \\ &= \Omega_L(t) + D(t)D^{\mathrm{T}}(t) \end{aligned} \tag{5.31}$$

with

$$D(t) = \left[-W_L^{\mathrm{T}}(t)P_L^{-1}(t)\eta(t) + w^{\mathrm{T}}(t-\tau_L) \right] U(t) \tag{5.32}$$

then, the *Sherman-Morrison-Woodbury identity* [Press et al. 2007] yields

$$\begin{aligned} \Omega_{L+1}^{-1}(t) &= \left[\Omega_L(t) + D(t)D^{\mathrm{T}}(t) \right]^{-1} \\ &= \Omega_L^{-1}(t) - \Omega_L^{-1}(t)D(t) \left[I + D^{\mathrm{T}}(t)\Omega_L^{-1}(t)D(t) \right]^{-1} D^{\mathrm{T}}(t)\Omega_L^{-1}(t) \end{aligned} \tag{5.33}$$

It can be clearly seen from (5.33) that state estimation error variance of the proposed CD-LTV-FMO, i.e. $\Omega_L^{-1}(t)$, satisfies the matrix riccati equation with respect to window length L. Based on the properties of RE stated in De Souza et al. [1986], the variance will asymptotically converge to a minimal value as the window length L increases. That means when L increases to a certain size, the estimation error will no longer decrease, which seems reasonable since the amount of information brought by increasing the window length is not significant any more. Hence, $L_{\max}$ can be decided either by the maximum tolerance on the dispersion of estimation or by the L chosen when the following condition meets:

$$\Omega_{L+1}^{-1}(t) \approx \Omega_L^{-1}(t)$$

.

5.5 Numerical Example

Consider a continuous-time LTV system [Kailath 1980], described by a state-space model as

$$\dot{x}(t) = A(t)x(t) + B(t)u(t) + \omega(t)$$
$$y(k) = Cx(t_k) + v(k)$$

with the other parameters settings are as follows:

$$A(t) = \begin{pmatrix} -4/t & -2/t^2 \\ 1 & 0 \end{pmatrix}; \quad B(t) = \begin{pmatrix} 1 \\ 0 \end{pmatrix}; \quad Q = \sigma_p \sigma_p^{\mathrm{T}} = \begin{pmatrix} 1\times 10^{-5} & 0 \\ 0 & 1\times 10^{-5} \end{pmatrix};$$

$$u(t) = \sin(20t); \quad C(t) = (0 \quad 1); \quad R = \sigma_m^2 = \left(2\times 10^{-5}\right)^2.$$

Before all the analyses, we firstly determine the state transition matrix as:

$$\Phi(t,\theta) = \begin{pmatrix} -\theta^2 t^{-2} + 2\theta^3 t^{-3} & -2\theta t^{-2} + 2\theta^2 t^{-3} \\ \theta^2 t^{-1} - \theta^3 t^{-2} & 2\theta t^{-1} - \theta^2 t^{-2} \end{pmatrix}$$

which one can check it by calculating $\frac{\mathrm{d}\Phi(t,\theta)}{\mathrm{d}t}$ and verifying that it is certainly equal to $A(t)\Phi(t,\theta)$.

5.5.1 Influence of window length L

It can be seen that the proposed CD-LTV-FMO (5.8) depends on the window length L. The influence of L is going to analyses through different aspects with the given example.

5.5.1.1 Variance of estimation error with respect to L

As theoretically proved in (5.15), the estimation variance of the proposed CD-LTV-FMO is $\Omega_L^{-1}(t)$, it can been clearly seen from Figure 5.2(a) that at any time instant t, $\Omega_L^{-1}(t)$ converges asymptotically while window length L augments.

Now let us note $\Sigma_L(t) = (x(t) - \hat{x}(t))(x(t) - \hat{x}(t))^{\mathrm{T}}$ as the practical estimation variance at each instant t calculated by the numerical simulation, the same convergence with respect to window length L can then be found in Figure 5.2(b). Comparing to 5.2(a), the "roughness" of $\Sigma_L(t)$ at beginning (when $L = 2$) is due to the numerical computation in the presence of noises. Take $t = 0.3s$ as an example, a detailed comparison between $\Sigma_L(t)$ and $\Omega_L^{-1}(t)$ with respect to window length L is shown in Figure 5.2(c). In the steady phase, $\Sigma_L(t) = \Omega_L^{-1}(t)$ is validated, which means $\Omega_L^{-1}(t)$ is surely validated as the variance of the proposed CD-LTV-FMO.

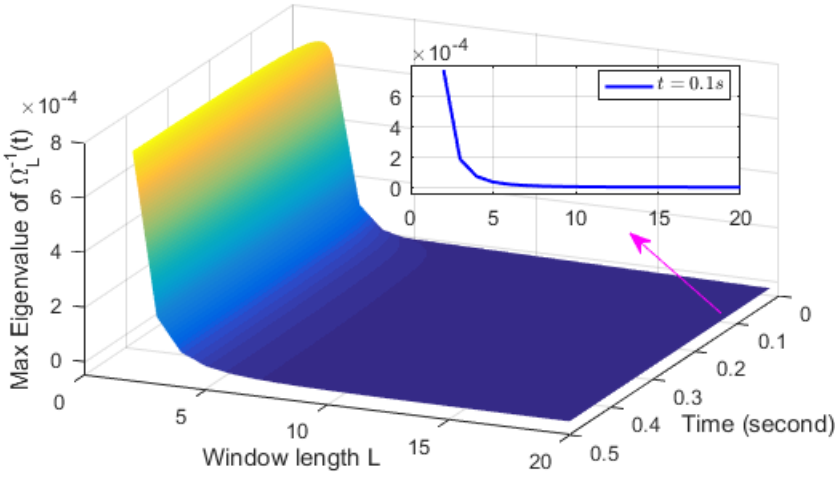

(a) Convergence of theoretical variance $\Omega_L^{-1}(t)$ over L

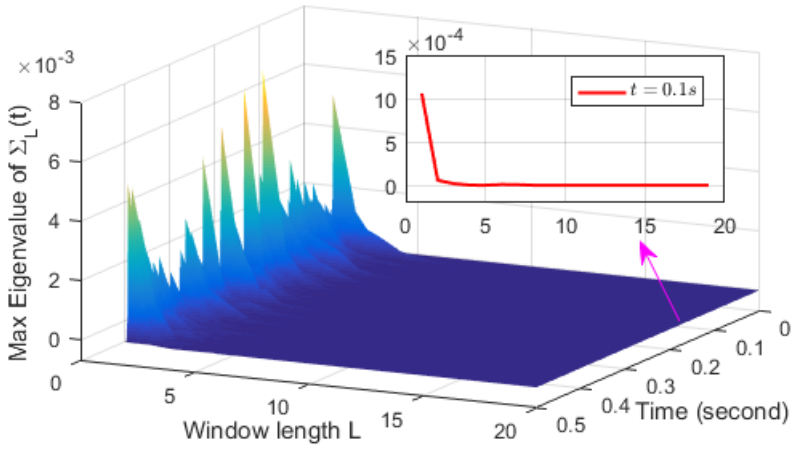

(b) Convergence of practical variance $\Sigma_L(t)$ over L

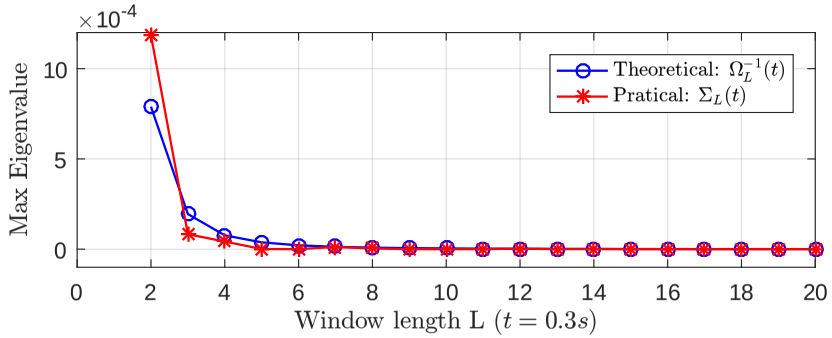

(c) Variance comparasion with respect to L when $t = 0.3s$

Figure 5.2: Convergence of variance with different window length L

5.5.1.2 Estimation performance with respect to L

As depicted in Figure 5.3 and Figure 5.4, the influence of window length L on the state estimation performance can be examined by comparing with true state. The longer the window length L is, the better the estimation is. Meanwhile, as usual, the window length L apparently has more impact on the state component without measurement since the measured state has enough amount of significant information and the unmeasured one mainly obtains the information by augmenting window length L.

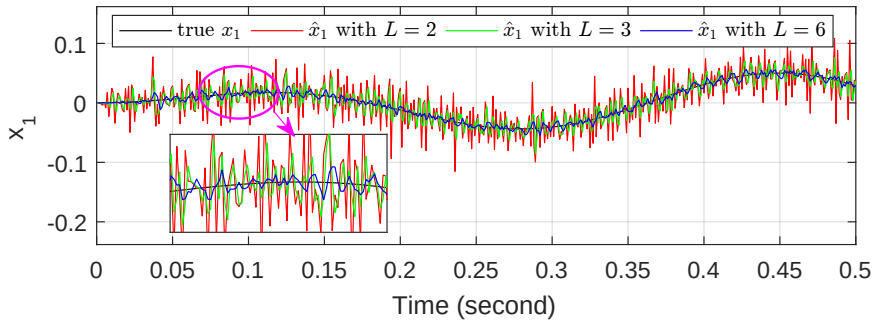

Figure 5.3: $\hat{x}_1$ over window length L

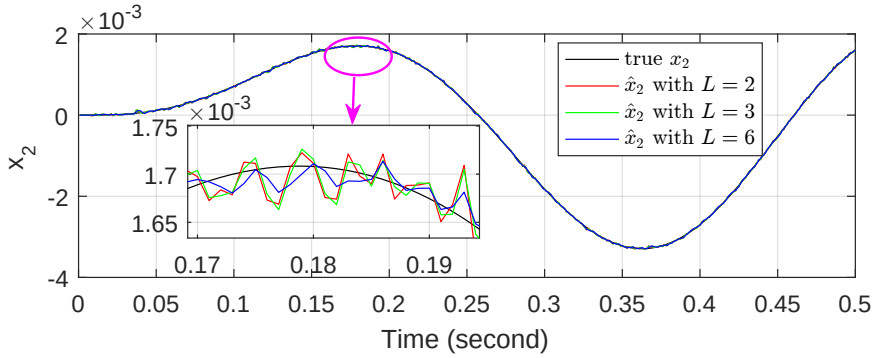

Figure 5.4: $\hat{x}_2$ over window length L

5.5.2 Cramér-Rao Lower Bound (CRLB) verification

As stated above in (5.22) and (5.23), the estimate variance of Kalman filter for LTV systems, which describes as the solution of Riccati equation, will converge to Cramér-Rao lower bound. As shown in Figure 5.5, the estimate variance $\Sigma_L(t)$ of the proposed CD-LTV-FMO is compared to both the CT-KF and CD-KF through the solutions of Riccati equation. By examining Figure 5.5, we see that the estimate variance $\Sigma_L(t)$ gets more and more closer (converge) to the CRLB as the window length L increases.

As a matter of fact, the proposed CD-LTV-FMO can be seen as a Kalman filter when the estimate variance no longer significantly changes as the window length L gets longer, namely $\Omega_{L+1}^{-1}(t) \approx \Omega_L^{-1}(t)$. In this case, thanks to the property of KF, the proposed CD-LTV-FMO is again validated as "BLUE".

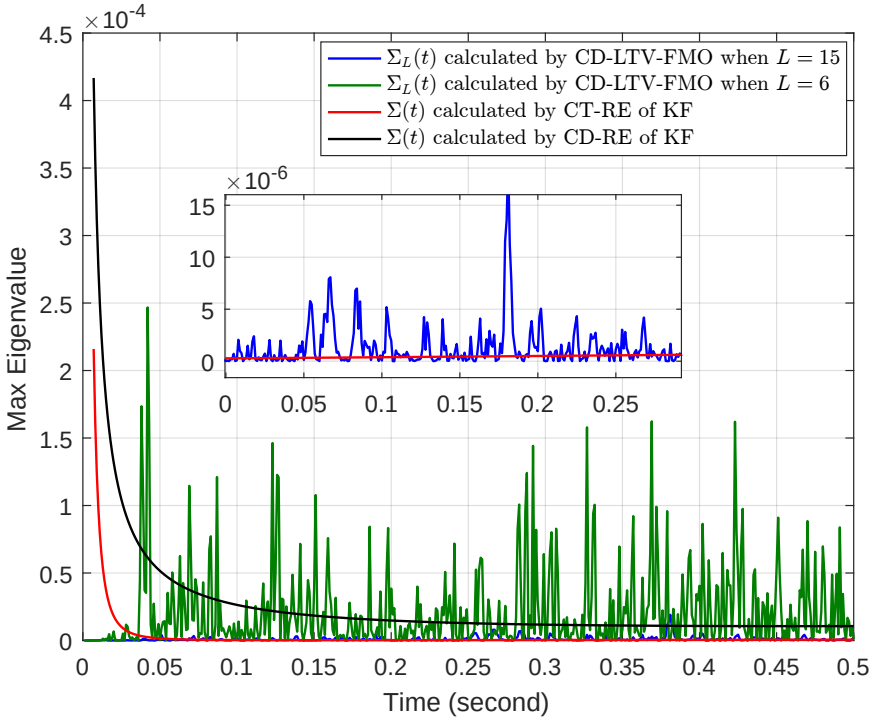

Figure 5.5: Estimate variance comparison with respect to KF by Riccati equation

5.5.3 Unbiased estimation performance via MC simulations

In order to evaluate the state estimation performance in stochastic case, we employ Monte Carlo (MC) simulations to check the unbiased property of the proposed observer, which is defined as

$$\bar{\hat{x}}(t) \triangleq \mathbb{E}\left[\hat{x}_L(t)\right] = \frac{1}{N_{\text{mc}}} \sum_{i=1}^{N_{\text{mc}}} \hat{x}_L^{(i)}$$

where N_{mc} is the number of MC runs. Let us set window length $L = 6$ and $N_{mc} = 500$. It can be seen by Figure 5.6 and Figure 5.7 that after performing 500 runs of MC simulations, the estimation expectation $\bar{\hat{x}}_2(t)$ is well rebuilt at the true value of state. Meanwhile, the upper and lower bounds of the sate estimation by the presented observer are also established in Figure 5.7, which are very close to the true state and vary in a quite small range.

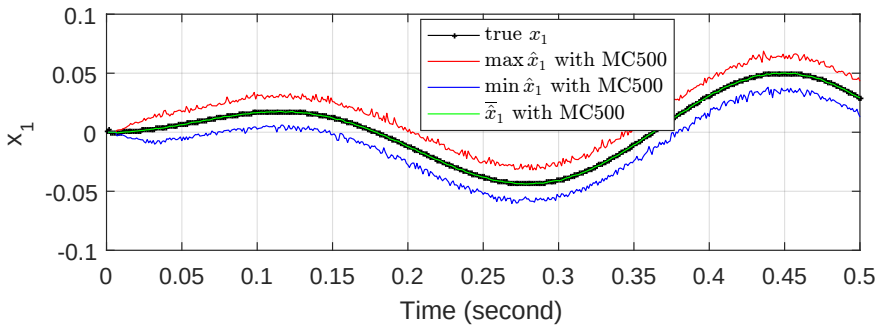

Figure 5.6: Expectation and bounds (upper / lower) of x_1 (LTV)

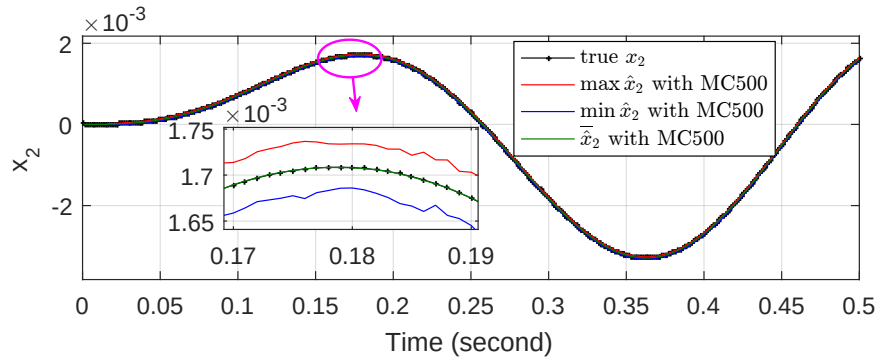

Figure 5.7: Expectation and bounds (upper / lower) of x_2 (LTV)

The RMSE (root-mean-square error) is further used as another measure of the differences between estimations and true value, which is defined as RMSE $= \sqrt{\frac{1}{N_{\text{mc}}}\sum_{i=1}^{N_{\text{mc}}}(\hat{x}_L^{(i)} - x)^2}$.

According to different window length and different numbers of MC runs, we establish six simulation scenarios, as shown in Table.5.1.

Table 5.1: MC simulation scenarios with respect to L and N_{mc}

	$N_{mc} = 100$ (N1)	$N_{mc} = 500$ (N2)
$L = 2$ (L1)	“L1N1"	“L1N2"
$L = 6$ (L2)	“L2N1"	“L2N2"
$L = 10$ (L3)	“L3N1"	“L3N2"

The RMSEs for different scenarios are depicted in Figure 5.8 and Figure 5.9. Through the examination of figure, the estimation performance may be analyzed in two aspects. On the one hand, seeing that there are three pairs of curves in the figure, the conclusion of “the longer the window length is, the better the estimations are" can be drawn immediately by comparing the RMSEs of the three pairs. This is by the way another evidence for the influence of window length.

On the other hand, examine the two different RMSEs of each pair, it can be obviously seen that how the increase of MC simulation times improves the state estimation accuracy, which appears to be reasonable since the more MC simulation times, the less uncertainty caused by process and measurement noises.

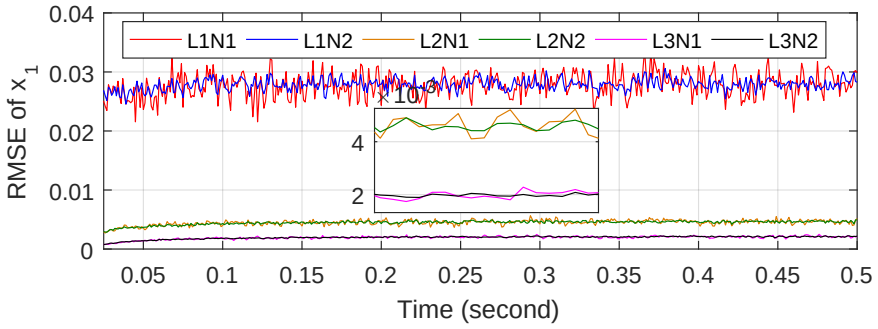

Figure 5.8: RMSE of $\hat{x}_1$ with different L and different N_{mc} (LTV)

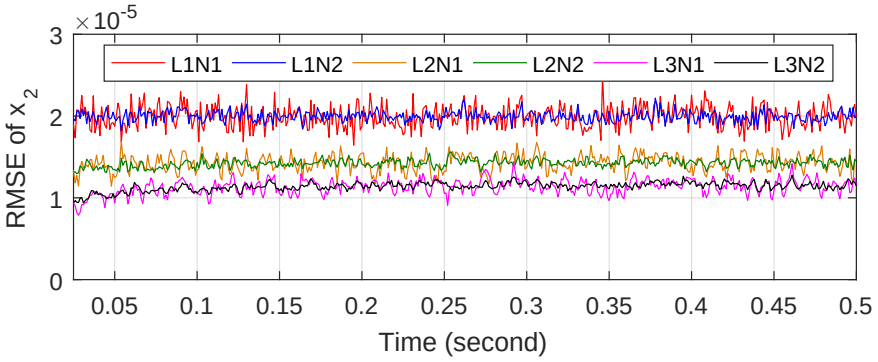

Figure 5.9: RMSE of $\hat{x}_2$ with different L and different N_{mc} (LTV)

5.6 FMO Design for CD-NLTV Systems (CD-NLTV-FMO)

Based on what we have designed above, the aim in this section is to extend the proposed CD-LTV-FMO to a class of continuous-discrete nonlinear time-varying (CD-NLTV) systems.

5.6.1 CD-NLTV-FMO formulation

The considered CD nonlinear time-varying (CD-NLTV) systems are described as

$$\dot{x}(t) = A(t)x(t) + B(t)u(t) + f(x,t) + \omega(t) \tag{5.34a}$$

$$y(k) = Cx(t_k) + v(k) \tag{5.34b}$$

where $x \in \mathbb{R}^n$, $y \in \mathbb{R}^p$ and $u \in \mathbb{R}^q$ are continuous state vector, discrete measurement vector and continuous input vector, respectively. The sampling period of measurement is T_s, i.e. $\exists k \in \mathbb{N} \mid t_k = k \times T_s$. In the meantime, $A(\cdot) \in \mathbb{R}^{n\times n}$, $B(\cdot) \in \mathbb{R}^{n\times q}$ and $C(\cdot) \in \mathbb{R}^{p\times n}$ are known matrices and are functions of time. The Gaussian measurement noise v and Gaussian process noise ω are independent with the properties described in (5.2). The nonlinearity $f(x,t)$ is at least *locally* Lipschitz with respect to x, i.e.

$$\|f(a,t) - f(b,t)\| \leq \kappa \|a-b\| \qquad (\kappa \text{ is Lipschtiz constant})$$

The continuous-discrete finite memory observer for NLTV systems, i.e. CD-NLTV-FMO, is then designed by the similar manner as the linear time-varying case based on **Assumption** 5.1, **Assumption** 5.2, **Definition** 5.1 and **Remark** 5.1.

Consider the time window $[t-\tau_{L-1}, t]$, use the state transition matrix $\Phi(t, t-\tau_i)$ to express the state mapping between $x(t)$ and $x(t-\tau_i)$ as:

$$\begin{aligned} x(t) = \Phi(t,t-\tau_i)x(t-\tau_i) + \int_{t-\tau_i}^{t} \Phi(t,\theta)B(\theta)u(\theta)\,\mathrm{d}\theta + \int_{t-\tau_i}^{t} \Phi(t,\theta)\omega(\theta)\,\mathrm{d}\theta \\ + \int_{t-\tau_i}^{t} \Phi(t,\theta)f(x(\theta),\theta)\,\mathrm{d}\theta \end{aligned} \tag{5.35}$$

both sides of (5.35) are left multiplied by a coefficient matrix $C(t-\tau_i)\Phi^{-1}(t,t-\tau_i)$, then take into consideration the measurement equation (5.34b) at time instant $t-\tau_i$ and rearrange with the properties of $\Phi(\cdot,\cdot)$ in **Remark** 5.1, we have

$$C(t-\tau_i)\Phi(t-\tau_i,t)x(t) = y(t-\tau_i) + \alpha_{[t-\tau_i,t]} - \beta_{[t-\tau_i,t]} + \gamma_{[t-\tau_i,t]} \tag{5.36}$$

with

$$\begin{aligned} \alpha_{[t-\tau_i,t]} &= \int_{t-\tau_i}^{t} C(t-\tau_i)\Phi(t-\tau_i,\theta)B(\theta)u(\theta)\,\mathrm{d}\theta \\ \beta_{[t-\tau_i,t]} &= v(t-\tau_i) - \int_{t-\tau_i}^{t} C(t-\tau_i)\Phi(t-\tau_i,\theta)\omega(\theta)\,\mathrm{d}\theta \\ \gamma_{[t-\tau_i,t]} &= \int_{t-\tau_i}^{t} C(t-\tau_i)\Phi(t-\tau_i,\theta)f(x(\theta),\theta)\,\mathrm{d}\theta \end{aligned}$$

Write equation (5.36) for every instant in time window $[t-\tau_{L-1}, t]$, a concatenated measurements can be denoted as the following linear equation:

$$Y_L(t) = W_L(t)x(t) + V_L(t) \tag{5.37}$$

where

$$Y_L(t) = \begin{pmatrix} y(t-\tau_0) + \alpha_{[t-\tau_0,t]} + \gamma_{[t-\tau_0,t]} \\ y(t-\tau_1) + \alpha_{[t-\tau_1,t]} + \gamma_{[t-\tau_1,t]} \\ \vdots \\ y(t-\tau_{L-1}) + \alpha_{[t-\tau_{L-1},t]} + \gamma_{[t-\tau_{L-1},t]} \end{pmatrix};$$

$$W_L(t) = \begin{pmatrix} C(t-\tau_0)\Phi(t-\tau_0,t) \\ C(t-\tau_1)\Phi(t-\tau_1,t) \\ \vdots \\ C(t-\tau_{L-1})\Phi(t-\tau_{L-1},t) \end{pmatrix}; \; V_L(t) = \begin{pmatrix} \beta_{[t-\tau_0,t]} \\ \beta_{[t-\tau_1,t]} \\ \vdots \\ \beta_{[t-\tau_{L-1},t]} \end{pmatrix}.$$

It can be seen that the noise term $V_L(t)$ is the same as the LTV case, so the variance matrix $P_L(t)$ remains the same as in (5.7).the least-squares solution of (5.6) as follows:

$$\begin{aligned} \hat{x}_L(t) &= \arg\min \frac{1}{2} ||Y_L(t) - W_L(t)x(t)||^2_{P_L^{-1}(t)} \\ &= \left[W_L^{\mathrm{T}}(t)P_L^{-1}(t)W_L(t)\right]^{-1} W_L^{\mathrm{T}}(t)P_L^{-1}(t)\hat{Y}_L(t) \end{aligned} \tag{5.38}$$

with

$$\hat{Y}_L(t) = \begin{pmatrix} y(t-\tau_0) + \alpha_{[t-\tau_0,t]} + \hat{\gamma}_{[t-\tau_0,t]} \\ y(t-\tau_1) + \alpha_{[t-\tau_1,t]} + \hat{\gamma}_{[t-\tau_1,t]} \\ \vdots \\ y(t-\tau_{L-1}) + \alpha_{[t-\tau_{L-1},t]} + \hat{\gamma}_{[t-\tau_{L-1},t]} \end{pmatrix}$$

$$\hat{\gamma}_{[t-\tau_i,t]} = \int_{t-\tau_i}^{t} C(t-\tau_i)\Phi(t-\tau_i,\theta) f(\hat{x}(\theta),\theta)\, \mathrm{d}\theta$$

Note that the calculation method for the integral term $\hat{\gamma}_{[t-\tau_i,t]}$ is the same as the one proposed in subsection 3.2.2.2 of Chapter 3. As a matter of fact, the CD-NLTV-FMO design idea can be referred as a combination of the CD-FMO designed in Chapter 3 and the FMO desgned for CD-LTV systems in section 5.2.

5.6.2 Numerical simulation

Consider adding a nonlinearity term $f(x,t)$ to the numerical example in section 5.5 while the other matrices and parameters remain unchanged:

$$f(x,t) = \begin{pmatrix} 0.1t \\ \sin(x_1) \end{pmatrix}$$

5.6.2.1 Influence of window length L

The same as the CD-FMO design for nonlinear systems in Chapter 3, the theoretical estimate variance of the nonlinear time-varying (NLTV) systems (5.34) cannot be currently given in this thesis. However, the practical estimate variance $\Sigma_L(t) = (x(t) - \hat{x}(t))(x(t) - \hat{x}(t))^{\mathrm{T}}$ numerically calculated by simulations at each instant t is given in Figure 5.10, from which we can still see the convergence of variance influenced by the size of window L.

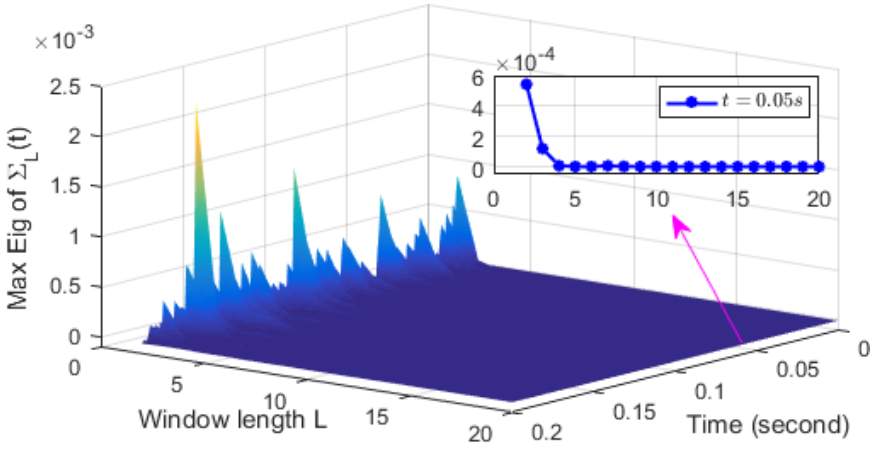

Figure 5.10: Practical variance $\Sigma_L(t)$ of CD-NLTV-FMO with respect to L

In the meantime, the comparison of state estimation through different window length L can be seen in Figure 5.11 by performing a single run of MC simulation, the convergence with respect to L depicted in Figure 5.10 is once again verified by state estimation performance.

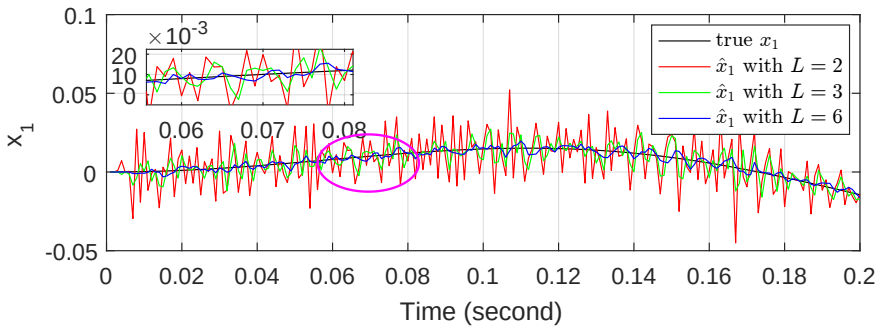

Figure 5.11: State estimation of CD-FMO-NLTV influenced by L

Note that we obtain the same convergence results as for the LTV systems case in the previous section. In next subsection, we are going to compare the estimate variance with the nonlinear Kalman filter, more specifically first-order extended Kalman filter (EKF), by the solution of the Riccati equation.

5.6.2.2 Comparison with the estimate variance of EKF

According to Simon [2006], the Riccati equations stated in (5.22) and (5.23) becomes as follows for the first-order EKF estimate variance $P(t)$ of nonlinear time-varying systems (NLTV) (5.34a), noted as

$$\dot{x}(t) = A(t)x(t) + B(t)u(t) + f(x,t) + \omega(t) \triangleq g(x,u,t,\omega)$$

$$\begin{aligned} &\text{CT-RE:} \quad \dot{P}(t) = F(t)P(t) + P(t)F^{\mathrm{T}}(t) - P(t)C^{\mathrm{T}}(t)R^{-1}C(t)P(t) + Q(t) \\ &\text{CD-RE:} \quad \dot{P}(t) = F(t)P(t) + P(t)F^{\mathrm{T}}(t) + Q(t) \end{aligned}$$

where

$$F(t) = \left.\frac{\partial g}{\partial x}\right|_{\hat{x}(t)} = A(t) + \left.\frac{\partial f}{\partial x}\right|_{\hat{x}(t)}$$

The estimate variance $\Sigma_L(t)$ of the proposed CD-NLTV-FMO is compared to both the first-order CT-EKF and CD-EKF through the solutions of Riccati equation in Figure 5.12. The same performance can be seen as in Figure 5.5. However, the estimation accuracy for NLTV systems is not as great as LTV systems due to the approximation of the nonlinearity.

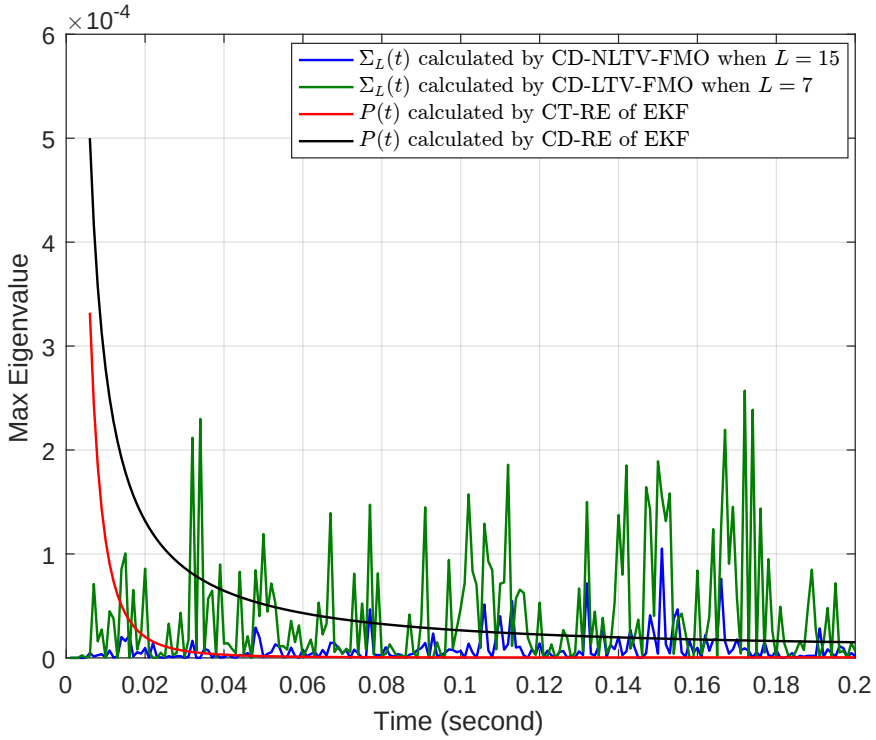

Figure 5.12: Estimate variance comparison with respect to EKF by Riccati equation

5.6.2.3 Unbiased estimation performance via MC simulations

The multiple MC simulations are run to test the unbiased property of CD-NLTV-FMO. The state estimation expectations and bounds with $N_{\text{mc}} = 500$ and $L = 6$ are shown in Figure 5.13 and Figure 5.14. Meanwhile the RMSE of different scenarios in Table.5.1 are shown in Figure 5.15 and Figure 5.16. By examining these figures, we can conclude that the proposed CD-NLTV-FMO shows a good performance.

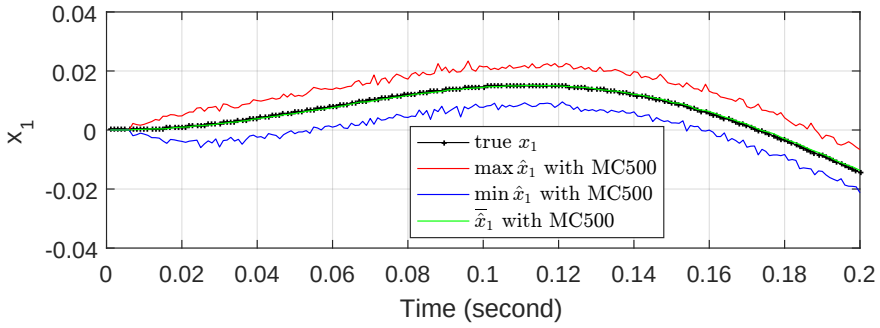

Figure 5.13: Expectation and bounds (upper / lower) of x_1 (NLTV)

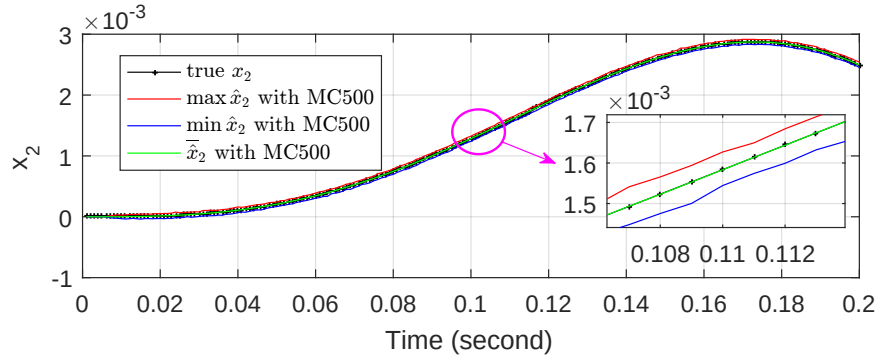

Figure 5.14: Expectation and bounds (upper / lower) of x_2 (NLTV)

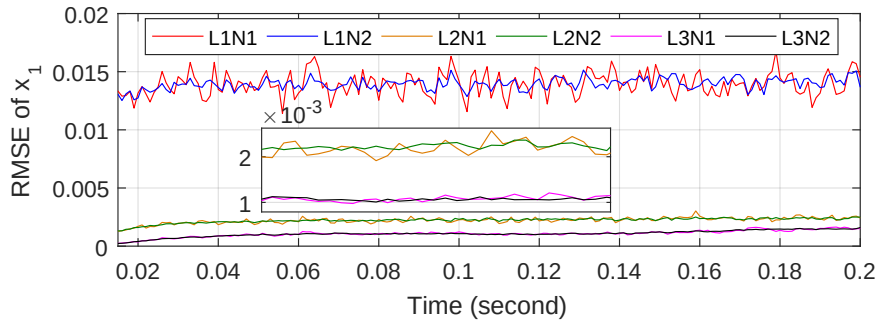

Figure 5.15: RMSE of $\hat{x}_1$ with different L and different N_{mc} (NLTV)

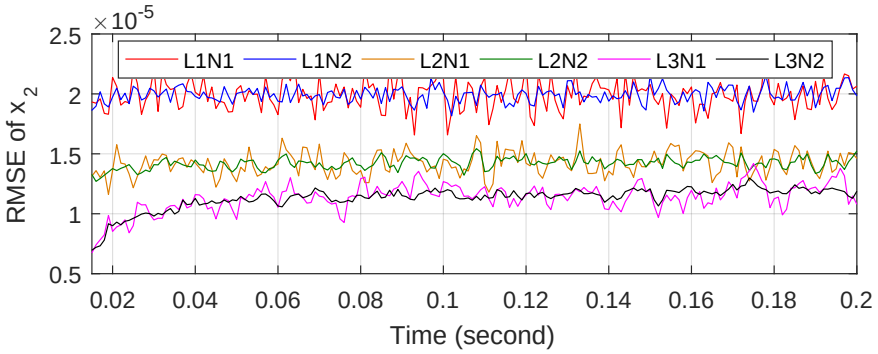

Figure 5.16: RMSE of $\hat{x}_2$ with different L and different N_{mc} (NLTV)

5.7 Conclusion

This chapter is dedicated to design a robust observer for continuous-discrete linear time-varying systems in noisy environment. The proposed approach has been proved unbiased and has the smallest estimation variance compared to other linear estimators. Furthermore, the presented observer also benefits from the finite time convergence and no initial value problem, which turns out to be an important consideration for practical applications. Like other moving horizon methods, the influence of window length has also been analysed both theoretically and practically, which a strategy of choosing the window length by dispersion tolerance are also provided. Monte Carlo simulations are used to examine and verify the performance of the proposed method, which appears to be robust and effective. It may be worth noting here that the presented observer framework also works well when sampling period is not a constant. At the last part, the proposed observer has been extended to the nonlinear time-varying systems through a brief demonstration and a numerical example is employed to test the performance of CD-FMO-NLTV.

Chapter 6

Conclusions and Future Research

This thesis set out to design a nonlinear observer for a class of dynamical systems, which are modeled by continuous-time nonlinear ordinary differential equations and are measured at discrete-time instant, and to use the proposed observer to perform fault diagnosis. A graphical representation of the structure of this thesis is given in Figure 6.1. In this final chapter, we will review the result conclusions of the work in this thesis, as well as discuss directions for future research.

6.1 Conclusions

The main conclusions of this thesis, which are drawn based on the obtained results, are summarized as follows in two aspects:

Nonlinear observer design

- **Time-invariant:** inspired by the existing optimization-based nonlinear observer design methods and the observer-based fault diagnosis approaches illustrated in Chapter 2, we have first devoted Chapter 3 to develop a continuous-discrete finite memory observer (CD-FMO) for a class of nonlinear dynamical time-invariant systems the presence of process and measurement noise, where a one-step prediction algorithm incorporated with an iterative-update scheme is performed to solve the integral problem caused by system nonlinearity, and an analysis of the unbiased estimation property has been proved in both deterministic and stochastic case.
- **Unknown input:** since there still remains a lack of study on nonlinear continuous-discrete observer design with the presence of unknown input, process and measurement noises at the same time, which serves as the motivation of the presented work in Chapter 4, where a CD-UI-FMO is constructed based upon an augmented model aiming to simultaneously estimate system state and UI of a noisy process with noisy measurements. The unbiased property of CD-FMO remains for the CD-UI-FMO case.

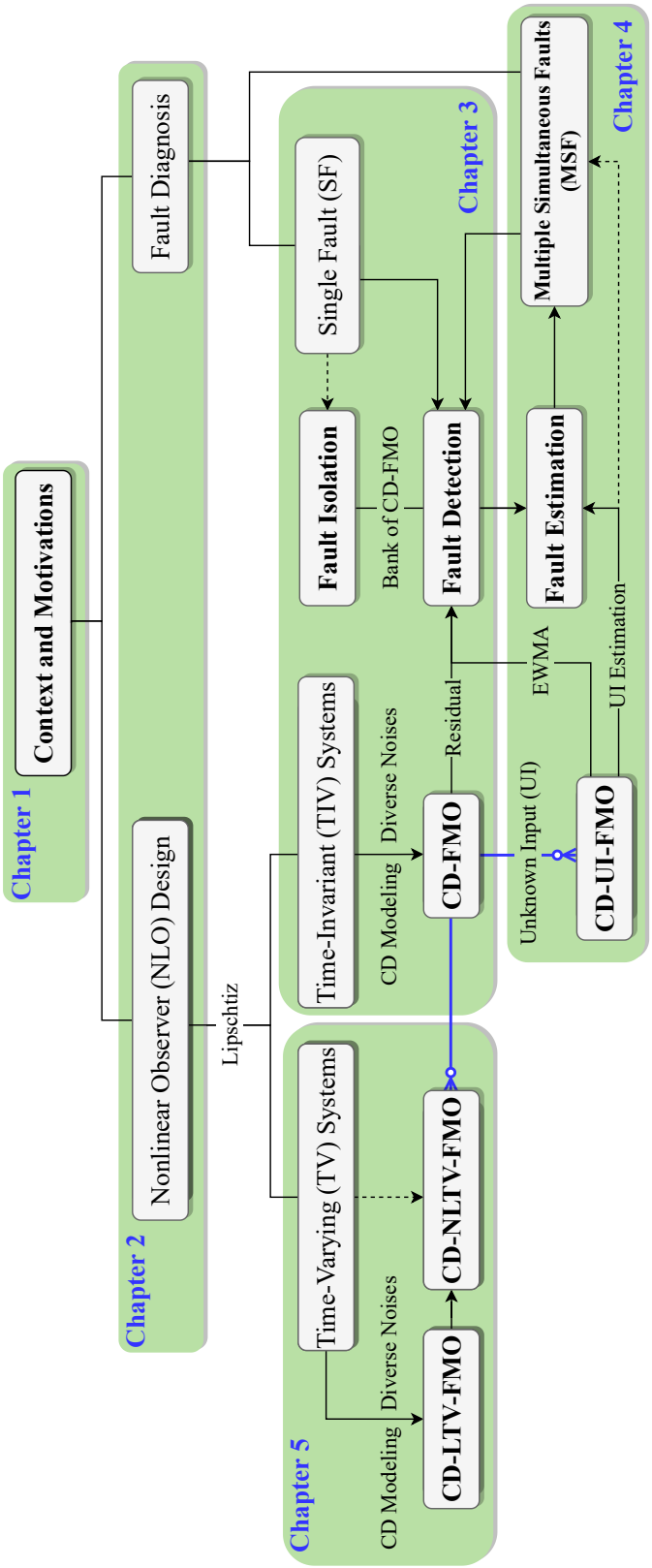

Figure 6.1: Conclusions and structure of the chapters in the thesis

- **Time-varying:** As for time-varying systems, an observer has been designed for both linear and nonlinear cases in Chapter 5, respectively called CD-LTV-FMO and CD-NLTV-FMO. A detailed proofs are provided for linear case while the formulation has been further extended to nonlinear case and illustrated by a given example.

Fault diagnosis

- **Detection,isolation and estimation:** for the application purpose, residuals generated by the proposed CD-FMO are employed in Chapter 3 to implement fault detection cooperated with the CUSUM algorithm, while a bank of CD-FMOs is adopted to realize fault isolation for different sensor and actuator faults of a considered nonlinear robotic systems. In the meantime, the proposed CD-UI-FMO structure in Chapter 4 has been applied to actuator fault estimation when the actuator fault is modeled as an unknown input of systems.
- **Multiple simultaneous faults detection and identification:** thanks to the unknown input estimation ability of CD-UI-FMO, fault detection and identification have been performed in Chapter 4 as well for multiple simultaneous sensor and actuator faults as the actuator fault has been estimated and compensated by CD-UI-FMO.

The above mentioned conclusions have been verified and validated by numerical simulations in this thesis. The provided results showed the good performance on both state estimation and fault diagnosis, as well as efficiency and robustness with respect to diverse noises.

6.2 Future Research

Even though my PhD journey is going to end very soon, my research is still going on. There still remains much research to be done in the future as the succession and continuity of the work in this thesis. These future research directions are also going to be listed in two aspects as follows:

Observer design aspect

- **Analytical form of the estimate variance:** it can be seen that the variance of estimation error obtained by CD-LTV-FMO in Chapter 5 are theoretically demonstrated by (5.15) and validated through simulations for linear time-varying systems. As for nonlinear case, the variance are shown by simulations while the analytical form of

estimate variance has not yet given, which refers to the proposed CD-FMO in Chapter 3, the CD-UI-FMO in Chapter 4 and the CD-NLTV-FMO in Chapter 5.

- **Incomplete or missing measurements:** missing measurements are a common occurrence in practical physical system and can cause a significant effect on system behavior. The proposed nonlinear finite memory observer is supposed to be robust with respect to the measurement missing thanks to the role of term "τ_i" in the formulation structure. It will be analyzed and validated in detail in the future.

- **Extension to general nonlinear systems:** since we have already built the observer for a class of nonlinear systems (3.1) and for time-varying nonlinear systems (5.34), it might be possible to extend the presented method to general nonlinear systems under the form $\hat{x} = f(x,u,t)$ by using the first-order or second-order Taylor expansion around $x = \hat{x}(t)$ at each instant t.

Fault diagnosis aspect

- **Detection sensitivity analyses with respect to different fault and noises:** in order to analyze the diagnostic performance according to different parameter configuration, it is then necessary to study the sensibility of the chosen fault indicator (for instance, the generated "residual" is used as fault indicator in this thesis) vis-a-vis different fault and noises. This type of study can help us theoretically analyze in advance the minimum fault detection amplitude with the known configuration parameters.

- **Integrate with the qualitative model-based diagnosis methods:** qualitative model-based diagnosis methods sometimes cannot give a correct diagnosis of failures. For example, fault tree (FT) will give false diagnosis when the true failure component is not the one whose failure rate is the highest. Since the failure rate is based on historical data and the current scenario may be more complex. To ensure more correct diagnosis results, one has to use other real-time information, where the proposed observer might give some help with it. It will make a significant improvement if the proposed observer can share information with the qualitative model-based methods.

This above non-exhaustive list forms our future research directions.

References

Abdelhedi, A., Sbita, L., and Boutat, D. (2016). Levenberg-marquardt and moving horizon estimation for the synthesis of nonlinear observers. *International Journal of Computer Science and Network Security*, 16(11):118–123.

Ahrens, J. H. and Khalil, H. K. (2009). High-gain observers in the presence of measurement noise: A switched-gain approach. *Automatica*, 45(4):936 – 943.

Alamir, M. (1999). Optimization based non-linear observers revisited. *International Journal of Control*, 72(13):1204–1217.

Alamir, M. (2007). Nonlinear moving horizon observers: Theory and real-time implementation. *Nonlinear Observers and Applications*, 363:139–179.

Alenezi, B., Hu, J., and Żak, S. H. (2019). Adaptive unknown input and state observers. In *2019 American Control Conference (ACC)*, pages 2434–2439.

Ali, S. A., Christen, A., Begg, S., and Langlois, N. (2016). Continuous–discrete time-observer design for state and disturbance estimation of electro-hydraulic actuator systems. *IEEE Transactions on Industrial Electronics*, 63(7):4314–4324.

Almasri, M., Tricot, N., and Lenain, R. (2020). Parameter estimation based-fdi method enhancement with mixed particle filter. *Neurocomputing*, 403:441 – 451.

Atkinson, K. E. (1989). *An introduction to numerical analysis*. Wiley, 2 edition.

Bellavia, S., Gratton, S., and Riccietti, E. (2018). A levenberg-marquardt method for large nonlinear least-squares problems with dynamic accuracy in functions and gradients. *Numerische Mathematik*, 140(3):791–825.

Bellman, R. (1943). The stability of solutions of linear differential equations. *Duke Mathematical Journal*, 10(4):643–647.

Blanke, M., Kinnaert, M., Lunze, J., and Staroswiecki, M. (2006). *Diagnosis and Fault-Tolerant Control*. Springer-Verlag Berlin Heidelberg, 2nd edition.

Bougatef, Z., Abdelkrim, N., Aitouche, A., and Abdelkrim, M. (2020). Fault detection of a pemfc system based on delayed lpv observer. *International Journal of Hydrogen Energy*, 45(19):11233–11241.

Canuto, E., Novara, C., Massotti, L., Carlucci, D., and Montenegro, C. P. (2018). *Spacecraft dynamics and control*. Butterworth-Heinemann, 1st edition.

Chen, C. (1999). *Linear system theory and design*. Oxford University Press.

Chen, J., Patton, R. J., and Zhang, H. Y. (1996). Design of unknown input observers and robust fault detection filters. *International Journal of Control*, 63(1):85–105.

Chow, E. and Willsky, A. (1984). Analytical redundancy and the design of robust failure detection systems. *IEEE Transactions on Automatic Control*, 29(7):603–614.

Ciccarella, G., Mora, M. D., and Germani, A. (1993). A luenberger-like observer for nonlinear systems. *International Journal of Control*, 57(3):537–556.

Cisar, P., Bošnjak, S., and Maravic Cisar, S. (2010). Ewma algorithm in network practice. *International Journal of Computers Communications & Control*, 5(2):160.

Coddington, E. A. and Levinson, N. (1987). *Theory of ordinary differential equations*. Krieger.

Cook, M. V. (2013). *Flight dynamics principles*. Butterworth-Heinemann.

De Souza, C., Gevers, M., and Goodwin, G. (1986). Riccati equations in optimal filtering of nonstabilizable systems having singular state transition matrices. *IEEE Transactions on Automatic Control*, 31(9):831–838.

Deza, F., Busvelle, E., Gauthier, J., and Rakotopara, D. (1992). High gain estimation for nonlinear systems. *Systems & Control Letters*, 18(4):295 – 299.

Ding, S. X. (2008). *Model-based fault diagnosis techniques*. Springer, 1st edition.

Dinh, T. N., Andrieu, V., Nadri, M., and Serres, U. (2015). Continuous-discrete time observer design for lipschitz systems with sampled measurements. *IEEE Transactions on Automatic Control*, 60(3):787–792.

El Merraoui, K., Ferdjouni, A., and Bounekhla, M. (2020). Real time observer-based stator fault diagnosis for im. *International Journal of Electrical and Computer Engineering (IJECE)*, 10(1):210.

Farza, M., M'Saad, M., and Busawon, K. (2014). Continuous-discrete-time observers for a class of uniformly observable systems. *Hybrid Dynamical Systems*, pages 261–275.

Farza, M., M'Saad, M., Ménard, T., Ltaief, A., and Maatoug, T. (2018). Adaptive observer design for a class of nonlinear systems. application to speed sensorless induction motor. *Automatica*, 90:239–247.

Fossard, A. J. and Normand-Cyrot, D. (1995). *Nonlinear Systems*. Springer US.

Frank, P. and Ding, X. (1997). Survey of robust residual generation and evaluation methods in observer-based fault detection systems. *Journal of Process Control*, 7(6):403–424.

Frank, P. M. (1987). Fault diagnosis in dynamic systems via state estimation - a survey. In Tzafestas, S., Singh, M., and Schmidt, G., editors, *System Fault Diagnostics, Reliability and Related Knowledge-Based Approaches*, pages 35–98, Dordrecht. Springer Netherlands.

Frank, P. M. (1990). Fault diagnosis in dynamic systems using analytical and knowledge-based redundancy. *Automatica*, 26(3):459–474.

Goupil, P. (2011). AIRBUS state of the art and practices on FDI and FTC in flight control system. *Control Engineering Practice*, 19(6):524–539.

Graton, G., Kratz, F., and Fantini, J. (2014). Finite memory observers for linear time-varying systems: Theory and diagnosis applications. *Journal of the Franklin Institute*, 351(2):785–810.

Grizzle, J. W. and Moraal, P. E. (1990). Newton, observers and nonlinear discrete-time control. In *29th IEEE Conference on Decision and Control*, volume vol.2, pages 760–767.

Hammouri, H. and Farza, M. (2003). Nonlinear observers for locally uniformly observable systems. *ESAIM: Control, Optimisation and Calculus of Variations*, 9:353–370.

Hammouri, H., Kinnaert, M., and El Yaagoubi, E. H. (1999). Observer-based approach to fault detection and isolation for nonlinear systems. *IEEE Transactions on Automatic Control*, 44(10):1879–1884.

Han, X., Li, Z., Dahhou, B., Cabassud, M., and He, M. (2019). Nonlinear observer based fault diagnosis for an innovative intensified heat-exchanger/reactor. *Proceedings of the 11th International Conference on Modelling, Identification and Control (ICMIC2019)*, pages 423–432.

Hao, J. and Kinnaert, M. (2017). Sensor fault detection and isolation over wireless sensor network based on hardware redundancy. *Journal of Physics: Conference Series*, 783:012006.

Hassani, S. (2009). *Mathematical methods*. Springer-Verlag.

Heffes, H. (1966). The effect of erroneous models on the kalman filter response. *IEEE Transactions on Automatic Control*, 11(3):541–543.

Hermann, R. and Krener, A. (1977). Nonlinear controllability and observability. *IEEE Transactions on Automatic Control*, 22(5):728–740.

Higham, N. J. (2009). Cholesky factorization. *Wiley Interdisciplinary Reviews: Computational Statistics*, 1(2):251–254.

Hou, M. and Muller, P. C. (1994). Disturbance decoupled observer design: a unified viewpoint. *IEEE Transactions on Automatic Control*, 39(6):1338–1341.

Hwang, I., Kim, S., Kim, Y., and Seah, C. E. (2010). A survey of fault detection, isolation, and reconfiguration methods. *IEEE Transactions on Control Systems Technology*, 18(3):636–653.

Isermann, R. (1984). Process fault detection based on modeling and estimation methods—a survey. *Automatica*, 20(4):387 – 404.

Isermann, R. (1991). Fault diagnosis of machines via parameter estimation and knowledge processing. *IFAC Proceedings Volumes*, 24(6):43 – 55. IFAC/IMACS Symposium on Fault Detection, Supervision and Safety for Technical Processes (SAFEPROCESS'91), Baden-Baden, Germany, 10-13 September 1991.

Isermann, R. (2005). Model-based fault-detection and diagnosis – status and applications. *Annual Reviews in Control*, 29(1):71 – 85.

Isermann, R. and Ballé, P. (1997). Trends in the application of model-based fault detection and diagnosis of technical processes. *Control Engineering Practice*, 5(5):709 – 719.

Jazwinski, A. H. (1970). *Stochastic processes and filtering theory*. Academic Press.

Johnson, S. C., Chakrabarty, A., Hu, J., Żak, S. H., and DeCarlo, R. A. (2018). Dual-mode robust fault estimation for switched linear systems with state jumps. *Nonlinear Analysis: Hybrid Systems*, 27:125 – 140.

Kailath, T. (1980). *Linear systems*. Prentice-Hall.

Kajdan, R., Graton, G., Aubry, D., and Kratz, F. (2006). Fault detection of a nonlinear switching system using finite memory observers. *IFAC Proceedings Volumes*, 39(13):992–997.

Kalman, R. E. (1963). Mathematical description of linear dynamical systems. *Journal of the Society for Industrial and Applied Mathematics Series A Control*, 1(2):152–192.

Kanzow, C., Yamashita, N., and Fukushima, M. (2004). Levenberg–marquardt methods with strong local convergence properties for solving nonlinear equations with convex constraints. *Journal of Computational and Applied Mathematics*, 172(2):375 – 397.

Kinnaert, M. (2003). Fault diagnosis based on analytical models for linear and nonlinear systems - a tutorial. *IFAC Proceedings Volumes*, 36(5):37 – 50. 5th IFAC Symposium on Fault Detection, Supervision and Safety of Technical Processes 2003, Washington DC, 9-11 June 1997.

Koenig, D. (2006). Observer design for unknown input nonlinear descriptor systems via convex optimization. *IEEE Transactions on Automatic Control*, 51(6):1047–1052.

Koshkouei, A., Burnham, K., and Sedighi, T. (2011). Nonlinear unknown input observer design for nonlinear systems: A new method. *IFAC Proceedings Volumes*, 44(1):11067 – 11072. 18th IFAC World Congress.

Kou, S., Tarn, T., and Elliott, D. (1973). Finite-time observer for nonlinear dynamic systems. *IEEE Conference on Decision and Control including the 12th Symposium on Adaptive Processes*.

Kratz, F. (1991). *Detection of sensor failures using instruments and analytic redundancies. Application to nuclear power plants*. PhD thesis, Université Henri Poincaré - Nancy 1.

Levenberg, K. (1944). A method for the solution of certain non-linear problems in least squares. *Quarterly of Applied Mathematics*, 2(2):164–168.

Li, L., Chadli, M., Ding, S. X., Qiu, J., and Yang, Y. (2018). Diagnostic observer design for t-s fuzzy systems: Application to real-time-weighted fault-detection approach. *IEEE Transactions on Fuzzy Systems*, 26(2):805–816.

Ling, C. and Kravaris, C. (2019). Multirate sampled-data observer design based on a continuous-time design. *IEEE Transactions on Automatic Control*, 64(12):5265–5272.

Marquardt, D. W. (1963). An algorithm for least-squares estimation of nonlinear parameters. *Journal of the Society for Industrial and Applied Mathematics*, 11(2):431–441.

Marx, B., Ichalal, D., Ragot, J., Maquin, D., and Mammar, S. (2019). Unknown input observer for lpv systems. *Automatica*, 100:67 – 74.

Mayne, D. Q. and Michalska, H. (1992). Moving horizon observer-based control. In *[1992] Proceedings of the 31st IEEE Conference on Decision and Control*, volume vol.2, pages 1512–1517.

Mazenc, F., Andrieu, V., and Malisoff, M. (2015). Design of continuous–discrete observers for time-varying nonlinear systems. *Automatica*, 57:135 – 144.

Mazenc, F. and Dinh, T. N. (2014). Construction of interval observers for continuous-time systems with discrete measurements. *Automatica*, 50(10):2555 – 2560.

Mazenc, F. and Fridman, E. (2014). Predictor-based sampled-data stabilization via continuous-discrete observers. In *53rd IEEE Conference on Decision and Control*, pages 1614–1619.

Mazenc, F. and Fridman, E. (2016). Predictor-based sampled-data exponential stabilization through continuous–discrete observers. *Automatica*, 63:74 – 81.

Mazenc, F. and Malisoff, M. (2020). Continuous discrete sequential observers for time-varying systems under sampling and input delays. *IEEE Transactions on Automatic Control*, 65(4):1704–1709.

Medvedev, A. (1994). Parity space method: a continuous time approach. In *Proceedings of 1994 American Control Conference - ACC '94*, volume 1, pages 662–665 vol.1.

Medvedev, A. V. and Toivonen, H. T. (1992). A continuous finite-memory deadbeat observer. In *1992 American Control Conference*, pages 1800–1804.

Meyer, L., Ichalal, D., and Vigneron, V. (2018). Interval observer for nonlinear lipschitz systems with unknown inputs. In *2018 Annual American Control Conference (ACC)*, pages 5962–5967.

Michalska, H. and Mayne, D. (1993). Moving horizon observers. In FLIESS, M., editor, *Nonlinear Control Systems Design 1992*, IFAC Symposia Series, pages 185 – 190. Pergamon, Oxford.

Michalska, H. and Mayne, D. Q. (1995). Moving horizon observers and observer-based control. *IEEE Transactions on Automatic Control*, 40(6):995–1006.

Montgomery, D. C. (2013). *Introduction to statistical quality control*. J. Wiley & Sons, 6 edition.

Moraal, P. E. (1994). *Nonlinear Observer Design: Theory and Applications to Automotive Control*. PhD thesis, University of Michigan.

Moraal, P. E. and Grizzle, J. W. (1995). Observer design for nonlinear systems with discrete-time measurements. *IEEE Transactions on Automatic Control*, 40(3):395–404.

M'Saad, M. and Farza, M. (2009). Identification of continuous-time linear systems with time-delay. *IFAC Proceedings Volumes*, 42(10):898 – 903. 15th IFAC Symposium on System Identification.

Nijmeijer, H. and Schaft, A. v. d. (2016). *Nonlinear dynamical control systems*. Springer Science+Business Media.

Nomizu, K. and Sasaki, T. (1994). *Affine differential geometry*. Cambridge University Press.

Nuninger, W., Kratz, F., and Ragot, J. (1998). Finite memory generalised state observer for failure detection in dynamic systems. *Proceedings of the 37th IEEE Conference on Decision and Control*, 1:581–585.

Nuninger, W., Kratz, F., and Ragot, J. (1998). Finite memory generalised state observer for failure detection in dynamic systems. In *Proceedings of the 37th IEEE Conference on Decision and Control (Cat. No.98CH36171)*, volume 1, pages 581–585 vol.1.

Prasov, A. A. and Khalil, H. K. (2013). A nonlinear high-gain observer for systems with measurement noise in a feedback control framework. *IEEE Transactions on Automatic Control*, 58(3):569–580.

Press, W. H., Teukolsky, S. A., Vetterling, W. T., and Flannery, B. P. (2007). *Numerical recipes*. Cambridge University Press, 3 edition.

Pujol, J. (2007). The solution of nonlinear inverse problems and the levenberg-marquardt method. *GEOPHYSICS*, 72(4):W1–W16.

Rajamani, R. (1998). Observers for lipschitz nonlinear systems. *IEEE Transactions on Automatic Control*, 43(3):397–401.

Rajamani, R. (2017). Observers for nonlinear systems: Introduction to part 1 of the special issue. *IEEE Control Systems Magazine*, 37(3):22–24.

Rudin, W. (2015). *Real and complex analysis*. McGraw Hill Education India, 3 edition.

Sanfelice, L. P. R. G. (2011). On the performance of high-gain observers with sign-indefinite gain adaptation under measurement noise. *Automatica*, 47(10):2165–2176.

Shields, D. N. (2005). Observer-based residual generation for fault diagnosis for non-affine non-linear polynomial systems. *International Journal of Control*, 78(5):363–384.

Simon, D. (2006). *Optimal state estimation*. Wiley-Interscience.

Sontag, E. D. (1998). *Mathematical control theory*. Springer-Verlag New York, Inc, 2 edition.

Sorenson, H. and Sacks, J. (1971). Recursive fading memory filtering. *Information Sciences*, 3(2):101–119.

Strube, H. (1982). Time-varying wave digital filters and vocal-tract models. In *ICASSP '82. IEEE International Conference on Acoustics, Speech, and Signal Processing*, volume 7, pages 923–926.

Tan, C., Crusca, F., and Aldeen, M. (2008). Extended results on robust state estimation and fault detection. *Automatica*, 44(8):2027 – 2033.

Termeche, A., Benazzouz, D., Bouamama, B. O., and Abdallah, I. (2018). Augmented analytical redundancy relations to improve the fault isolation. *Mechatronics*, 55:129 – 140.

Thuillier, J., Delouche, D., Fantini, J., and Kratz, F. (2018). Finite memory observer - based sensor fault detection and isolation for system when measurements are correlated with process noise. *IFAC-PapersOnLine*, 51(24):320–325.

Toda, M. and Patel, R. (1978). Performance bounds for continuous-time filters in the presence of modeling errors. *IEEE Transactions on Aerospace and Electronic Systems*, AES-14(6):912–919.

Toumi, D., Boucherit, M., and Tadjine, M. (2012). Observer-based fault diagnosis and field oriented fault tolerant control of induction motor with stator inter-turn fault. *Archives of Electrical Engineering*, 61(2):165–188.

Transtrum, M. and Sethna, J. (2012). Improvements to the levenberg-marquardt algorithm for nonlinear least-squares minimization. *arXiv: Data Analysis, Statistics and Probability*.

Tréangle, C., Farza, M., and M'Saad, M. (2019). Observer design for a class of disturbed nonlinear systems with time-varying delayed outputs using mixed time-continuous and sampled measurements. *Automatica*, 107:231 – 240.

Van Schrick, D. (1997). Remarks on terminology in the field of supervision, fault detection and diagnosis. *IFAC Proceedings Volumes*, 30(18):959 – 964. IFAC Symposium on Fault Detection, Supervision and Safety for Technical Processes (SAFEPROCESS 97), Kingston upon Hull, UK, 26-28 August 1997.

Venkatasubramanian, V., Rengaswamy, R., Yin, K., and Kavuri, S. N. (2003). A review of process fault detection and diagnosis: Part i: Quantitative model-based methods. *Computers & Chemical Engineering*, 27(3):293 – 311.

Wang, D., Yu, M., Low, C. B., and Arogeti, S. (2013). *Model-based Health Monitoring of Hybrid Systems*. Springer New York.

Wilamowski, B. M. and Yu, H. (2010). Improved computation for levenberg–marquardt training. *IEEE Transactions on Neural Networks*, 21(6):930–937.

Yang, H. and Saif, M. (1996). Monitoring and diagnostics of a class of nonlinear systems using a nonlinear unknown input observer. In *Proceeding of the 1996 IEEE International Conference on Control Applications IEEE International Conference on Control Applications held together with IEEE International Symposium on Intelligent Contro*, pages 1006–1011.

Zemouche, A. and Boutayeb, M. (2013). On LMI conditions to design observers for lipschitz nonlinear systems. *Automatica*, 49(2):585 – 591.

Zhang, F. (2010). *The Schur complement and its applications*. Springer.

Zhang, J., Swain, A. K., and Nguang, S. K. (2016a). *Robust Observer-Based Fault Diagnosis for Nonlinear Systems Using MATLAB*. Springer International Publishing.

Zhang, K., Jiang, B., and Shi, P. (2013). *Observer-Based Fault Estimation and Accomodation for Dynamic Systems*. Springer.

Zhang, K., Liu, G., and Jiang, B. (2016b). Robust unknown input observer-based fault estimation of leader-follower linear multi-agent systems. *Circuits, Systems, and Signal Processing*, 36(2):525–542.

Zhang, T., Kratz, F., Hou, Y., and Idasiak, V. (2020). A continuous-discrete finite memory observer design for a class of nonlinear systems: Application to fault diagnosis. *Mathematical Problems in Engineering*, 2020:1–14.

Zhang, W., Su, H., Zhu, F., and Azar, G. M. (2014). Unknown input observer design for one-sided lipschitz nonlinear systems. *Nonlinear Dynamics*, 79(2):1469–1479.

Zhang, X., Polycarpou, M. M., and Parisini, T. (2008). Design and analysis of a fault isolation scheme for a class of uncertain nonlinear systems. *Annual Reviews in Control*, 32(1):107–121.

Zimmer, G. (1993a). A new algorithm for approximating the state of nonlinear systems. *International Journal of Systems Science*, 24(4):777–788.

Zimmer, G. (1993b). Newton step observer for nonlinear feedback systems. In *Proceedings of the 2nd European Control Conference*, pages 391–395.

Zimmer, G. (1993c). Newton-verfahren zur zustandsapproximation nichtlinearer systerne. *VDI-Bericht*, Nr. 1026:81–90.

Zimmer, G. (1994). State observation by on-line minimization. *International Journal of Control*, 60(4):595–606.

Appendix A

Calculation of the noise variance matrix P

This appendix presents the detailed calculation of the noise variance matrix P in equation (3.8) of chapter 3.

A note on notation

Three dots between delimiters (parenthesis, brackets, or braces) means that the quantity between the delimiters is the same as the quantity between the previous set of identical delimiters in the same equation. For example,

$$(A+BCD)+(\cdots)^{\mathrm{T}} = (A+BCD)+(A+BCD)^{\mathrm{T}}$$
$$A+[B(C+D)]^{-1}E[\cdots] = A+[B(C+D)]^{-1}E[B(C+D)]$$

According to the definition of *Variance* and zero mean, i.e. $\mathbb{E}(V_L)=0$, we have

$$\begin{aligned}
P &= \mathbb{E}\left\{[V_L-\mathbb{E}(V_L)][V_L-\mathbb{E}(V_L)]^{\mathrm{T}}\right\} \\
&= \mathbb{E}\left\{V_L V_L^{\mathrm{T}}\right\} \\
&= \mathbb{E}\left\{\begin{pmatrix} v(t-\tau_0)-\int_{t-\tau_0}^{t} Ce^{A(t-\tau_0-\theta)}G\omega(\theta)\,\mathrm{d}\theta \\ v(t-\tau_1)-\int_{t-\tau_1}^{t} Ce^{A(t-\tau_1-\theta)}G\omega(\theta)\,\mathrm{d}\theta \\ \vdots \\ v(t-\tau_{L-1}-\int_{t-\tau_{L-1}}^{t} Ce^{A(t-\tau_{L-1}-\theta)}G\omega(\theta)\,\mathrm{d}\theta) \end{pmatrix} \begin{pmatrix} \\ \cdots \\ \\ \end{pmatrix}^{\mathrm{T}}\right\} \\
&\triangleq \begin{pmatrix} p_{0,0} & p_{0,1} & \cdots & p_{0,L-1} \\ p_{1,0} & p_{1,1} & \cdots & p_{1,L-1} \\ \vdots & \vdots & \ddots & \vdots \\ p_{L-1,0} & p_{L-1,1} & \cdots & p_{L-1,L-1} \end{pmatrix} \\
&\triangleq (p_{i,j}) \in \mathbb{R}^{L\times L}
\end{aligned} \tag{A.1}$$

where the elements $p_{i,j}$ are indexed by $0 \le i \le L-1$ and $0 \le j \le L-1$. Using the noise properties of w and v in (3.3), we know that $p_{i,j}$ satisfy

$$\begin{aligned} p_{i,j} &= \mathbb{E}\left(\left[v(t-\tau_i) - \int_{t-\tau_i}^{t} e^{A(t-\tau_i-\theta_1)} G\omega(\theta_1)\,\mathrm{d}\theta_1\right]\left[\cdots\right]^{\mathrm{T}}_{(i\leftarrow j;\theta_1\leftarrow\theta_2)}\right) \\ &= \mathbb{E}\left(\left[\cdots\right]\left[v(t-\tau_j)^{\mathrm{T}} - \int_{t-\tau_j}^{t} \omega^{\mathrm{T}}(\theta_2) G^{\mathrm{T}} e^{A^{\mathrm{T}}(t-\tau_j-\theta_2)} C^{\mathrm{T}}\,\mathrm{d}\theta_2\right]\right) \\ &\triangleq ① - ② - ③ + ④ \end{aligned} \tag{A.2}$$

with

$$① = \mathbb{E}\left(v(t-\tau_i)v(t-\tau_j)^{\mathrm{T}}\right) = R\delta_{i,j} = \begin{cases} 0 & \text{if } i \neq j \\ R & \text{if } i = j \end{cases} \tag{A.3a}$$

$$② = \mathbb{E}\left(v(t-\tau_i)\cdot\int_{t-\tau_j}^{t} \omega^{\mathrm{T}}(\theta_2) G^{\mathrm{T}} e^{A^{\mathrm{T}}(t-\tau_j-\theta_2)} C^{\mathrm{T}}\,\mathrm{d}\theta_2\right) = 0 \quad \forall i,j \tag{A.3b}$$

$$③ = \mathbb{E}\left(\int_{t-\tau_i}^{t} e^{A(t-\tau_i-\theta_1)} G\omega(\theta_1)\,\mathrm{d}\theta_1 \cdot v(t-\tau_j)\right) = 0 \quad \forall i,j \tag{A.3c}$$

$$④ = \mathbb{E}\left(\int_{t-\tau_i}^{t} Ce^{A(t-\tau_i-\theta_1)} G\omega(\theta_1)\,\mathrm{d}\theta_1 \cdot \int_{t-\tau_j}^{t} \omega^{\mathrm{T}}(\theta_2) G^{\mathrm{T}} e^{A^{\mathrm{T}}(t-\tau_j-\theta_2)} C^{\mathrm{T}}\,\mathrm{d}\theta_2\right) \tag{A.3d}$$

Note that term ④ in the above equation needs to be deduced. In order to derived ④, the following corollary of Fubini's theorem is introduced first

Corollary 1. *Given a rectangle $\Delta := [a,b]\times[c,d]$, let $f(x)$ be defined in $a \le x \le b$ and $g(y)$ be defined in $c \le y \le d$. Then, if f and g are continuous, we have*

$$\iint_{\Delta} f(x)g(y)\,\mathrm{d}x\,\mathrm{d}y = \left(\int_a^b f(x)\,\mathrm{d}x\right)\left(\int_c^d g(y)\,\mathrm{d}y\right)$$

Applying Corollary 1 to (A.3d), we obtain

$$\begin{aligned} ④ &= \mathbb{E}\left(\int_{t-\tau_i}^{t} Ce^{A(t-\tau_i-\theta_1)} G\omega(\theta_1)\,\mathrm{d}\theta_1 \cdot \int_{t-\tau_j}^{t} \omega^{\mathrm{T}}(\theta_2) G^{\mathrm{T}} e^{A^{\mathrm{T}}(t-\tau_j-\theta_2)} C^{\mathrm{T}}\,\mathrm{d}\theta_2\right) \\ &= \mathbb{E}\left(\int_{t-\tau_i}^{t}\int_{t-\tau_j}^{t} Ce^{A(t-\tau_i-\theta_1)} G\omega(\theta_1)\omega^{\mathrm{T}}(\theta_2) G^{\mathrm{T}} e^{A^{\mathrm{T}}(t-\tau_j-\theta_2)} C^{\mathrm{T}}\,\mathrm{d}\theta_2\,\mathrm{d}\theta_1\right) \\ &= \int_{t-\tau_i}^{t}\int_{t-\tau_j}^{t} Ce^{A(t-\tau_i-\theta_1)} G\mathbb{E}\left(\omega(\theta_1)\omega^{\mathrm{T}}(\theta_2)\right) G^{\mathrm{T}} e^{A^{\mathrm{T}}(t-\tau_j-\theta_2)} C^{\mathrm{T}}\,\mathrm{d}\theta_2\,\mathrm{d}\theta_1 \\ &= \int_{t-\tau_i}^{t}\int_{t-\tau_j}^{t} Ce^{A(t-\tau_i-\theta_1)} GQ\delta(\theta_1-\theta_2) G^{\mathrm{T}} e^{A^{\mathrm{T}}(t-\tau_j-\theta_2)} C^{\mathrm{T}}\,\mathrm{d}\theta_2\,\mathrm{d}\theta_1 \end{aligned} \tag{A.4}$$

Since the *Dirac delta function* is even, then $\delta(\theta_1-\theta_2)=\delta(\theta_2-\theta_1)$. Furthermore, the shifting property of *Dirac delta function* is recalled as follows:

Corollary 2 ([Hassani 2009]). *For any real or complex valued continuous function f on $\mathbb{R}$, the Dirac delta satisfies the shifting property*

$$\int_a^b f(x)\delta(x-x_0)\,\mathrm{d}x=\begin{cases}f(x_0) & \text{if } a<x_0<b\\ 0 & \text{otherwise}\end{cases}$$

Then, let $k\triangleq\min[i,j]=0,1,...,L-1$, Corollary 2 allows us to continue deriving (A.4) as follows

$$\begin{aligned}
④ &= \int_{t-\tau_i}^{t}\int_{t-\tau_j}^{t} Ce^{A(t-\tau_i-\theta_1)}GQ\delta(\theta_1-\theta_2)G^{\mathrm{T}}e^{A^{\mathrm{T}}(t-\tau_j-\theta_2)}C^{\mathrm{T}}\,\mathrm{d}\theta_2\,\mathrm{d}\theta_1\\
&= \int_{t-\tau_i}^{t}\int_{t-\tau_j}^{t} Ce^{A(t-\tau_i-\theta_1)}GQ\delta(\theta_2-\theta_1)G^{\mathrm{T}}e^{A^{\mathrm{T}}(t-\tau_j-\theta_2)}C^{\mathrm{T}}\,\mathrm{d}\theta_2\,\mathrm{d}\theta_1\\
&= \int_{t-\tau_k}^{t} Ce^{A(t-\tau_k-\theta_1)}GQG^{\mathrm{T}}e^{A^{\mathrm{T}}(t-\tau_k-\theta_1)}C^{\mathrm{T}}\,\mathrm{d}\theta_1\\
\xrightarrow[s=t-\tau_k-\theta_1]{\text{substitution}} &= \int_{-\tau_k}^{0} Ce^{As}GQG^{\mathrm{T}}e^{A^{\mathrm{T}}s}C^{\mathrm{T}}\,\mathrm{d}s \quad \forall i,j
\end{aligned} \tag{A.5}$$

Let $S_k=\int_{-\tau_k}^{0}Ce^{As}GQG^{\mathrm{T}}e^{A^{\mathrm{T}}s}C^{\mathrm{T}}\,\mathrm{d}s$, based upon (A.1)-(A.5), we finally obtain

$$P=\begin{pmatrix}S_0 & S_0 & \cdots & S_0\\ S_0 & S_1 & \cdots & S_1\\ \vdots & \vdots & \ddots & \vdots\\ S_0 & S_1 & \cdots & S_{L-1}\end{pmatrix}+\begin{pmatrix}R & 0 & \cdots & 0\\ 0 & R & \ddots & \vdots\\ \vdots & \ddots & \ddots & 0\\ 0 & \cdots & 0 & R\end{pmatrix} \tag{A.6}$$

Note that block matrix P is symmetric, which is only logic since it is a variance matrix.

Appendix B

Proof of the unbiased estimation property of the CD-FMO in stochastic case

This appendix intends to give a detailed proof that the state estimation of the proposed CD-FMO (3.10) in Chapter 3 is unbiased in stochastic case, namely

$$\mathbb{E}\left(\hat{x}(t)-x(t)\right)=0 \qquad t\in[L\times T_s,+\infty) \tag{B.1}$$

First of all, let K_i with $i=0,1,\cdots,L-1$ represents the $i+1^{\text{th}}$ column of the inverse of variance matrix P^{-1} in (3.8) as follows

$$P^{-1}\triangleq[K_0,K_1,\cdots,K_{L-1}] \tag{B.2}$$

Recall the proposed CD-FMO here as in (3.9) and (3.10)

$$\hat{x}(t)=\arg\min J(x)=\left(W_L^{\mathrm{T}}P^{-1}W_L\right)^{-1}W_L^{\mathrm{T}}P^{-1}\hat{Y}_L \tag{B.3}$$

where

$$\hat{Y}_L=\begin{pmatrix} y(t-\tau_0)+\alpha_{t-\tau_0,t}+\hat{\beta}_{t-\tau_0,t}\\ y(t-\tau_1)+\alpha_{t-\tau_1,t}+\hat{\beta}_{t-\tau_1,t}\\ \vdots\\ y(t-\tau_{L-1})+\alpha_{t-\tau_{L-1},t}+\hat{\beta}_{t-\tau_{L-1},t}\end{pmatrix};\quad W_L=\begin{pmatrix} Ce^{-A\tau_0}\\ Ce^{-A\tau_1}\\ \vdots\\ Ce^{-A\tau_{L-1}}\end{pmatrix}$$

with

$$\hat{\beta}_{t-\tau_i,t}=\int_{t-\tau_i}^{t}Ce^{A(t-\tau_i-\theta)}\Phi(\hat{x}(\theta))\,\mathrm{d}\theta \tag{B.4a}$$

Rewrite the CD-FMO (B.3) as follows

$$\begin{aligned}\hat{x}(t)&=\Omega_L^{-1}W_L^{\mathrm{T}}P^{-1}\hat{Y}_L\\ &=\Omega_L^{-1}\sum_{i=0}^{L-1}\left\{e^{-A^{\mathrm{T}}\tau_i}C^{\mathrm{T}}K_i\left[y(t-\tau_i)+\alpha_{t-\tau_i,t}+\hat{\beta}_{t-\tau_i,t}\right]\right\}\end{aligned} \tag{B.5}$$

with

$$\Omega_L = W_L^{\mathrm{T}} P^{-1} W_L = \sum_{i=0}^{L-1} e^{-A^{\mathrm{T}}\tau_i} C^{\mathrm{T}} K_i C e^{-A\tau_i} \tag{B.6}$$

from (3.5) and (3.6) we have

$$y(t-\tau_i) = Ce^{-A\tau_i}x(t) + v(t-\tau_i) - \alpha_{t-\tau_i,t} - \beta_{t-\tau_i,t} - \gamma_{t-\tau_i,t} \tag{B.7}$$

where

$$\beta_{t-\tau_i,t} = \int_{t-\tau_i}^{t} Ce^{A(t-\tau_i-\theta)}\Phi(x(\theta))\,\mathrm{d}\theta \tag{B.8a}$$

$$\gamma_{t-\tau_i,t} = \int_{t-\tau_i}^{t} Ce^{A(t-\tau_i-\theta)}G\omega(\theta)\,\mathrm{d}\theta \tag{B.8b}$$

replace $y(t-\tau_i)$ in (B.5) by (B.7), we obtain

$$\begin{aligned}\hat{x}(t) &= \Omega_L^{-1}\sum_{i=0}^{L-1}\left\{e^{-A^{\mathrm{T}}\tau_i}C^{\mathrm{T}}K_i\left[Ce^{-A\tau_i}x(t) + v(t-\tau_i) - \beta_{t-\tau_i,t} - \gamma_{t-\tau_i,t} + \hat{\beta}_{t-\tau_i,t}\right]\right\} \\ &\triangleq ① + ② + ③\end{aligned} \tag{B.9}$$

with

$$① = \Omega_L^{-1}\sum_{i=0}^{L-1}\left\{e^{-A^{\mathrm{T}}\tau_i}C^{\mathrm{T}}K_iCe^{-A\tau_i}x(t)\right\} \overset{(B.6)}{=} x(t) \tag{B.10a}$$

$$② = \Omega_L^{-1}\sum_{i=0}^{L-1}\left\{e^{-A^{\mathrm{T}}\tau_i}C^{\mathrm{T}}K_i\left[v(t-\tau_i) - \gamma_{t-\tau_i,t}\right]\right\} \to \mathbb{E}\left(②\right) = 0 \tag{B.10b}$$

$$③ = \Omega_L^{-1}\sum_{i=0}^{L-1}\left\{e^{-A^{\mathrm{T}}\tau_i}C^{\mathrm{T}}K_i\left[\hat{\beta}_{t-\tau_i,t} - \beta_{t-\tau_i,t}\right]\right\} \tag{B.10c}$$

According to (B.9) and (B.10), the following mathematical expectation is given

$$\begin{aligned}\mathbb{E}\left(\hat{x}(t) - x(t)\right) &= \mathbb{E}\left(②\ +\ ③\right) = \mathbb{E}\left(③\right) \\ &= \mathbb{E}\left(\Omega_L^{-1}\sum_{i=0}^{L-1}\left\{e^{-A^{\mathrm{T}}\tau_i}C^{\mathrm{T}}K_i\left[\hat{\beta}_{t-\tau_i,t} - \beta_{t-\tau_i,t}\right]\right\}\right) \\ &= \Omega_L^{-1}\sum_{i=0}^{L-1}\left\{e^{-A^{\mathrm{T}}\tau_i}C^{\mathrm{T}}K_i\mathbb{E}\left[\hat{\beta}_{t-\tau_i,t} - \beta_{t-\tau_i,t}\right]\right\}\end{aligned} \tag{B.11}$$

Before we go any further, let us write the first-order Taylor series of the nonlinear term $\Phi(\hat{x})$ at the point $\hat{x} = x$ as follows

$$\Phi(\hat{x}) \approx \Phi(x) + \left.\frac{\mathrm{d}\Phi}{\mathrm{d}x}\right|_x \cdot (\hat{x} - x) \tag{B.12}$$

since x is not stochastic, it is then straightforward that

$$\mathbb{E}\left[\Phi(\hat{x}) - \Phi(x)\right] = \left.\frac{\mathrm{d}\Phi}{\mathrm{d}x}\right|_x \cdot \mathbb{E}\left(\hat{x} - x\right) \tag{B.13}$$

write (B.11) with (B.4a), (B.8a) and (B.13) as

$$\begin{aligned}
\mathbb{E}\left(\hat{x}(t) - x(t)\right) &= \Omega_L^{-1} \sum_{i=0}^{L-1} \left\{ e^{-A^{\mathrm{T}}\tau_i} C^{\mathrm{T}} K_i \mathbb{E}\left[\hat{\beta}_{t-\tau_i,t} - \beta_{t-\tau_i,t}\right] \right\} \\
&= \Omega_L^{-1} \sum_{i=0}^{L-1} \left\{ e^{-A^{\mathrm{T}}\tau_i} C^{\mathrm{T}} K_i \mathbb{E}\left(\int_{t-\tau_i}^{t} C e^{A(t-\tau_i-\theta)} \left[\Phi(\hat{x}(\theta)) - \Phi(x(\theta))\right] \mathrm{d}\theta \right) \right\} \\
&= \Omega_L^{-1} \sum_{i=0}^{L-1} \left\{ e^{-A^{\mathrm{T}}\tau_i} C^{\mathrm{T}} K_i \int_{t-\tau_i}^{t} C e^{A(t-\tau_i-\theta)} \mathbb{E}\left[\Phi(\hat{x}(\theta)) - \Phi(x(\theta))\right] \mathrm{d}\theta \right\} \\
&= \Omega_L^{-1} \sum_{i=0}^{L-1} \left\{ e^{-A^{\mathrm{T}}\tau_i} C^{\mathrm{T}} K_i \int_{t-\tau_i}^{t} C e^{A(t-\tau_i-\theta)} \cdot \left.\frac{\mathrm{d}\Phi}{\mathrm{d}x}\right|_x \cdot \mathbb{E}\left(\hat{x}(\theta) - x(\theta)\right) \mathrm{d}\theta \right\}
\end{aligned} \tag{B.14}$$

Note that $t \in [L \times T_s, \infty)$, let us take the norm for both side of (B.14), we have

$$\begin{aligned}
\left\|\mathbb{E}\left(\hat{x}(t) - x(t)\right)\right\| &= \left\| \Omega_L^{-1} \sum_{i=0}^{L-1} \left\{ e^{-A^{\mathrm{T}}\tau_i} C^{\mathrm{T}} K_i \int_{t-\tau_i}^{t} C e^{A(t-\tau_i-\theta)} \cdot \left.\frac{\mathrm{d}\Phi}{\mathrm{d}x}\right|_x \cdot \mathbb{E}\left(\hat{x}(\theta) - x(\theta)\right) \mathrm{d}\theta \right\} \right\| \\
&\le \sum_{i=0}^{L-1} \left\{ \left\| \Omega_L^{-1} e^{-A^{\mathrm{T}}\tau_i} C^{\mathrm{T}} K_i \int_{t-\tau_i}^{t} C e^{A(t-\tau_i-\theta)} \cdot \left.\frac{\mathrm{d}\Phi}{\mathrm{d}x}\right|_x \cdot \mathbb{E}\left(\hat{x}(\theta) - x(\theta)\right) \mathrm{d}\theta \right\| \right\} \\
&\le \sum_{i=0}^{L-1} \left\{ \int_{t-\tau_i}^{t} \left\| \Omega_L^{-1} e^{-A^{\mathrm{T}}\tau_i} C^{\mathrm{T}} K_i C e^{A(t-\tau_i-\theta)} \cdot \left.\frac{\mathrm{d}\Phi}{\mathrm{d}x}\right|_x \cdot \mathbb{E}\left(\hat{x}(\theta) - x(\theta)\right) \right\| \mathrm{d}\theta \right\} \\
&\le L \int_{t-\tau_{L-1}}^{t} \left\| \Omega_L^{-1} e^{-A^{\mathrm{T}}\tau_{L-1}} C^{\mathrm{T}} K_i C e^{A(t-\tau_{L-1}-\theta)} \cdot \left.\frac{\mathrm{d}\Phi}{\mathrm{d}x}\right|_x \cdot \mathbb{E}\left(\hat{x}(\theta) - x(\theta)\right) \right\| \mathrm{d}\theta \\
&\le L \int_{t-\tau_{L-1}}^{t} \left\| \Omega_L^{-1} e^{-A^{\mathrm{T}}\tau_{L-1}} C^{\mathrm{T}} K_i C e^{A(t-\tau_{L-1}-\theta)} \cdot \left.\frac{\mathrm{d}\Phi}{\mathrm{d}x}\right|_x \right\| \left\|\mathbb{E}\left(\hat{x}(\theta) - x(\theta)\right)\right\| \mathrm{d}\theta \\
&\le L \int_{L\times T_s}^{t} \left\| \Omega_L^{-1} e^{-A^{\mathrm{T}}\tau_{L-1}} C^{\mathrm{T}} K_i C e^{A(t-\tau_{L-1}-\theta)} \cdot \left.\frac{\mathrm{d}\Phi}{\mathrm{d}x}\right|_x \right\| \left\|\mathbb{E}\left(\hat{x}(\theta) - x(\theta)\right)\right\| \mathrm{d}\theta
\end{aligned} \tag{B.15}$$

then, the Gronwall inequality [Bellman 1943] yields

$$\begin{aligned} \|\mathbb{E}\left(\hat{x}(t)-x(t)\right)\| &\leq \mathbf{0}\cdot e^{L\int_{L\times T_s}^{t}\left\|\Omega_L^{-1}e^{-A^{\mathrm{T}}\tau_{L-1}}C^{\mathrm{T}}K_iCe^{A(t-\tau_{L-1}-\theta)}\cdot\frac{\mathrm{d}\Phi}{\mathrm{d}x}\big|_x\right\|\mathrm{d}\theta} \\ &\leq 0 \end{aligned} \tag{B.16}$$

hence,

$$\|\mathbb{E}\left(\hat{x}(t)-x(t)\right)\|\leq 0 \;\Rightarrow\; \|\mathbb{E}\left(\hat{x}(t)-x(t)\right)\|=0 \;\Rightarrow\; \mathbb{E}\left(\hat{x}(t)-x(t)\right)=0$$

The proof is completed.

Appendix C

Proof of the "positive definiteness" for the Schur complement $\mathbb{S}(t) := P_{L+1}(t) \backslash P_L(t)$

In order to prove $\mathbb{S}(t) = r^{\mathrm{T}}(t)r(t) - \eta^{\mathrm{T}}(t)P_L^{-1}(t)\eta(t)$ in (5.28) is positive-definite, let us firstly note $P_{L+1}(t)$ in (5.26) as follows

$$P_{L+1}(t) = \begin{bmatrix} P_L(t) & \eta(t) \\ \eta^{\mathrm{T}}(t) & r^{\mathrm{T}}(t)r(t) \end{bmatrix} \quad \xrightarrow{\text{note as}} \quad \mathbb{M} = \begin{bmatrix} \mathbb{A} & \mathbb{B} \\ \mathbb{C} & \mathbb{D} \end{bmatrix} \tag{C.1}$$

then we need to prove that when $\mathbb{M}$ and $\mathbb{A}$ are positive-definite and invertible, the Schur complement of $\mathbb{A}$ in $\mathbb{M}$, i.e. $\mathbb{A}\backslash\mathbb{M} = \mathbb{D} - \mathbb{C}\mathbb{A}^{-1}\mathbb{B}$, are positive-definite.

Since $\mathbb{M}$ and $\mathbb{A}$ are positive-definite and invertible, then $\det(\mathbb{M}) > 0$ and $\det(\mathbb{A}^{-1}) > 0$. Therefore, the following equation naturally holds

$$\begin{bmatrix} \mathbb{A}^{-1} & 0 \\ -\mathbb{C}\mathbb{A}^{-1} & I \end{bmatrix} \begin{bmatrix} \mathbb{A} & \mathbb{B} \\ \mathbb{C} & \mathbb{D} \end{bmatrix} = \begin{bmatrix} I & \mathbb{A}^{-1}\mathbb{B} \\ 0 & \mathbb{D} - \mathbb{C}\mathbb{A}^{-1}\mathbb{B} \end{bmatrix} \tag{C.2}$$

Take the determinant on both sides of (C.2) as

$$\det(\mathbb{A}^{-1})\det(\mathbb{M}) = \det(\mathbb{D} - \mathbb{C}\mathbb{A}^{-1}\mathbb{B}) \tag{C.3}$$

Since $\det(\mathbb{M}) > 0$ and $\det(\mathbb{A}^{-1}) > 0$, we then obtain from (C.3) that

$$\det(\mathbb{D} - \mathbb{C}\mathbb{A}^{-1}\mathbb{B}) > 0 \tag{C.4}$$

namely,

$$\mathbb{S}(t) = r^{\mathrm{T}}(t)r(t) - \eta^{\mathrm{T}}(t)P_L^{-1}(t)\eta(t) > 0 \tag{C.5}$$

which proves that the Schur complement of $P_L(t)$, $\mathbb{S}(t)$, is positive-definite.

Tingting ZHANG

Observateur à mémoire finie pour les systèmes non linéaires à temps continu et à mesures discrètes : application au diagnostic

Résumé : L'objectif de cette thèse est de développer un observateur non linéaire pour un outil de diagnostic pour des systèmes non linéaires à temps continu et à mesures discrètes. Ce mémoire débute par l'étude de notions d'observabilité faisant le point sur l'observation de ces systèmes. Nous enchaînons ensuite par l'analyse d'observateurs non linéaires obtenu par optimisation, puis nous présentons les méthodes de diagnostic à l'aide d'observateurs. Un observateur à mémoire finie est ensuite synthétisé pour détecter et localiser les défauts capteurs et actionneurs d'une classe de systèmes non linéaires en présence à la fois de bruit de processus et de bruit de mesures. De plus, un observateur non linéaire est également construit sur un modèle augmenté pour estimer simultanément les états du système et les entrées inconnues. Une étude de robustesse vis à vis des divers bruits a été menée, ainsi que l'étude de la définition des défaut d'amplitude minimale pour la détection. L'utilisation de l'algorithme EWMA a également été introduit pour ses performance en détection. Multiple défauts simultanés ont été détectés et identifiés dans cette partie. À la fin de cette thèse, un observateur à mémoire finie est développé pour les systèmes non linéaires à temps variants.

Mots-clés : synthèse d'observateurs, systèmes non linéaires, diagnostic de défauts, temps-variant, entrée inconnue, observateur à mémoire finie

Finite memory observer design for continuous-time nonlinear systems with discrete-time measurements: application to diagnosis

Abstract: The aim of this thesis is to design a nonlinear observer as a diagnostic tool for continuous-time nonlinear systems with discrete-time measurements. We begin with the study of some observability notions concerning the considered nonlinear systems, following by the presents of three typical optimization-based nonlinear observers and observer-based diagnostic methods. Inspired by the existing approaches, a finite memory observer is then designed for a class of nonlinear systems in the presence of both process and measurement noises in order to perform fault detection and isolation of sensor and actuator faults. In the second part, a nonlinear observer based on augmented model is then designed to simultaneously estimate both system states and unknown inputs. The robustness with respect to the diverse noises is studied, as well as the study of the minimum amplitude of fault for the detection. The EWMA algorithm was also introduced and analyzed for its performance in detection. Multiple simultaneous faults are also detected and identified in this part. At the end of this thesis, a finite memory observer is designed for the nonlinear time-varying systems on the basis of the fundamental synthesis for linear time-varying systems.

Keywords: observer design, nonlinear dynamical systems, fault diagnosis, time-varying, unknown input, finite memory observer

INSA INSTITUT NATIONAL DES SCIENCES APPLIQUÉES CENTRE VAL DE LOIRE

Laboratoire PRISME
INSA Centre Val de Loire (Campus de Bourges)
88, Boulevard Lahitolle
18000 Bourges

PRISME Laboratoire Pluridisciplinaire de Recherche Ingénierie des Systèmes, Mécanique, Énergétique